57

A Design for a High Energy X-Ray Computed Tomography Sensor for the Study of Solidification Fronts in Aluminum

by

Imad Maurice Jureidini

B.S., Applied Physics, Columbia University, 1994

SUBMITTED TO THE DEPARTMENT OF NUCLEAR ENGINEERING IN PARTIAL FULFILLMENT OF THE REQUIREMENTS FOR THE DEGREE OF

MASTER OF SCIENCE IN NUCLEAR ENGINEERING

AT THE

MASSACHUSETTS INSTITUTE OF TECHNOLOGY

February 1997

Signature of Author: _____
Department of Nuclear Engineering
January 17, 1997

Certified by: _____
Richard Lanza
Research Scientist, Nuclear Engineering Department
Thesis Supervisor

Certified by: _____
Lawrence Lidsky
Professor of Nuclear Engineering
Thesis Reader

Accepted by: _____
Jeffrey Freidberg
Professor of Nuclear Engineering
Chairman, Department Committee on Graduate Students

A Design for a High Energy X-Ray Computed Tomography Sensor for the Study of Solidification Fronts in Aluminum

by

Imad Jureidini

Submitted to the Department of Nuclear Engineering
on January 17, 1997 in Partial Fulfillment of the Requirements for the Degree of
Master of Science in Nuclear Engineering

ABSTRACT

CastScan, a computed tomography sensor, has been designed to study the solidification front of aluminum in a laboratory environment. The characteristics of this scanner are presented, along with the motivations behind its design and its expected performance.

X-ray computed tomography systems allow one to obtain two-dimensional, cross-sectional images of the density within a scanned sample. Liquid and solid metals vary in density by a few percent, making them a potential object of CT study. Because of the high density of metals, traditional low-energy CT systems such as those used in medicine are not useful. CastScan uses a 6 MeV electron linac to produces an intense beam of highly energetic, highly penetrative x-ray photons. To detect these photons, the system uses 120 channels of high density cadmium tungstate scintillation crystals coupled to silicon photodiodes. An aluminum sample is melted in a cylindrical furnace that resides on a computer controlled rotary and translational stage. The temperature of the sample is measured at 16 positions. A computer system allows the remote operation of the sensor from outside a shielded facility.

The CastScan system is expected to be capable of yielding images of the density of the aluminum sample within a 1.2 cm thick slab and with a maximum resolution of 1.1 mm, in a time on the order of one to a few minutes. This capability will allow the operator to resolve the profile of the solidification front within the aluminum sample. This system opens the possibility of real-time monitoring of the solidification front of metals in an industrial environment.

Thesis Advisor: Richard Lanza
Title: Principal Research Scientist

Acknowledgments

I would like to thank Dr. Richard Lanza for introducing me to this project and for his guidance and advice over the past year. My thanks also go to Prof. Jung-Hoon Chun and Dr. Nannaji Saka. The three of them are the backbone of this project and allow it to be an ongoing success.

I am grateful to have such great colleagues and friends as my fellow graduate students Mark Hytros and DongSik Kim, who are not a bunch of freaks, even though they may think so. My gratitude goes to our undergraduate branch, Eric Empey.

I would like to thank Jeff DiTullio of the MIT Manufacturing Institute, as well as Dr. Tim Roney and Dr. Dennis Kunerth of the Idaho National Engineering Laboratory. The staff at the Bates Linear Accelerator Center, and particularly Kenneth Hatch, have proven invaluable to the advancement of our project. I would also like to thank our partners at Analogic Corporation, in particular John Dobbs and Hans Weedon, for their commitment and efforts at providing us a detector system. Finally, I extend my appreciation to Russ Schonberg and the folks at Schonberg corporation for their willingness to help and their friendliness.

This work was in part funded by the National Science Foundation (Grant No. DMI-9522973) and the Idaho National Engineering Laboratory - University Research Consortium (Contract No. C95-175002-LKK-267-95).

Table of Contents

List of Tables

List of Figures

1. INTRODUCTION

1.1. Continuous Casting

In 1995, the raw steel production in North America represented 134 million net tons. More than 60 % of this production is the result of a continuous casting process, up from 5 % in 1970 for the worldwide production [1]. This investment on continuous casting, which is reflected in the $20 billion in plant and equipment investment by the U.S. steel producers, has yielded a payback in a significant increase in productivity from 10.1 man hours per finished ton (MHPT) in 1982 to 3.9 MHPT in 1995, with many North American facilities under 2.0 MHPT.

In March 1996, the annual rate of aluminum production in the U.S. was 3.58 million tons per year.

The advantages of continuous casting are the following:

- Energy savings
- Improved yield
- Improved labor productivity
- improved steel quality
- reduced pollution
- reduced capital costs

Traditional casting methods consist of pouring molten metal into an ingot mold. The solidified metal is then reheated in soaking pits for rolling to semi-finished or finished products. In continuous casting, the re-heating process is bypassed, leading to a significant reduction in energy costs. The molten metal is poured into a water cooled mold which is open at the bottom. As the hot liquid makes contact with the surface of the mold, its outer skin solidifies. The resulting strand then descends into the open air, cooling down. As a result, the skin thickens until eventually the entire section is

solidified. During this process, the strand can be rolled into its final shape. A diagram representing the basic principles of continuous casting is shown in Figure 1.1.

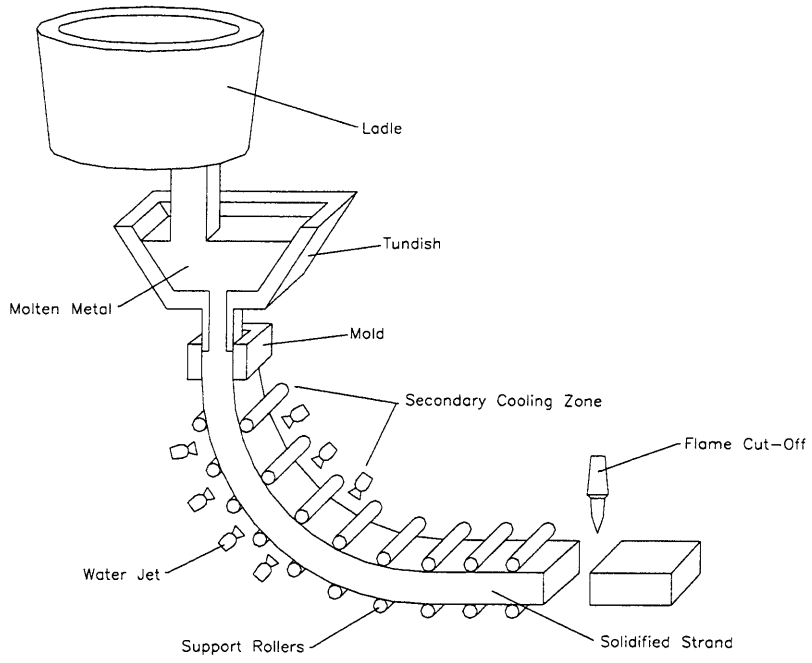

Figure 1.1. Schematic of a continuous casting facility

1.2. Sensor Benefits

A real-time sensor that could obtain a two- or three-dimensional image of the solidifying metal would be very beneficial to the casting industry. Among the many issues of importance for this industry are the following:

- Productivity depends on the rate at which the strand is pulled and the quality of the cast.
- *Breakout* may occur if the strand is pulled too fast: production is stopped and repairs are costly.
- Steel quality may suffer depending on the cooling rate.

As is apparent, there is conflict between the desire to produce metal at a faster rate and the risk of a costly accident. In addition to helping to prevent such occurrences, a sensor

could provide valuable information about the steel quality and the manufacturing process in general.

The concept of an x-ray computed tomography (CT) sensor has been proposed [2][3][4]. Because such a sensor is sensitive to density variations within an object, it is capable of discriminating between solid and liquid metal. Typical density variations for steel, aluminum and tin are presented in Table 1.1.

	Solid Density [kg/m^3]	Liquid Density [kg/m^3]	Difference
Steel	~7800	~7400	4%-7%
Aluminum	~2700	~2400	9%-12%
Tin	~7300	~7000	4%-5%

Table 1.1. Density variation between solid and liquid steel, aluminum and tin

In this document, we propose to describe the CastScan experiment. Its goal is to design and construct a fast, high energy x-ray CT sensor to study the solidification properties of aluminum melted in a laboratory environment. The topics covered include the principles of computed tomography. We will examine how x-rays interact with matter and how these properties are used to measure the density variations of a sample within a two-dimensional plane.

The focus will then be turned towards the x-ray source appropriate for this application, an electron linear accelerator (linac). We will review the fundamentals of the operation of a linac, and explain the process by which x-rays are produced. We will then review the configuration of the MINAC 6 accelerator which will be used in this experiment, as well as the physical characteristics of the x-ray beam it emits.

The CastScan CT sensor images an aluminum sample placed within a laboratory furnace. We will survey the furnace setup and the design of the cooling system used to create a solidification front within the melted aluminum sample. The assembly used to move the furnace will be briefly examined.

The x-ray detection system is a critical part of a CT sensor. After reviewing the principles of x-ray detector systems, we will present the system chosen for the CastScan project. Particular attention is paid to issue of the scattering of x-rays and its potentially "nefarious" consequences on image quality.

With the basic components specified, we will turn our attention towards the overall experimental layout. Because the x-ray beam produced by the linear accelerator can be lethal in little more than a minute for an unprotected operator, we probe into the issue of shielding and the overall room design.

Some of the scanner's constituents must be adjusted prior to an imaging sequence, while the others need to be precisely synchronized by a computer during data acquisition. We will therefore cover the topic of the devices and the software that controls them.

With all the experimental parameters established, the expected performance goals of the CastScan system will be discussed, both in terms of resolution and acquisition time.

2. X-RAY COMPUTED TOMOGRAPHY

Since the early 70's when it was first made practical, the technique of computed tomography has revolutionized the field of medical imaging. Standard radiography, which originated soon after the discovery of radioactivity and x-rays in the late 19^{th} century, provides images which are essentially the "shadows" of x-rays through an object or person. The information obtained represents the superimposition of the properties of the medium the photons traverse. Only the trained eye of a radiologist can, after years of experience, interpret this data and extract the depth-dependent information required for diagnostics in the medical field. Almost a century later, computed tomography has solved this problem by allowing one to obtain two-dimensional images of cross-sections through a body or object.

To understand the basis x-ray CT, we will first explore the issue of how high-energy photons interact with matter. From this foundation, we will explain the standard model used to quantify photon attenuation. Finally, we will overview the mathematical basis of computed tomography.

2.1. Photon Interactions

X-rays interactions with matter can be classified into three categories: photoelectric absorption, Compton-scattering and pair production. A brief explanation of the physical principles of these three important phenomena is now presented.

2.1.1. Photoelectric Absorption

An important stepping stone towards the establishment of quantum mechanics early this century, the phenomenon of photoelectric absorption was first described by

Albert Einstein in 1905. Einstein described how photons impinging upon matter are absorbed and cause the expulsion of an electron with a well-defined kinetic energy. Indeed it was observed that the energy of an outgoing electron was nearly proportional to the frequency of the incoming electromagnetic radiation, as shown in equation Eq. 2.1.

$$E_{electron} = h\nu - B_e \qquad \text{Eq. 2.1}$$

In this equation, ν represents the frequency of the light, h is Planck's constant, and B_e is the binding energy of the electron in the atom. This observation lead to the understanding that light, considered until then to be a wave phenomenon as described by Maxwell's equations, also behaves like a particle. Indeed, through Planck's constant, light is bundled into *quanta* of energy proportional to the frequency of the light.

In the context of computed tomography, the important property of photoelectric absorption is that the incoming photon disappears completely after the interaction with the electron.

The interaction probability for the photoelectric effect, as well as those for the other interaction schemes that will be discussed in the following sections, is dependent upon the photon energy E and the atomic number of the target material Z. This issue will be reviewed in section 2.2.

2.1.2. Compton Scattering

Another mode of interaction between photons and matter is Compton scattering. As described in Figure 2.1, an incoming photon interacts with an atomic electron and causes it to be ejected.

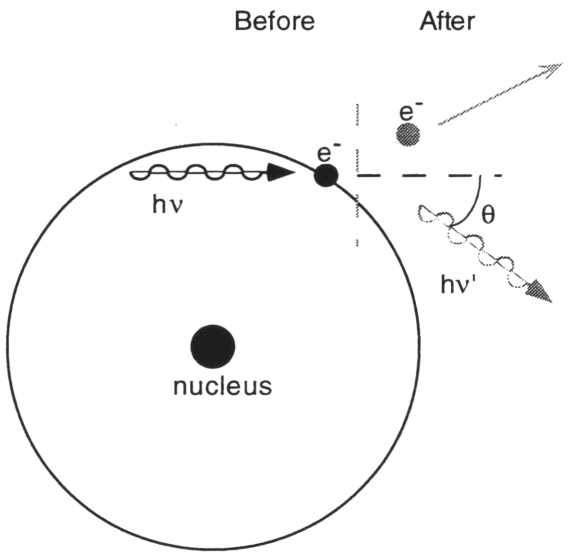

Figure 2.1. Schematic of the Compton scattering process

In contrast to photoelectric absorption, the incoming photon is not completely absorbed. Instead it scatters at an angle θ from its original path. The outgoing photon and the ejected electron share the incoming photon's energy. The energy of the outgoing photon can be calculated by applying the relativistic laws of conservation of energy and momentum to the photon and the electron [5], and is given by:

$$h\nu' = \frac{h\nu}{1 + \frac{h\nu}{m_e c^2}(1 - \cos\theta)} \qquad \text{Eq. 2.2}$$

where m_e is the rest mass of the electron, such that $m_e c^2$ is equal to 511 keV. The binding energy B_e of the electron is not taken into account in this formulation. The scattered photon energy as a function of θ is shown in Figure 2.2.

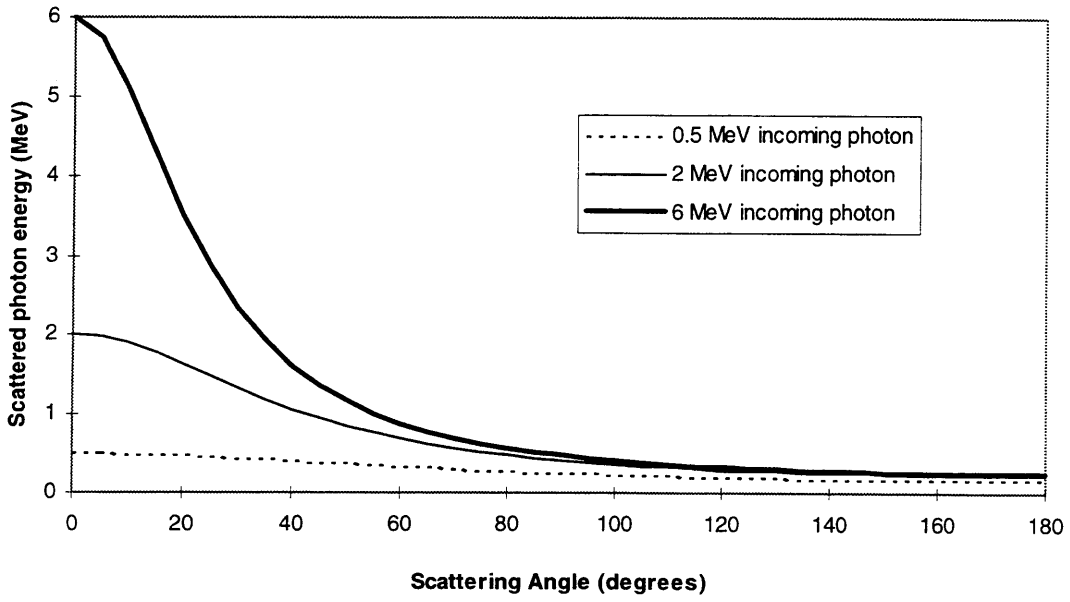

Figure 2.2. Energy of Compton scattered photons as function of the scatter angle

One can distinguish a number of interesting features in these curves. First, when the angle of scatter θ is close to 0°, one finds, as expected by intuition, that the photon energy is unchanged. At 90°, the scattered energies for photons above 1 MeV converge towards the rest mass of the electron, 0.511 MeV. Finally, at the backscattering angle 180°, the scattered photon energies converge towards $m_e c^2/2$.

The angular distribution of Compton scattered photons is both a function of the angle θ of this scatter with respect to the trajectory of the incoming photon, and of this photon's energy. The theoretical expression for this distribution is known as the Klein-Nishina formula [6]:

$$\frac{d\mu_{cs}}{d\Omega} \propto \left(\frac{1}{1+\alpha(1-\cos\theta)}\right)^2 \left(\frac{1+\cos^2\theta}{2}\right) \cdot \left(1+\frac{\alpha^2(1-\cos\theta)^2}{(1+\cos^2\theta)[1+\alpha(1-\cos\theta)]}\right) \qquad \text{Eq. 2.3}$$

A graph of this expression is shown in Figure 2.3, where it is evaluated for energies of 10 keV, 100 keV, 1 MeV and 6 MeV.

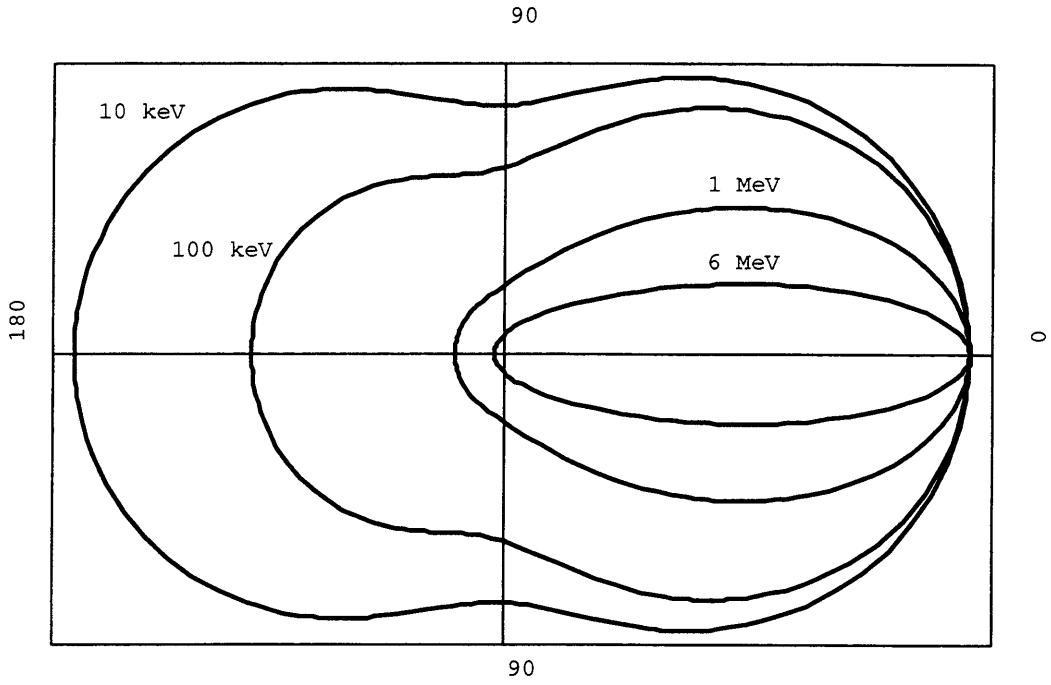

Figure 2.3. Polar plots of the probability of Compton scattering as a function of the scattering angle θ for a variety of photon energies .

In the context of computed tomography, it is important to note that the more energetic the photons, the shallower the angle of scatter will tend to be; and as a consequence, the photons scattered at small angles retain most of their energy.

2.1.3. Pair Production

Above a certain threshold, a photon's energy can be directly converted into matter. In this process, a particle and its corresponding antimatter conjugate are created. For reasons of conservation of energy, the pair production of an electron and its antimatter counterpart, the positron, requires a minimum photon energy equal to twice the electron rest mass m_e, i.e. 1.022 MeV. A schematic of this process is shown in Figure 2.4.

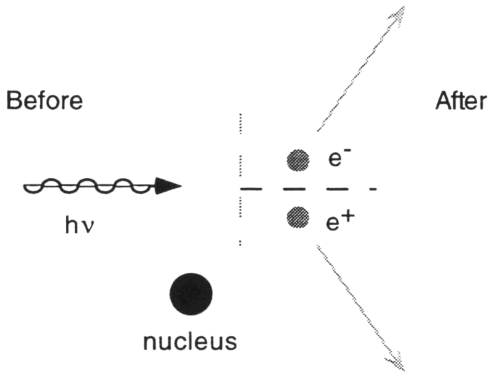

Figure 2.4. Schematic of the pair production process

As shown above, the pair production process requires the presence of a nucleus to satisfy the laws of conservation of energy and momentum. The electron and the positron have an equal kinetic energy T_e, given by Eq. 2.4.

$$T_e = \frac{h\nu}{2} - m_e c^2 \qquad \text{Eq. 2.4}$$

Because they are electrically charged, the electron and the positron rapidly loose their kinetic energy and nearly stop. Whereas the electron is absorbed by the medium, the positron interacts with an atomic electron and annihilates with it. As a result, two x-ray photons of 0.511 MeV each are created. Because the electron and positron involved are nearly at rest, the annihilation x-rays travel in nearly opposite directions.

Overall, the important features of the pair production process are its threshold of 1.022 MeV, and the creation of two lower energy x-rays emitted isotropically.

2.2. Photon Attenuation

The probability of interaction of a photon as it travels in a medium is constant. In the case of a thin target of thickness Δx, the probability of interaction is proportional to this thickness Δx, with a constant of proportionality defined as μ, the *linear attenuation*

coefficient. Given a number of photons N_0 entering the thin target, the number that will interact ΔN is given by Eq. 2.5.

$$\Delta N = \mu N_0 \cdot \Delta x \qquad \text{Eq. 2.5}$$

This model can be extended to thick targets by integrating Eq. 2.5 over a distance l:

$$N(x) = N_0 - \int_0^l \mu N(x) dx \qquad \text{Eq. 2.6}$$

The result of this integral equation is given next:

$$N(x) = N_0 e^{-\mu l} \qquad \text{Eq. 2.7}$$

This equation shows that the number of photons in a target decreases exponentially. This model assumes that the photons that interact are removed completely, which is the case for the photoelectric effect, but is not in the case of Compton scattering nor pair production. Although we will adopt this standard attenuation model in the remainder of this text, the issue of scattered photons will be addressed in section 5.3.

The attenuation coefficient μ takes into account all three interaction types described in section 2.1. It can be decomposed into three components, μ_{pe}, μ_{cs}, and μ_{pp}, representing the attenuation coefficient for the photoelectric effect, Compton scattering and pair production respectively. Because these phenomena rely on different physical basis, their importance is a function of the photon energy, the material density, and its composition.

The photoelectric effect attenuation coefficient per atom increases with the atomic number Z of the target material and decreases with the photon energy E. An approximate relation is given in Eq. 2.8 [6].

$$\mu_{pe} \propto \frac{Z^n}{E^{3.5}} \qquad \text{Eq. 2.8}$$

where n depends on the material and varies between 4 and 5. This equation signifies that the photoelectric effect is much more important for high Z materials such as tungsten (Z=74) and lead (Z=82) than for lower Z materials such as aluminum (Z=27). Also, one can expect that the photoelectric effect will be dominant at low photon energies, and will drop off quickly as the photon energy increases.

The attenuation coefficient for the Compton scattering process is almost independent of the atomic number Z, and generally decreases as the photon energy E increases.

Pair production doesn't contribute to attenuation at all until the threshold energy 1.022 MeV is reached. Above this energy, the attenuation coefficient increases swiftly. In terms of the atomic number, the coefficient per atom varies approximately as Z^2.

Figure 2.5 shows these coefficients for aluminum. [The coefficients where calculated using the PhotCoef software package for IBM PC compatible, published by Applied Inventions Corporation].

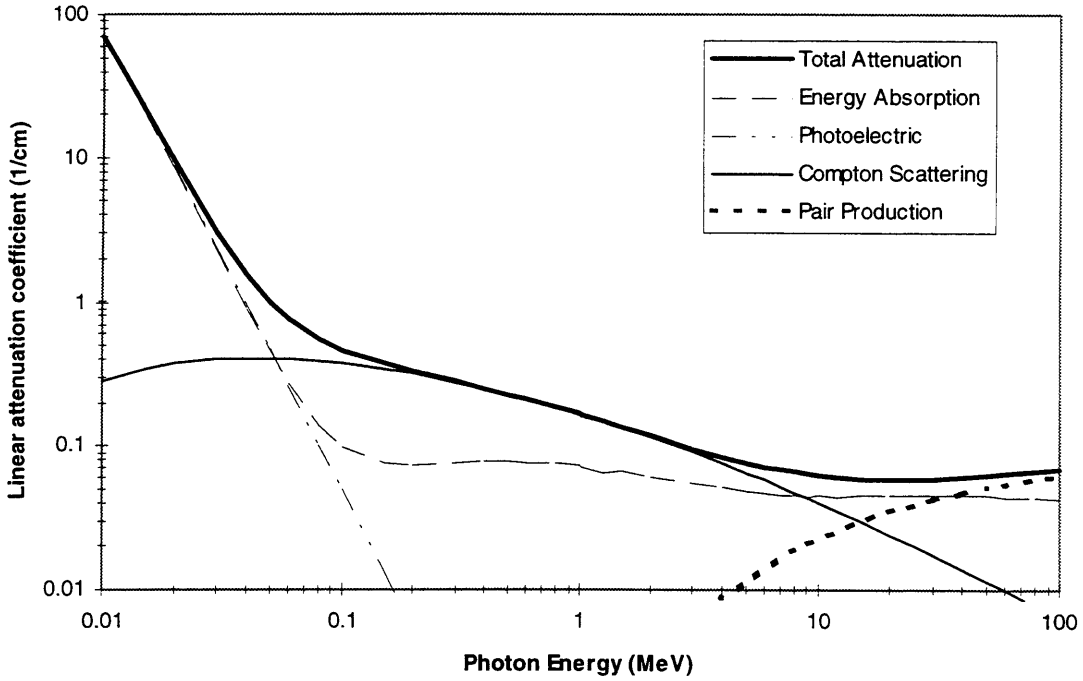

Figure 2.5. Linear attenuation coefficients for aluminum for photon energies ranging from 10 keV to 100 MeV.

At energies below 100 keV, the photoelectric effect dominates all other phenomena due to its strong inverse dependence on E. As we increase photon energies, the probability of photoelectric absorption drops, and because the threshold for pair production hasn't been reached, the Compton scattering phenomenon dominates, decreasing slowly with energy. Finally, for energies greater than 1.022 MeV, μ_{pp} increases slowly until it supersedes μ_{cs} between 10 and 100 MeV.

An interesting feature of Figure 2.5 is the energy absorption coefficient μ_A. As we have seen, the amount of energy deposited by a photon depends on the interaction type. For the photoelectric effect, all the photon energy is deposited. This is apparent in Figure 2.5 at low energies when only μ_{pe} is important and $\mu_A=\mu_{pe}$. In Compton scattering, only a fraction of the incoming photon energy is carried by the recoiling electron, meaning that in the energy range in which μ_{cs} is dominant, the energy absorption coefficient μ_A is smaller than the linear attenuation coefficient μ. Finally, in the regions where pair

production dominates, the energy carried by the annihilation x-rays is not accounted for in μ_A, again meaning that $\mu_A<\mu$.

For a given target material and photon energy, the attenuation coefficient μ will be proportional to the target atom density, which in turn is proportional to the mass density ρ of the material in question. Because of this, it is often easier to use the *mass attenuation coefficient,* μ_m. The definition of μ_m is given in Eq. 2.9.

$$\mu_m = \frac{\mu}{\rho} \qquad \text{Eq. 2.9}$$

We can now compare the attenuation properties of different materials. The following figure shows the mass attenuation coefficient μ_m for air, water, aluminum and lead, for photon energies ranging from 10 keV to 100 MeV.

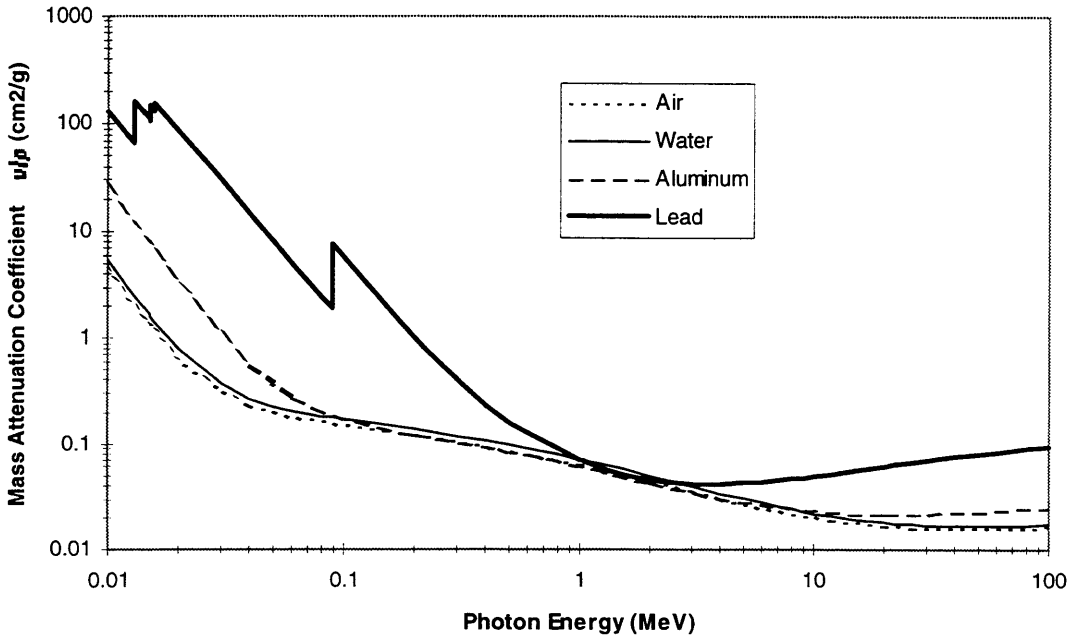

Figure 2.6. Mass attenuation coefficients of air, water, aluminum and lead as a function of photon energy

As we will see in section 2.4, an important feature of this graph is the fact that between 1 and 5 MeV the mass attenuation coefficient is independent of the material type, meaning that the attenuation coefficient μ is proportional only to the material density ρ.

Before applying these observations to the experiment described in this text, we will examine how computed tomography relies on the concepts developed above.

2.3. Principles of Computed Tomography

In standard radiography, x-rays are transmitted through an object, and the attenuation of these x-rays is measured using a film. A radiograph is essentially a map of this attenuation. Because the object under study is made of a variety of materials of varying densities, the attenuation coefficient μ is a function of the position within the object. Measuring the attenuation of an x-ray beam along a given path allows one to calculate an average attenuation coefficient $\overline{\mu}$. This concept is illustrated by Figure 2.7.

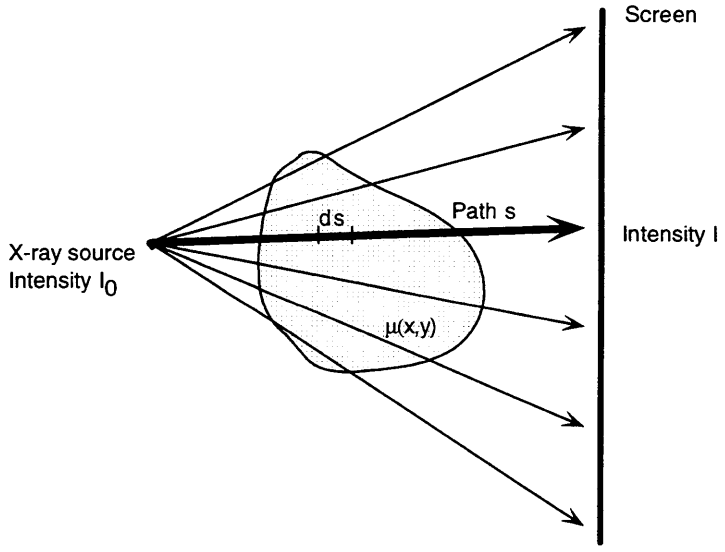

Figure 2.7. Schematic of a radiography experiment

The photon intensity I measured by the screen is related to the intensity I_0 emanating from the x-ray source by the following equation:

$$I = I_0 e^{-\int_0^s \mu(s')ds'} \qquad \text{Eq. 2.10}$$

The average attenuation coefficient along the path s is given by:

$$\bar{\mu} = \frac{\int_0^s \mu(s')ds'}{s} = \ln\left(\frac{I_0}{I}\right) \qquad \text{Eq. 2.11}$$

The limitation of traditional radiography is apparent in this equation: the depth information in $\mu(s)$ is lost. Computed tomography allows one to obtain this information using a set of radiographs taken at a number of angles around the object. This process amounts to performing a *Radon transform*, which will now be described.

2.3.1. The Radon Transform

The linear attenuation coefficient $\mu(x,y)$ within an object varies with position as shown in Figure 2.8.

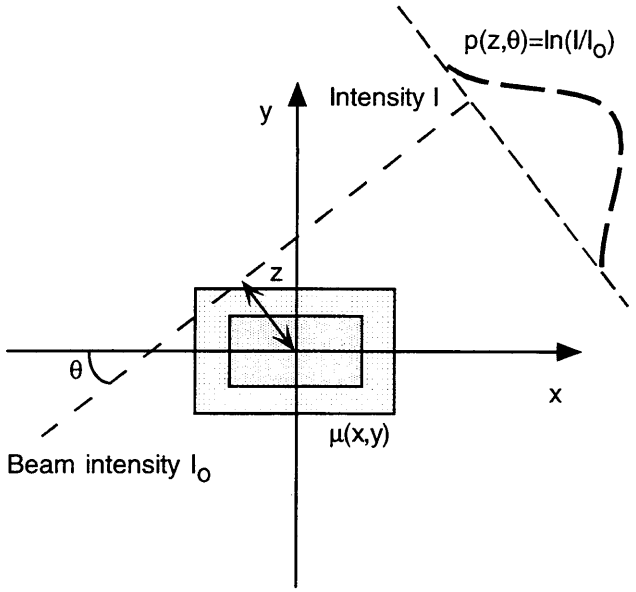

Figure 2.8. Radon transform geometry

An x-ray beam traverses the object at an angle θ from the x-axis, at a distance z from the center of the reference frame. The quantity $p(z,\theta)$ is a function of both z and θ. Its analytical form is:

$$p(z,\theta) = \int\int \mu(x,y)\delta(x\cos\theta + y\sin\theta - z)dxdy \qquad \text{Eq. 2.12}$$

This transformation from $\{x,y\}$ to $\{z,\theta\}$ is named the *Radon transform* [7]. The result of this transformation is a two-dimensional function called a *sinogram*. An example of an object and its corresponding sinogram are shown in Figure 2.9.

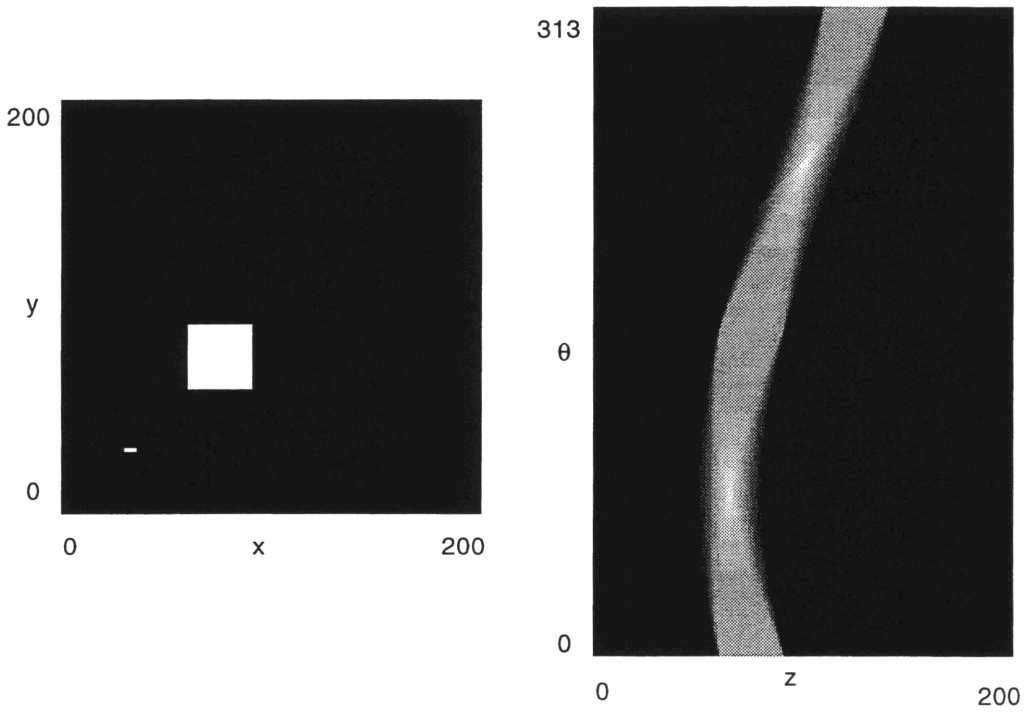

Figure 2.9. Sample bitmap (left) and its corresponding sinogram (right)

When an x-ray CT experiment is carried out and a sinogram is obtained, the goal is to reconstruct the object map from the sinogram. The issue is therefore to process the sinogram $p(z,\theta)$ with an inverse Radon transform.

2.3.2. The Inverse Radon Transform

The Fourier transform $F(w)$ of a function $f(x)$ is defined as follows:

$$F(w) = \int_{-\infty}^{\infty} f(x)e^{-iwx}dx \qquad \text{Eq. 2.13}$$

The inverse Fourier transform is itself defined such that:

$$f(x) = \frac{1}{2\pi} \int_{-\infty}^{\infty} F(w) e^{-iwx} dw \qquad \text{Eq. 2.14}$$

The Fourier transform of $p(z,\theta)$ along the z-axis is derived next:

$$\begin{aligned} P(w_z,\theta) &= \int_{-\infty}^{\infty}\int_{-\infty}^{\infty}\int_{-\infty}^{\infty} \mu(x,y)\delta(x\cos\theta + y\sin\theta - z) e^{-iw_z z} dx dy dz \\ &= \int_{-\infty}^{\infty}\int_{-\infty}^{\infty} \mu(x,y) e^{-iw_z(x\cos\theta + y\sin\theta)} dx dy \\ &= \mathrm{M}(w_x, w_y) \end{aligned} \qquad \text{Eq. 2.15}$$

This result constitutes the *central slice theorem.* It states that the one-dimensional Fourier transform of the sinogram is equal to the two dimensional Fourier transform of the map of the object. The function $\mu(x,y)$ can now be obtained by taking the two dimensional inverse Fourier transform of $M(w_x,w_y)$.

$$\begin{aligned} \mu(x,y) &= \frac{1}{4\pi^2} \int_{-\infty}^{\infty}\int_{-\infty}^{\infty} \mathrm{M}(w_x, w_y) e^{i(w_x x + w_y y)} dw_x dw_y \\ &= \frac{1}{4\pi^2} \int_{0}^{2\pi}\int_{-\infty}^{\infty} P(w_z,\theta) e^{iw_z z} |J| dw_z d\theta \end{aligned} \qquad \text{Eq. 2.16}$$

where $|J|$ is the Jacobian of the transformation from $\{w_x,w_y\}$ to $\{w_z,\theta\}$, and equal to $|w_z|$. If we denote the Fourier transform operation and its inverse as F and F^{-1} respectively, the inverse Radon transform operation can be summarized as follows:

$$\mu(x,y) = \frac{1}{\pi} \int_{0}^{\pi} F^{-1}\left\{ P(w_z,\theta) \cdot |w_z| \right\} d\theta \qquad \text{Eq. 2.17}$$

This function μ at a point (x,y) is therefore proportional to the sum of the function inside the integral, evaluated along all paths traversing (x,y) and over a 180° angular range. This

type of operation is called a *backprojection*. Equation 2.17 signifies that the linear attenuation coefficient distribution in an object can be reconstructed in five operations:

- obtain the sinogram $p(z,\theta)$ experimentally,
- take the z-axis Fourier transform of $p(z,\theta)$ to obtain $P(w_z,\theta)$,
- multiply $P(w_z,\theta)$ by the filter function $|w_z|$,
- take the inverse Fourier transform $p'(z,\theta)$ of the result,
- backproject this filtered sinogram.

This algorithm for the reconstruction of $\mu(x,y)$ is known as the *filtered backprojection* (FBP) algorithm. The result of the FBP algorithm for the example of Figure 2.9 is now contrasted to the result of standard backprojection, for which no filter is applied to the sinogram.

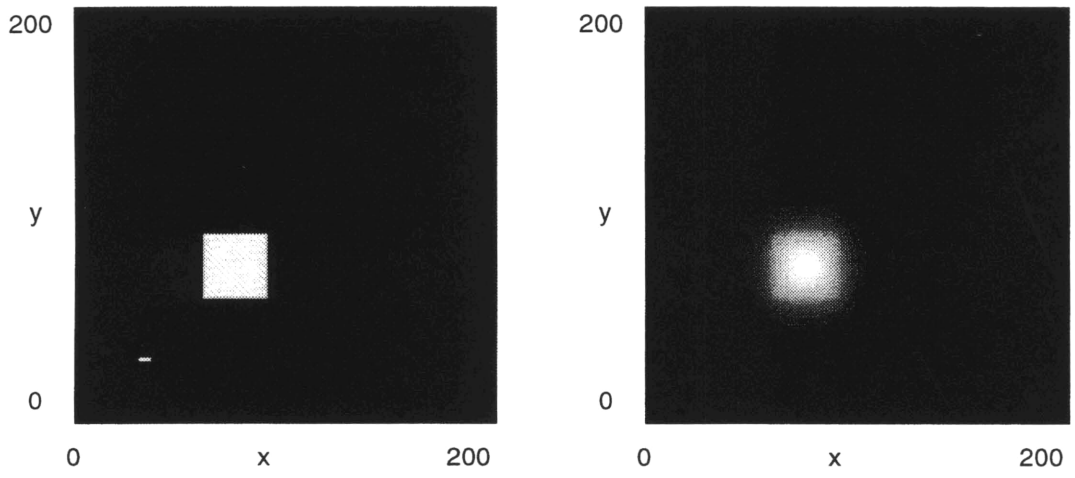

Figure 2.10. Filtered backprojection of a sample sinogram (left) and unfiltered backprojection of the same sinogram (right)

It is apparent that the $|w_z|$ filter described serves to compensate for the blurring effect apparent in the usage of unfiltered backprojection. This filter is appropriate if the region examined is sampled without noise and if the information one seeks to recover is bandwidth limited to less than half of the spatial sampling resolution. This is a result of the Nyquist sampling theorem [8], which states that in order to properly reconstruct a

continuous signal limited in bandwidth to a frequency Ω_{signal}, it must be sampled at a frequency equal to or greater than twice Ω_{signal}.

$$\text{Nyquist theorem: } \omega_{sampling} \geq 2 \cdot \Omega_{signal} \qquad \text{Eq. 2.18}$$

Other filters exist that should be used when these conditions are not met [7]. This is in general the case.

Now that the mathematical foundation of x-ray computed tomography has been presented, we will explore the issue of the optimal photon energy for our experiment.

2.4. Photon Energy Requirements

The goal of this experiment is to obtain a two-dimensional map of the density changes within an sample of liquid and solid aluminum. As we have seen, x-ray CT will yield a map of the linear attenuation coefficient of the object under examination. Because the mass attenuation coefficients μ_m of liquid and solid aluminum are the same, dividing $\mu(x,y)$ by $\mu_{m,Al}$ will result in $\rho(x,y)$, the quantity we are interested in.

A number of issues arise when one considers the fact that most x-ray sources are not monoenergetic and that the object imaged is not exclusively composed of aluminum. These conditions imply that the map of μ obtained by CT reconstruction will represent an average over all the energies present in the x-ray beam, as well as an average of the mass attenuation coefficients of the materials in the object under study. This is illustrated by the following equation.

$$p(z,\theta) = \int_{path} ds\rho(s) \int_{E_{\min}(s)}^{E_{\max}(s)} f(E',s)\mu_m(Z(s),E')dE' \qquad \text{Eq. 2.19}$$

where $f(E,s)=\left.\frac{dN}{dE}\right|_s$ is the energy distribution of the x-ray beam at the position s along the beam path. Indeed as an x-ray beam penetrates into a target, its spectrum changes due to the dependence in the interaction probability of a photon on its energy. Because lower energy photons have a higher attenuation coefficient, the lower end of the spectrum will tend to decrease in size with depth. This phenomenon is called *beam hardening*.

To reconcile Eq. 2.19 with Eq. 2.10, a solution is to choose the beam energy range so that μ_m remains independent of energy and material composition. Examining Figure 2.6 reveals that in the 1 to 3 MeV energy range these conditions are nearly satisfied. In this region, the mass attenuation coefficients of the variety of materials presented converge near 0.03-0.05 cm^2/g. In addition, the coefficients vary slowly with energy.

Assuming a mass attenuation coefficient of 0.04 cm^2/g for a photon energy in the range described above and considering an aluminum sample of density 2.7 g/cm^3, we calculate an attenuation coefficient of 0.11 cm^{-1}. To better understand this number, it is preferable to introduce the concept of the *half-value layer* (HVL). The HVL is defined as the thickness of target material that will diminish the intensity of a photon beam by a half. The relationship between the *HVL* and the attenuation coefficient μ is simple:

$$HVL = \frac{\ln 2}{\mu} \qquad \text{Eq. 2.20}$$

The half-value layer of aluminum for the case considered above is calculated to be equal to 6.4 cm. As we will see, this number is appropriate for a CT application in which the studied object is on the order of a few tens of centimeters in size, such as in this experiment.

These observations lead one to consider an x-ray source that will produce a beam the energy spectrum of which shows strong component between 1 and 3 MeV. The MINAC 6 linear accelerator is a source that meets these criteria, and is the topic of the next chapter.

3. X-RAY SOURCE: THE LINAC

As we have seen in Chapter 3, high-energy photons are an appropriate particle to use as a probe to measure the density fluctuations within an aluminum sample such as the one used in this experiment. There are several sources of such high energy photons, two of which are of particular interest. The first one is a radioactive source that emits gamma rays. The important characteristics of radioactive emitters are the following:

- the photons emitted are monoenergetic,
- the rate of emission follows an exponential decay which can be characterized by a half-life,
- the source cannot be turned off.

An example of such a source would be Cobalt-60 (Co^{60}), which emits two gamma-rays per disintegration, with energies of 1.17 and 1.33 MeV. The half-life of Co^{60} is 5.3 years, removing the concern with the exponential decrease in the source activity during an experiment that can arise with shorter half-lives. On the other hand, a long half-life translates into a smaller specific activity, which is equal to the activity per unit mass of the sample. The highest specific activities achievable today for Co^{60} are on the order of 200 Ci/g [9], where one Curie corresponds to 3.7×10^{10} disintegrations per second. As we will see further, these characteristics do not compare favorably with our second source of high energy photons, the linear accelerator.

3.1. Principles of the Linac

Traditionally, intense x-ray beams are produced using x-ray tubes. The photons are emitted when bombarding a target with high energy electrons. The electrons are produced by heating a thin filament surrounded by a cup-shaped cathode. As the electrons boil off the filament, they find themselves accelerated in a DC electric field towards an anode. The anode serves as the target for the bombardment, and is at an electric potential that is up to several hundred kilovolts greater than that of the cathode.

After acceleration, the electrons are nearly monoenergetic and carry an energy in electron-volts that is equal to the voltage applied between the cathode and anode. As the electrons impinge upon the target, they are slowed down through collisions with the electrons surrounding the atoms in the material, and are submitted to abrupt accelerations. As electromagnetic theory states, accelerating charged particles emit radiation. In the case of charged particles colliding with a target, the photons produced are called *bremsstrahlung* radiation. One property of this type of radiation is that it consists of photons that carry a spectrum of energies, the maximum of which is equal to the energy the electrons are accelerated to.

One drawback of traditional x-ray tubes is that the energy of the accelerated electrons is limited to a few hundred kilovolts because of the risks of arcing between the anode and the cathode. To reach higher energies, machines were developed that did not rely on DC electric fields for acceleration, but rather on radio-frequency (RF) alternating electromagnetic fields. These machines are linear accelerators (linac), and we will now describe the principles behind their operation, as well as the characteristics of bremsstrahlung radiation.

3.1.1. Electron Acceleration in Linacs

The contrast between linacs and x-ray tubes lies in the manner in which the electrons are accelerated. Linear accelerators are classified into two categories: traveling-wave accelerators, and standing-wave accelerators. Both are based upon a waveguide structure divided into sections separated by conducting discs. Pulses of electromagnetic radio-frequency fields are fed into this structure. In a traveling-wave accelerator, the wave travels only in one direction. In a standing-wave machine, two waves of equal amplitude travel in opposite directions, creating a standing pattern similar to that observed in vibrating strings. We will now discuss how the electric field patterns in both systems work to accelerate a fraction of the electrons to very high energies.

Electromagnetic fields travel at the speed of light c, equal to 3×10^{10} m/s. As a consequence, the wavelength λ is inversely proportional to the frequency ν of the wave following the relation:

$$\lambda = \frac{c}{\nu} \qquad \text{Eq. 3.1}$$

Let's consider a waveguide structure in which each section is separated by a quarter of a wavelength, λ/4. In the case of a traveling wave linac, we describe the evolution of the longitudinal component of the electric field in Figure 3.1.

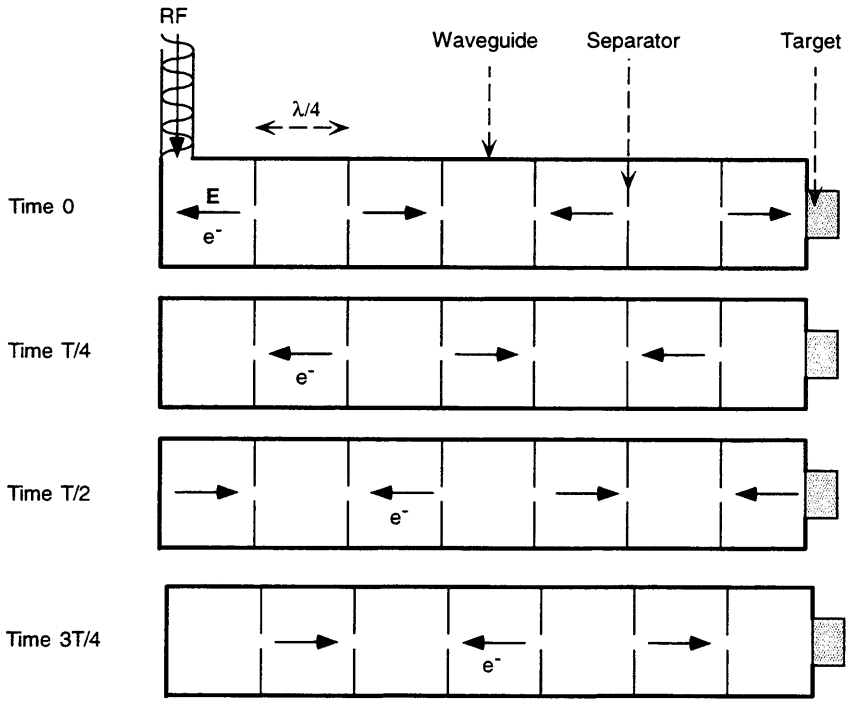

Figure 3.1. Time evolution of the longitudinal electric field in a traveling wave linac

In this illustration, time is expressed in terms of the period T equal to the inverse of the frequency, $1/\nu$. The arrows inside the waveguide indicate the direction in which the electric field points. In a quarter of a period, the wave propagates by a distance equal to λ/4. If electrons, represented by the symbol e^-, are injected into the waveguide at a velocity close to that of light, they will be accelerated over the entire length of the linac by the longitudinal component of the electric field $\mathbf{E}$. The acceleration scheme is slightly different in a standing wave linac, as illustrated in Figure 3.2.

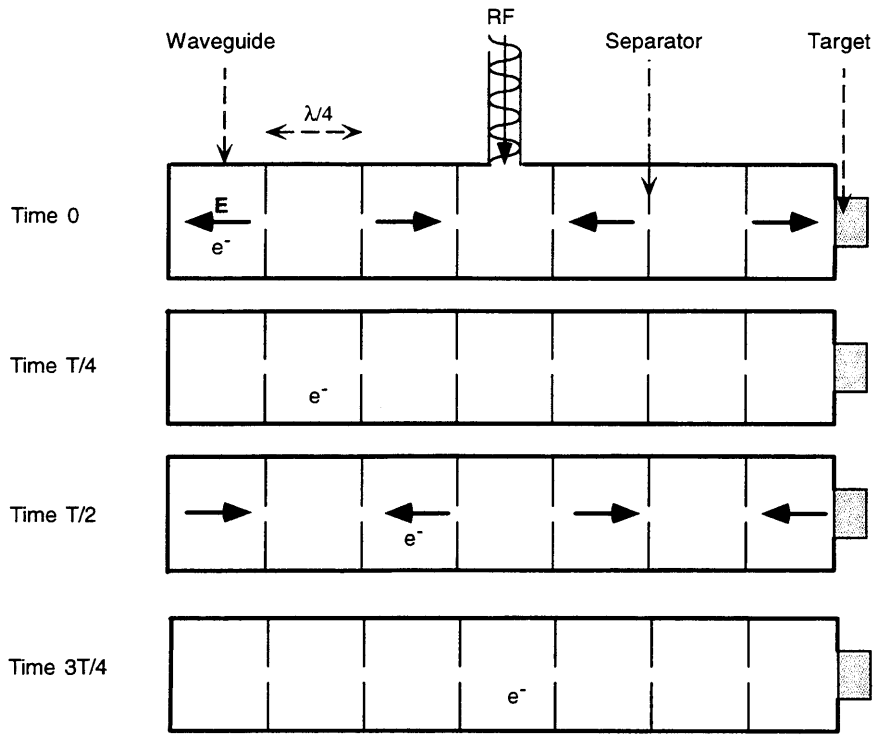

Figure 3.2. Time evolution of the longitudinal electric field in a standing wave linac

In the standing wave linac, two RF waves travel in opposite directions and either cancel or re-enforce each other. In contrast with the traveling wave accelerator, the electrons are accelerated half of the time. This loss is made up by the electric field which is twice as strong. The overall acceleration is equal in both standing wave and traveling wave linacs.

In the previous treatment, we assumed the electrons entered the accelerating structure at a velocity close to c. The velocity of a particle v is related to its kinetic energy T by the following relativistic formula:

$$T = m_0\left[\frac{1}{\sqrt{1-(v/c)^2}} - 1\right] \qquad \text{Eq. 3.2}$$

where m_0 is the rest mass of the particle. If the kinetic energy of an electron is equal to its rest mass m_0=0.511 MeV, one finds that $\beta=v/c$ is equal to 0.87, meaning that the electron travels at 87% of the speed of light. At energies of 1 MeV and above, our assumption that the velocity of the electron is constant is justified. At lower energies, the acceleration is achieved by making the initial waveguide cells shorter in length, so that the velocity of the electrons matches the phase velocity of the electromagnetic wave. In this way, the electrons that find themselves in phase with the accelerating portion of the longitudinal electric field receive energy from the RF field and can be accelerated in short distances.

The development of linacs was in great part possible because of the emergence of devices capable of creating strong pulses of RF radiation in the decimeter range and below. Such devices, magnetrons and klystrons, were invented to satisfy the requirements of radar during World War II [10] [11].

3.1.2. Bremsstrahlung Radiation

X-rays are produced by smashing the high energy electrons produced by either an x-ray tube or a linac into a target. Electrons lose their kinetic energy through two types of interactions. First, as they collide with the electronic cloud surrounding an nucleus, they can excite or ionize an atom. This results in the heating of the target and in the production of characteristic x-rays that are radiated as an electron drops into a lower energy level after excitation or ionization.

The second process occurs as an electron travels in the vicinity of a nucleus. Its trajectory bends significantly due to the electric attraction between the negative charge of the electron and the generally greater positive charge of the nucleus. The nucleus essentially remains in place during this interaction due to its rest mass which is three to five orders of magnitude greater than that of the electron. According to electromagnetic theory, as a charge accelerates, it emits radiation. An electron slowing down in the presence of a nucleus consequently emits *bremsstrahlung* ("braking radiation" in German) radiation. Depending on how much kinetic energy the electron loses, the radiation can consists of a photon carrying up to the full electron energy. In the thin target approximation, in which the target is considered thin enough that each electron will

at most collide once, the intensity of the emitted radiation is constant from zero to E, the electron kinetic energy [9]. One can extrapolate this result to a thick target by realizing that after each collision, an electron will emit bremsstrahlung radiation similar to that described above for the thin target, but with a maximum energy reduced to the electron energy after the first collision. By superposing all these individual thin target spectra, one obtains a thick target spectrum similar to the one shown in Figure 3.3.

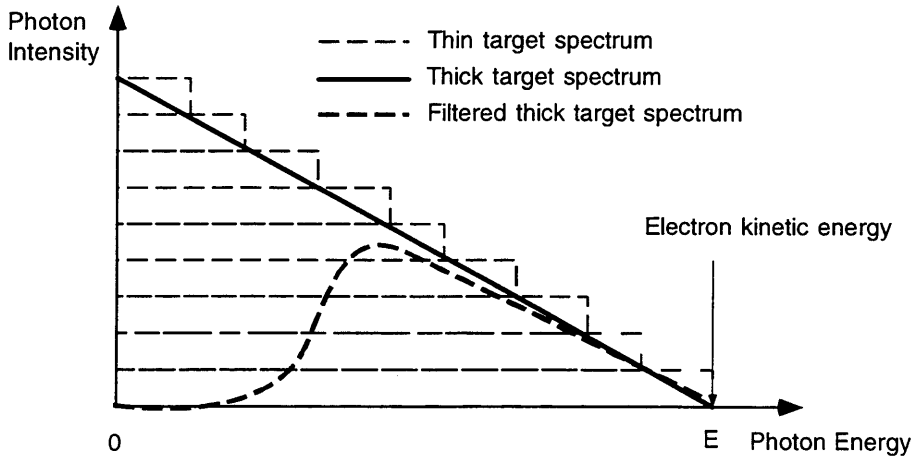

Figure 3.3. Thin and thick target bremsstrahlung spectra for an electron kinetic energy E.

Of course when photons travel through a thick target, they are attenuated via absorption and scatter. As seen in Section 3.2, low energy photons are absorbed more efficiently than higher energy radiation. As bremsstrahlung photons travel through the thick target, the low energy part of the spectrum is preferentially absorbed by the medium, resulting in a drop in intensity in the lower part of the spectrum. This is illustrated by the filtered thick target spectrum curve in Figure 3.3.

It is of interest to note that the ratio of the radiative (bremsstrahlung) to the collisional stopping power is given approximately equal by the following equation:

$$\frac{(-dE/dx)_{rad}}{(-dE/dx)_{col}} \cong \frac{ZE}{800} \qquad \text{Eq. 3.3}$$

Here *dE/dx* is equal to the energy loss rate of the electron over a distance *dx* along its travel path, *Z* is the atomic number of the target material, and *E* is the electron kinetic energy, expressed in MeV. This equation will prove useful in justifying the choice of tungsten as the target material for the production of x-rays in MINAC 6, which will be done in section 3.2.3.

3.2. Characteristics of MINAC 6

The MINAC 6 linear accelerator is manufactured by Schonberg Research Corporation, of Santa Clara, CA. We will examine its physical characteristics, its operating characteristics, and the type of x-ray beam it creates.

3.2.1. Physical Characteristics

The MINAC 6 accelerator consists of six components. Their name, dimensions and weight are described in Table 3.1.

Component name	Dimensions (l x w x h) [cm]	Weight
Modulator	89 x 51 x 58	181 kg
RF Unit	102 x 46 x 46	113 kg
X-Ray Head	69 x 10 x 18	41 kg
Water cooling system	66 x 53 x 97	145 kg
Control Console	64 x 51 x 28	18 kg
Remote Monitor and Interlock	36 x 38 x 33	11 kg

Table 3.1. Components of the MINAC 6 linear accelerator.

The various modules are interconnected as shown in Figure 3.4.

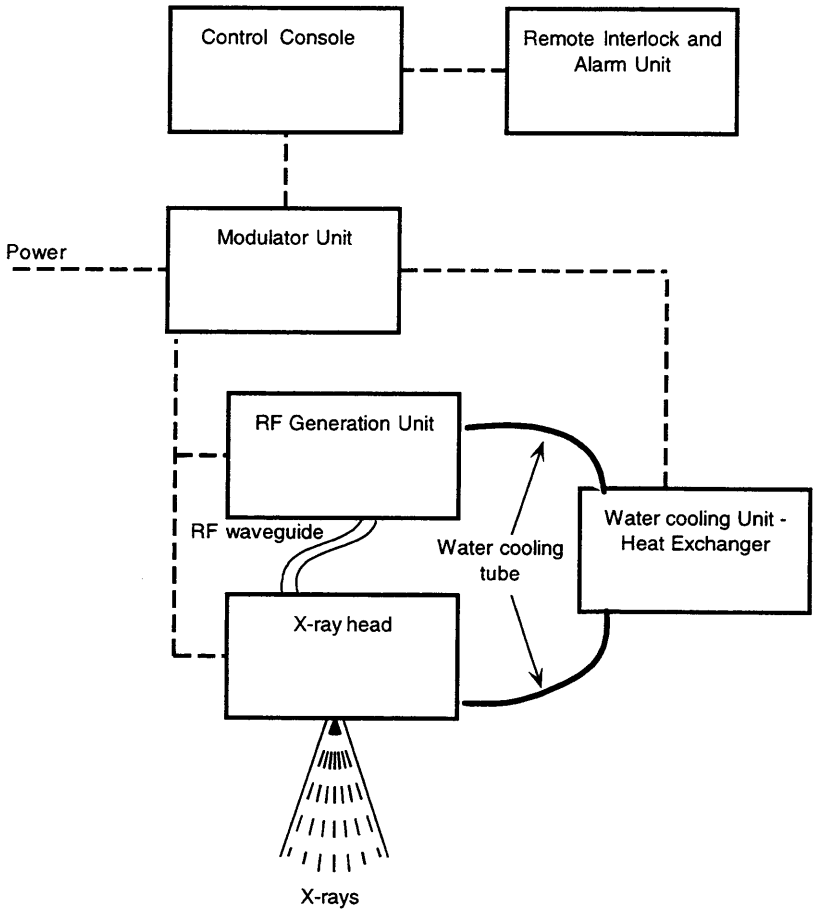

Figure 3.4. Diagram of the MINAC 6 components

3.2.2. Operating Characteristics

The modulator contains circuits that produce high voltage pulses used by the magnetron and the x-ray head. This assembly can produce pulses between rates of 50 and 200 pulses per second. Each pulse lasts 4 μs, with a rise and fall time of 0.5 μs

The RF unit contains the magnetron which produces pulses of radio-frequency radiation. It is driven by the high voltage pulses of the modulator. The radiation is produced in the X-band frequency, at exactly 9303 MHz. It is output via a flexible waveguide. The waveguide is filled with SF_6 (sulfur hexafluoride) gas to prevent arcing.

The x-ray head is responsible for accelerating electrons and producing bremsstrahlung x-rays. It includes an electron gun driven by the modulator's voltage pulses, a 52 cm long standing-wave accelerating section, a high-density tungsten target, and a collimator. The x-ray head receives the RF waves from the flexible waveguide via a side port. The electron current during a pulse is 50 mA, with an average current of 50 μA, corresponding to a 1000-to-1 duty factor. The electron gun is a triode-type gun, and injects 15 keV electrons into the accelerating section. Before colliding with the target, the electrons reach an energy of 6 MeV. The target itself is made of a thin sheet of tungsten. The x-rays produced are then restricted into a 30° cone by a tungsten collimator.

The MINAC 6 x-ray head is shown in Figure 3.5, where the collimator is visible as a metallic cylinder on the right. The center section, in white, is the housing for the RF coupling window and the connections for the water cooling tubes. On the left, one can distinguish the high voltage pulse plug.

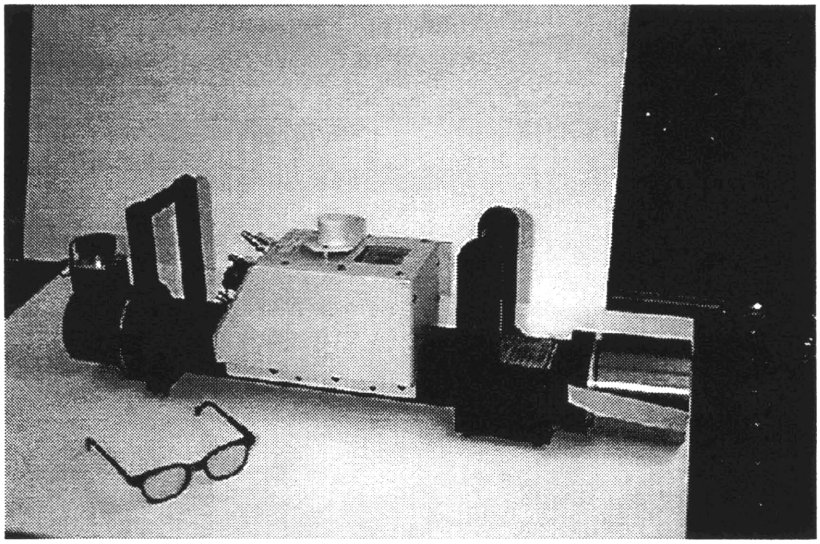

Figure 3.5. Photograph of the MINAC 6 x-ray head

The heat exchanger is a closed-loop water-cooling system that circulates water at 20°C through the RF module and the x-ray head to dissipate the heat produced by those units.

The control console is used to operate the linac and monitor its performance. It is equipped with readouts for the radiation output and the status of the accelerator. It also features a series of LED's that turn on in a sequence corresponding to the power-on procedure.

Finally, the remote interlock and alarm unit is designed to reside in the vault in which x-ray head is used. Prior to the emission of any radiation, a visual and audible alarm is given, warning any personnel that the beam is about to be turned on. A "panic button" is located on the unit, allowing anyone in the facility to power down the system and avoid exposure to harmful radiation in the case of an operational error.

3.2.3. X-Ray Beam Characteristics

The atomic number of tungsten is 74, and its density is 17.3 g/cm^3. Applying Eq. 3.3, one finds that for 6 MeV electrons 36% of the lost electron kinetic energy is used for the creation of bremsstrahlung x-rays. The high atomic number of tungsten is indeed a major reason for its choice as a target for the production of x-rays in most devices. Its high density contributes to keeping the electron paths short; this translates into a smaller spot size than obtainable with other materials. The MINAC 6 target consists of a 0.889 mm thick tungsten sheet welded to a .965 mm thick copper support. In addition a 1 mm thick lead sheet is added at the exit of the collimator. The collimator itself is made of tungsten because its high density translates into a large linear attenuation coefficient. The role of the collimator is to restrict the x-rays emitted by the target into a 30° cone. It is configured as a 9.5 cm long cylinder with a cone-shaped hole the aperture of which is 4.45 cm.

Using the geometry specified above as an input to a photon transport simulation program, one can compute the energy spectrum of the MINAC 6 x-ray beam. This was done using MCNP (Monte Carlo N-Particle Transport Code System) published by the Los Alamos National Laboratory, New Mexico. A total of 400,000 electrons were simulated. The x-ray energy flux was measured at a distance of 1 m away from the tungsten target, and integrated over an angle of 30°. Energy bins 50 keV wide where used to tally the

measured photons. The MCNP input code is given in Appendix A. The spectrum obtained is shown in Figure 3.6.

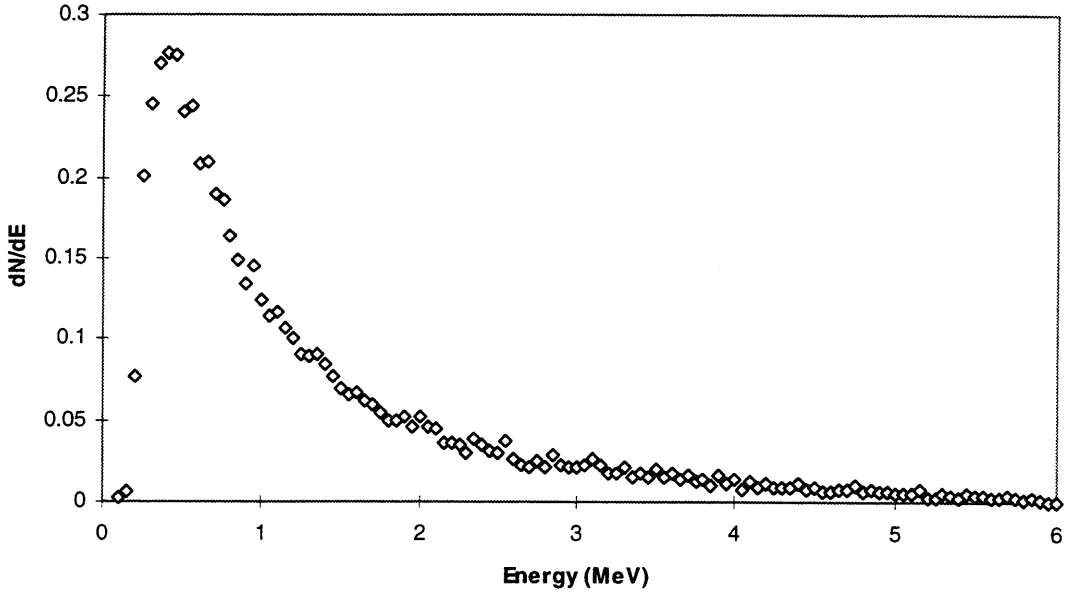

Figure 3.6. Calculated MINAC 6 photon number spectrum
dN/dE

This spectrum can be more easily compared with the type of result expected from section 3.1.2 if it is expressed in terms of intensity rather than photon number. This transformation is carried out by multiplying dN/dE by E. The resulting intensity spectrum is presented in Figure 3.7.

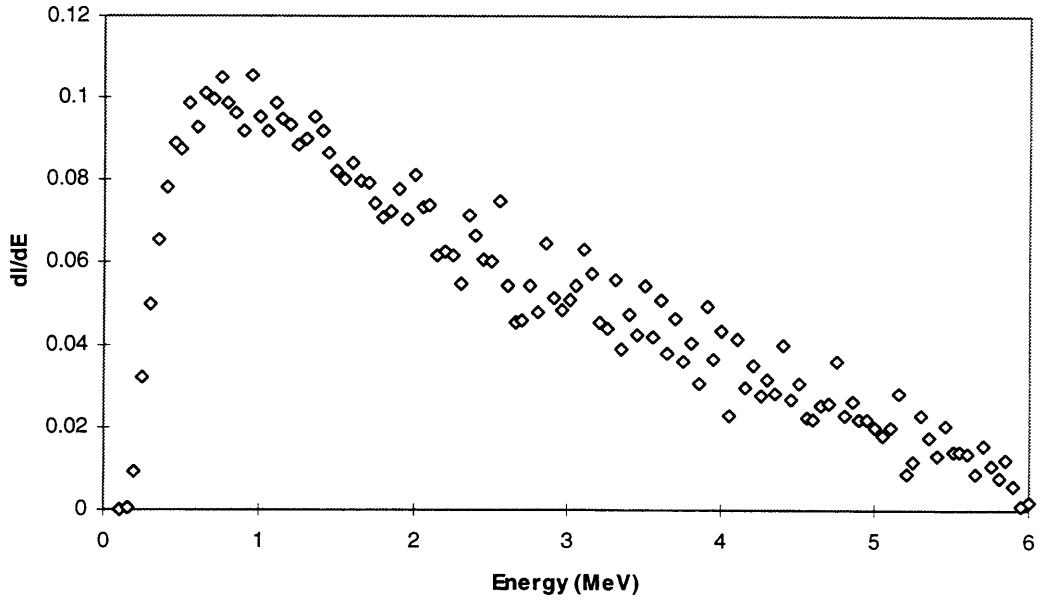

Figure 3.7. Calculated MINAC 6 photon intensity spectrum
dI/dE

As expected from theory, the photon intensity decreases linearly with energy. The drop in the low end of the spectrum is caused by the shielding effect of the lead sheet. Indeed, because the low energy photons are subjected to a greater linear attenuation coefficient, they are more easily stopped by the thin sheet. This is a manifestation of the beam hardening phenomenon discussed in section 2.4. As expected, no photons are observed above 6 MeV, the electron energy.

This spectrum can be used to calculate the average energy of the photons. The result was found to be 1.29 MeV. This number may appear low, but one must remember that as the beam progresses through the imaged object, the low end of the spectrum will be filtered out, leading to an increase of the average energy. Overall, the average energy of the beam will remain within the target range specified in section 2.4.

The MINAC 6 linac produces 300 R/min of ionizing x-rays. One Roentgen [R] is equivalent to a charge of 2.58×10^{-4} C created in a mass of one kilogram of air by ionizing photons. The average energy required to ionize an atom in air is equal to 34 eV. Because each ionization involves the creation of a charge of 1.6×10^{-19} C, the MINAC 6 output can

therefore be translated into an energy deposition rate of 2.7×10^{17} eV/kg/s, or 2.7×10^{8} MeV/g/s.

If we assume that this energy is deposited in a volume of area A and very small thickness Δx, we can calculate the photon flux ϕ traversing the volume using the following equation:

$$\Delta E_{deposited} = \phi \cdot A \cdot \overline{E} \cdot \overline{\mu}(A \cdot \Delta x)$$
$$\Leftrightarrow \phi = \frac{1}{\overline{E} \cdot \overline{\mu}_{m,air}} \cdot \frac{\Delta E}{(A \cdot \Delta x \cdot \rho_{air})} = \frac{1}{\overline{E} \cdot \overline{\mu}_{m,air}} \cdot \frac{\Delta E}{\Delta M} \qquad \text{Eq. 3.4}$$

where $\overline{E}$ is the average energy of the photons in the beam, $\overline{\mu}_{,m,air}$ is the average mass attenuation coefficient of air for energy deposition in the beam, and ΔM is the mass of the volume of air we consider. As established from the beam spectrum analysis, the average energy of the photons is $\overline{E}$=1.29 MeV. To determine $\overline{\mu}_{,m,air}$, we consider the following figure.

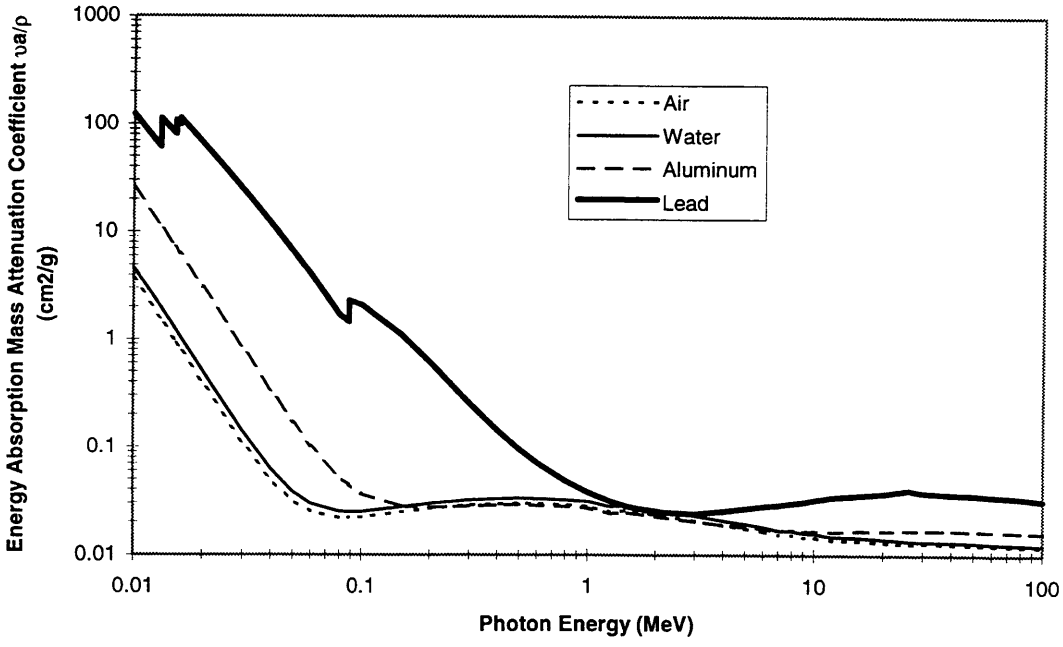

Figure 3.8. Energy absorption mass attenuation coefficient of a variety of materials for energies ranging from 10 keV to 100 MeV.

At an energy of 1.29 MeV, the mass attenuation coefficient of air for energy absorption is 0.025 cm^2/g. Using this value in Eq. 3.4, we obtain a photon flux equal to $\phi = 8.4 \times 10^9$ photons/cm^2/s.

This photon flux figure can be used to verify the validity of the Monte Carlo simulation used to obtain the spectrum. Its results indicate that the photon flux per electron at 1 meter is equal to 3.25×10^{-5} photons/electron/cm^2. Dividing the 50 μA electron output of MINAC 6 by the charge of the electron e, equal to 1.6×10^{-19} C, tells us that MINAC 6 produces 3.13×10^{14} electrons/s. Multiplying this number by the predicted photon flux per electron gives us the photon flux per unit time. The result, $\phi_{MCNP} = 1.02 \times 10^{10}$ photons/cm^2/s, is close to the figure obtained in the previous paragraph from the MINAC 6 specifications. This is a good indication that the Monte Carlo simulation's results are valid.

The determination of the x-ray properties of the MINAC 6 beam are essential to the characterization this experiment's performance. Before that step can be carried out, it is necessary to specify the properties of the aluminum sample we propose to image as well as those of the apparatus needed to create the stable solid/liquid phase transition. This is the topic of the next chapter.

4. SOLIDIFICATION FRONT

In computed tomography, the object imaged needs to be scanned through an angular range of at least 180°. For this reason, we need to have a system that will rotate an aluminum sample. Before we describe this system, the experimental setup of the sample is presented.

4.1. Furnace and Cooling System

A cylindrical furnace is used to create an aluminum sample in which a stable solid/liquid phase interface can be maintained. A schematic of the cross section of this furnace is shown in Figure 4.1.

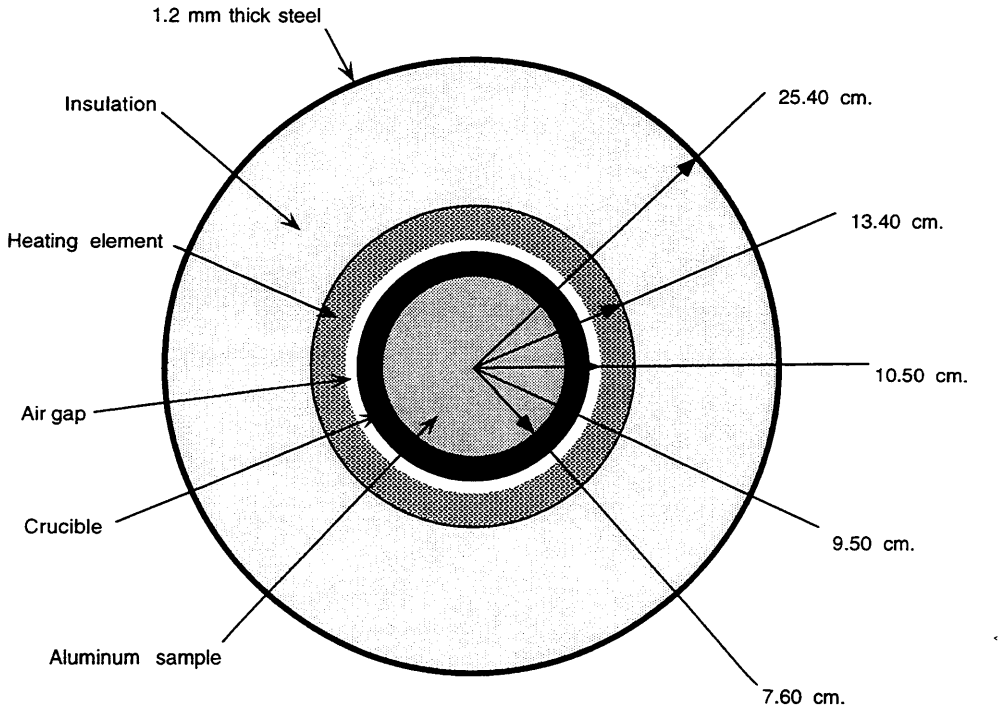

Figure 4.1. Cross sectional schematic of furnace with dimensions

This furnace is integrated into the experimental setup shown in Figure 4.2. This schematic shows a cylindrical furnace 16 inches high manufactured by Mellen, Webster, NH. At the core of the furnace is a cavity in which lies a graphite crucible. The crucible is heated by resistive heating elements placed around the perimeter of the cavity. These heating elements are in turn surrounded by low density insulation material. Finally the furnace is surrounded by a thin steel sheet to provide protection to the insulation. The following figure shows a cross sectional view of the furnace.

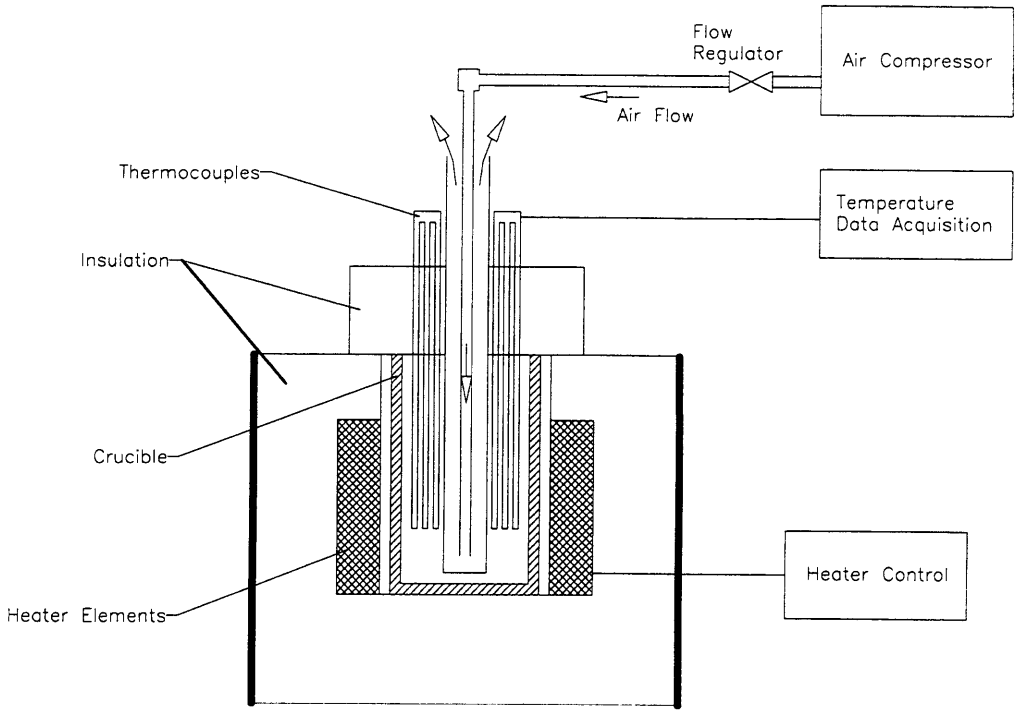

Figure 4.2. Schematic of the experimental setup for the creation of a liquid/solid interface in aluminum

The temperature of the air gap is measured by a built-in thermocouple. The furnace controller monitors this temperature and pulses current through the heating elements to regulate this temperature.

The cavity in the crucible is topped by an insulated cover. A cooling tube penetrates through the cover into the inside of the crucible. As compressed air flows down the inner core (OD of 1.59 cm) of the cooling tube and up the outer boundary (OD

An interesting feature of this experimental setup is its cylindrical symmetry. Because of it, the solidification front is also expected to show some radial symmetry, which should allow an improved analysis of the solidification front geometry.

4.2. Motion system

To allow the furnace to be rotated through any angular range, it is placed on a rotational table driven by stepping motor. The rotational stage itself is placed on top of a translational stage, which allows the furnace's position within the x-ray beam to be changed. The tables are manufactured by New England Affiliated Technologies, Lowell, MA. The stepping motors are controlled by an amplifier manufactured by Nulogic, Needham, MA.

5. DETECTOR SYSTEM

X-rays are an appropriate probe for computed tomography because they are a highly penetrating radiation. This very property makes them difficult to detect. As we will see, x-ray detection relies on sensitive measurements of the charge created by an x-ray photon as atoms become ionized. There are several methods to perform this measurement which we will explore in the following section. As will appear from this review, the combination of cadmium tungstate ($CdWO_4$) scintillation crystals and photodiodes is an appropriate choice for our application. Our experimental detection setup will be described, with particular attention focused on the issue of Compton scattered photons and means to reduce their contribution.

5.1. Principles of X-Ray Detection

The photoelectric effect, Compton scattering and pair production all lead in the end to ionization of atoms in the target material. The task is to find methods of measuring the extent of this ionization, and to detect it fast and efficiently. We will review the most widely used techniques used to achieve this, and will determine which characteristics are sought in an x-ray CT context.

5.1.1. Gas-filled Chambers

A very popular means of x-ray detection relies on a gas-filled chamber in which a strong electric field is generated. The basic principle behind the operation of such devices is the following. As radiation penetrates the volume inside the chamber, gas atoms and molecules ionize into separate electrons and heavy ions. An anode and a cathode connected to a voltage source cause a strong electric field to pervade within the volume, and because of their opposite charges, the electrons and ions diffuse towards the

plates. Eventually, their charge, and any charge created by their collisions with neutral molecules and atoms in the gas, are collected by the anode and cathode and a current is generated and measured. The information obtained from this type of detector depends on the strength of the applied electric field and its geometry. These are generally classified in the following categories:

- **Ionization Chambers:** The electric field is low enough that the electrons it accelerates do not ionize more atoms. As a consequence, the current measured is a direct consequence of the collection of the charge created by the x-rays. In general, this signal is small and requires careful amplification to measure.
- **Proportional Counters:** At a certain electric field threshold, the electrons produced by the ionizing radiation gain enough energy between collisions with neutrals to ionize them. The newly created charge is itself capable of ionizing more atoms, leading to the formation of an *avalanche* of charge. The result is a current that is proportional to the original energy deposition in the chamber, but is easier to measure.
- **Geiger-Mueller Counters:** As the electric field is increased, one avalanche process can lead to further avalanches, causing a current pulse of equal amplitude regardless of the amount of energy deposition.

5.1.2. Scintillation

Another means of quantifying the energy deposition of x-rays is to rely on the property of certain materials to emit visible light when excited. Two major types of scintillation materials exist: *organic* and *inorganic* scintillators.

Organic scintillators

These materials contain molecules with an electronic structure such as the one shown in Figure 5.1.

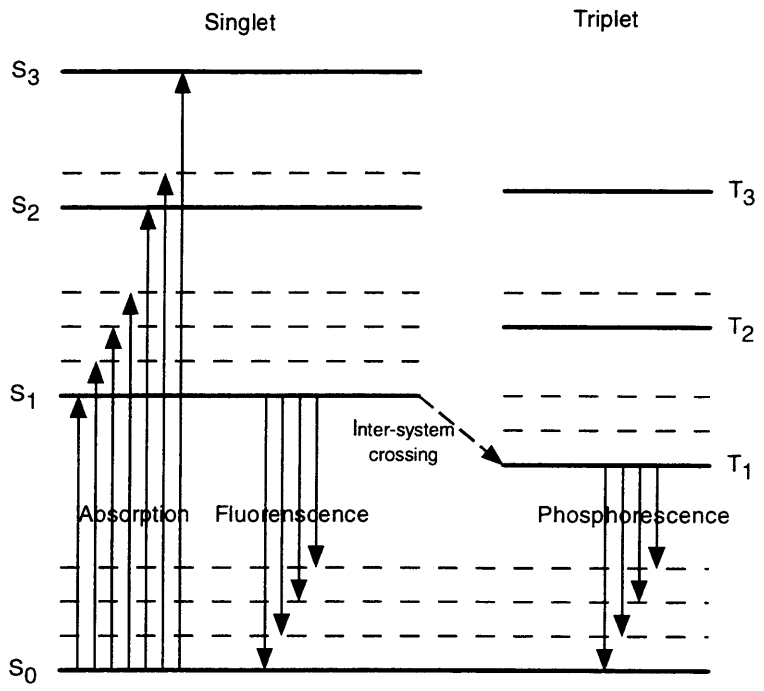

Figure 5.1. Energy levels of an organic molecule with π-electron structure [6]

The electrons produced by the x-rays transfer their kinetic energy to the molecules. This is represented as the absorption arrows. The excited singlet states quickly deexcite to the S_1 level, which is 3 to 4 eV above ground state. The transition from S_1 to S_0, which occurs in a few nanoseconds, is characterized by the emission of a visible photon, and the process is named *fluorescence*. Occasionally the system will transition from the S_1 state to the T_1 triplet state, which itself decays by *phosphorescence*. A molecule in T_1 state can be further excited back into S_1, resulting in a delayed fluorescence that can occur as much as 10^{-3} s after the main flash.

Inorganic scintillators

Most inorganic scintillators are crystals with an activator. This combination leads to an energy band structure similar to the one shown in the following figure.

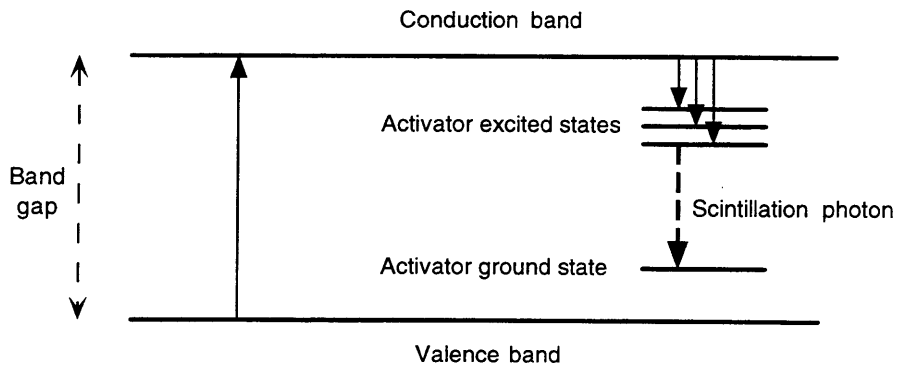

Figure 5.2. Energy band structure of a typical activated inorganic scintillation crystal [6]

As the electrons released by the x-ray interactions travel within the crystal, electron-hole pairs are created. The holes quickly migrate in the crystal lattice until they reach an activator site and leave it ionized. Meanwhile the electrons find themselves in the conduction band, where they travel. Eventually the electrons reach an activator site and drop into an excited state. The energy gap between these excited states and the activator ground state is such that a visible photon is emitted. Other processes compete with the one presented above and can lead to phosphorescence. These excited states decay at a much slower rate, causing light to be emitted long after the initial pulse. This phenomenon is called *afterglow*.

The most commonly used inorganic scintillation crystal is thallium iodide activated sodium iodide, NaI(Tl). Other inorganic scintillation materials exist that don't rely on the mechanism describe in Figure 5.2., and can exist in the gas phase.

Although the amount of visible light emitted by scintillation materials is proportional to the amount of energy deposited by x-rays, an important task remains to accurately measure the amount of visible light emitted. This is the topic of the following section.

5.1.3. Photomultiplier Tubes and Photodiodes

Measuring a signal involves translating it into an electric current. Two mechanisms are particularly useful to measure the visible photon output of scintillation materials in x-ray detection. These are the usage of *photomultiplier tubes* and *photodiodes*.

Photomultiplier tubes

A schematic of a typical photomultiplier tube is presented in Figure 5.3.

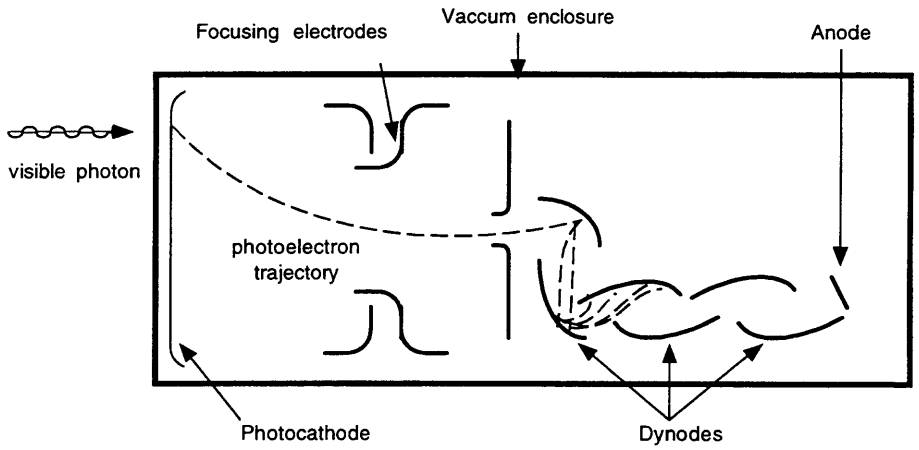

Figure 5.3. Schematic of a photomultiplier tube

The light emitted during the scintillation process impinges upon a photocathode. In response to this excitation, the photocathode emits a photoelectron. The number of electrons emitted per incoming photon is called the *quantum efficiency*. The electrons are accelerated towards a dynode, while being focused by electrodes. As a photoelectron collides with a dynode, its kinetic energy is transferred to other electrons. In turn these electrons are accelerated towards the next dynode, creating even more electrons in the process. By the time they reach the anode, the electrons form a measurable current that is proportional to the amount of light received by the photocathode.

Photodiodes

The operating principles of photodiodes is quite simple. An electric field is applied across a semiconductor material with a band gap of 1 to 2 eV. Visible photons, with energies of 3-4 eV, easily create electron-hole pairs in the lattice. These are then collected by the electrodes, so that a current is measured. This process does not involve any amplification. As a consequence signals are much smaller with photodiodes than with photomultiplier tubes. On the other hand, because of the lesser energy required to create a electron-hole pair compared to that needed to eject an electron in a photocathode, the quantum efficiency of photodiodes is greater than that of a photomultiplier tube.

5.1.4. X-ray detection for CT

Because in computed tomography we are mainly interested in the beam intensity at a certain location, it is important to obtain a signal proportional to the x-ray energy deposited. For this reason G-M counters cannot be considered. Because the contribution of individual photons need not be distinguished, and because the photon flux in CT is typically high, detection systems that do not amplify the charge created by ionizing radiation may be appropriate.

As we have seen in section 2.2, the linear attenuation coefficient of x-rays is proportional to the density of the target material. For this reason it is preferable to choose a high-density detector. This requirement rules out the usage of non-pressurized gas-filled systems. In fact it is a strong justification for the employment of high-density scintillation crystals for x-ray CT.

Another argument in favor of scintillation crystals is the flexibility in shaping them and obtaining them in a small size. Indeed using a thin detector allows one to increase the number of x-ray beam paths that can be monitored. Because of their bulky size, photomultiplier tubes do not combine well with small scintillation crystals. For this reason and because of their greater quantum efficiency, photodiodes appear to be the a good counterpart to scintillation crystals in CT.

From this discussion it was established that the best x-ray detection system for computed tomography is a combination of a high-density scintillation crystal with a photodiode. Because one wishes to acquire attenuation data as fast as possible, the afterglow of the scintillation crystal must be chosen to decay fast in order to avoid contaminating a signal with light emitted from a previous measurement.

5.2. Experimental Detection System

The x-ray detection system for this experiment is provided by Analogic Corporation, Peabody, MA. It consists of an array of 384 scintillation crystal - photodiode pairs placed around an arc spanning an angular range of 48°, corresponding to 0.125° per channel. The radius of the arc is 84.5 cm. The scintillation crystal used, cadmium tungstate ($CdWO_4$), is inorganic. Each crystal is 2 cm high, 1.8 mm wide and 3 mm deep. The properties of $CdWO_4$ are contrasted with those of NaI(Tl) in the following table:

	NaI(Tl)	$CdWO_4$
Density [g/cm^3]	3.67	7.9
Melting Point [K]	924	1598
Wavelength of maximum emission [nm]	415	470/540
Primary Decay Time [μs]	0.23	20/5
Afterglow [%]	0.3 after 6ms	0.1 after 3 ms
Light Yield [photons/MeV γ]	$3.8x10^4$	$1.2\text{-}1.5x10^4$

Table 5.1. Physical properties of NaI(Tl) and $CdWO_4$

The afterglow of cadmium tungstate decays quickly, making it appropriate for CT usage. Its light yield is three times lower than that of sodium iodide, but this is in part compensated by the higher wavelengths of photon emission which in general are more efficiently measured by photodiodes than with photocathodes.

The density of cadmium tungstate is 7.9 g/cm^3, making it particularly efficient at stopping x-rays. The energy absorption coefficient μ_a of this material for 1.29 MeV x-rays is equal to 0.204 cm^{-1}. The energy deposition efficiency of the crystals can be calculated:

$$\eta_E = 1 - e^{-\mu_a \cdot t} \qquad \text{Eq. 5.1}$$

where t is the thickness of a crystal. Using the information given above, we find η_e = 5.9%. This efficiency is not very good and could easily be improved by making the scintillation crystal thicker. The crystal's shallowness is due to the fact this detector system is designed primarily for medical CT, where x-ray energies on the order of 100 keV are used. $CdWO_4$ crystals exhibit to some extent a tendency to absorb the visible photons emitted during scintillation. This *self-absorption* phenomenon limits the thickness $CdWO_4$ crystals to 3 cm; the energy deposition efficiency of such crystals is on the order of 45 %.

5.3. Scatter and Collimation

5.3.1. Detector Angular Sensitivity Characterization

As we explained in section 2.2, Compton scattered photons are a concern because they contribute signal to the detectors. These are not capable of distinguishing the contribution of scattered photons from that of unscattered ones. Because their depth is greater than their width, the crystals are inherently more sensitive at measuring photons coming from the focus point. Compton scattered photons can arrive from any point within the studied object, so that they will not be detected as efficiently as unscattered photons. To improve upon this quality, the system also includes a system of anti-scatter plates. These plates are made of tungsten to effectively attenuate x-rays. They are placed in front of every other crystal and extend towards the focus point as shown in Figure 5.4.

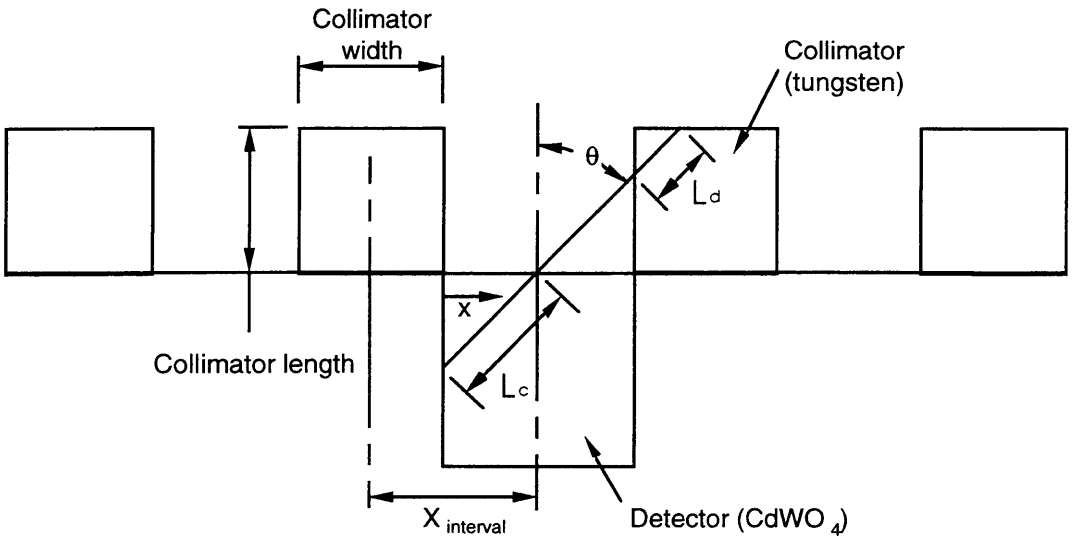

Figure 5.4. Collimator and crystal geometry

After traveling through a collimator plate for a distance L_d, an x-ray impinges upon a scintillation crystal at an angle θ from the vertical. It then travels through the crystal for a distance L_c. The energy deposition efficiency for this x-ray is dependent upon θ, and is given by:

$$\eta_E(\theta) = e^{-\mu_c L_c(\theta)} \cdot \left(1 - e^{-\mu_{dc} L_d(\theta)}\right) \qquad \text{Eq. 5.2}$$

where μ_c and μ_d are the linear attenuation coefficients of the collimator and the detector material respectively. When designing a collimator/detector system, one can vary a number of parameters, including the scintillation crystal depth, the collimator width and the collimator length. The function $\eta_e(\theta)$ was evaluated numerically for a number of different parameter configurations. A baseline function was computed using a detector width of 1.5 mm, a crystal thickness of 3 mm, a collimator width of 0.5 mm and a collimator depth of 40 mm. The following figures shows how this baseline (dotted) changes when the crystal thickness is increased to 25 mm; when the collimator width is increased to 2 mm; when the collimator length increased to 100 mm; and when all these

changes are applied at the same time. In each calculation, 100 collimators are included on either side of the detector crystal.

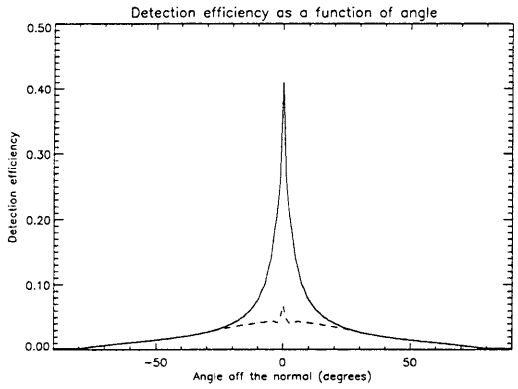

a. Crystal thickness: 3 to 25 mm

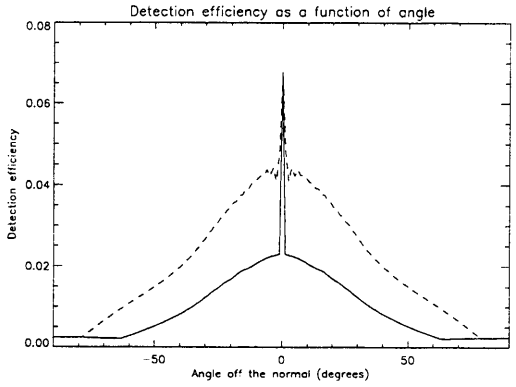

c. Collimator length: 4 to 10 cm

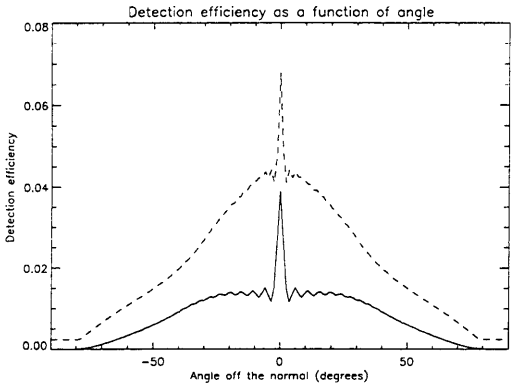

b. Collimator width: 0.5 to 2 mm

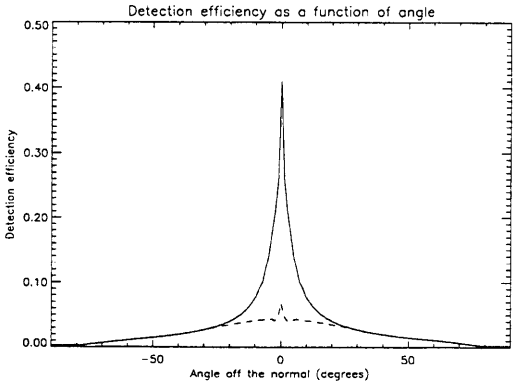

d. Combination of a, b and c

Figure 5.5. Sensitivity of detector systems as a function of the x-ray incidence angle

As expected, increasing the crystal thickness dramatically improves efficiency and also increases the ratio of unscattered to scattered photon detected. Increasing the collimator width also achieves this result, but at the detriment of overall efficiency. Indeed increasing the width of the anti-scatter plates decreases the geometrical efficiency of the system by reducing the fraction of useful detection surface. Finally, increasing the collimator length does not affect the detection efficiency of unscattered photons, but

significantly decreases the system's efficiency at detecting photons arriving at $\theta \neq 0°$. Combining all three techniques yields a tremendously improved $\eta_e(\theta)$.

Because of the ease of using the crystals in their original dimensions, using deeper ones is not considered for the immediate execution of this experiment. The collimator plates were chosen to be as long as possible, the limiting factor being the presence of the furnace to be imaged. Their length is 8cm. Finally the thickness of the collimator plates is chosen to be the same as that of the scintillation crystals, i.e. 1.8mm. Although this reduces the number of usable detection channels by a half, it is a necessary decision as the next section will illustrate.

5.3.2. Scatter Discrimination Properties

The contrast of in the measurement of the linear attenuation coefficient μ_{object} in an object is equal to:

$$Contrast = \frac{\left|\mu_{object} - \mu_{background}\right|}{\mu_{background}} \qquad \text{Eq. 5.3}$$

where $\mu_{background}$ is the linear attenuation coefficient of the medium the object lies in. Recall that μ is determined using equation Eq. 2.11. In the presence of many scattered photons, the intensity I measured by the detectors increases while the intensity emitted by the source I_0 remains unchanged. As a consequence because of the detection of Compton scattered photons, linear attenuation will tend to be underestimated. As Eq. 5.3 shows, this translates into a loss of contrast.

To determine whether the detection system is designed to successfully eliminate the risk of contrast reduction due to scattered x-rays, a Monte-Carlo simulation was executed. The geometry of the problem includes a source of x-rays with the spectrum characteristics shown in Figure 3.6. The furnace, the crucible and the aluminum sample are included in the problem. Also included are 383 $CdWO_4$ crystals of dimensions equal

to those of the Analogic detector system. A point source of x-rays emits a beam that is aimed at the detector at the center of the array, and distributes photons over its surface uniformly. The photons traverses the center of the furnace, and have the same spectral characteristics as MINAC 6's beam. MCNP is used to measure the energy deposited per emitted photon into each of the detectors. Because the beam is only aimed at the center detector, any photons that land into the other crystals must have originated from a Compton scattering event. The geometry can also include scatter plates of any size, material and density. For this application, we chose to compare the scatter characteristics of the detection system without any anti-scatter plates to its properties in the presence of the anti-scatter plates specified in the previous section. Finally we added a layer of lead above and below the detectors and scatter plates if present. This layer is in the shape of an arc centered on the source, spanning 48°, with an inner radius of 76.5 cm and an outer diameter of 86.6 cm. The lead thickness is 5.1 cm. In each simulation, 5 million photons were simulated. A sample MCNP input file is given in Appendix B. A ray-traced image of the furnace and detection system geometry is shown in Figure 5.6.

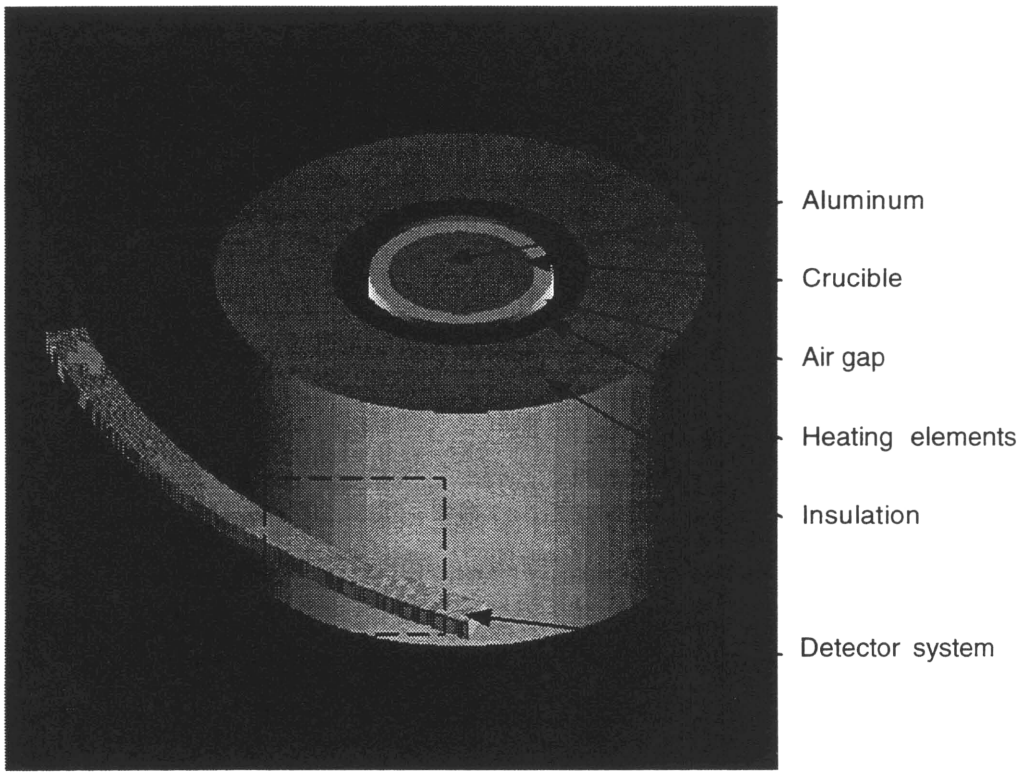

Figure 5.6. Ray-traced image of the MCNP model used to calculated scatter functions. The square represents the detail shown in Figure 5.7.

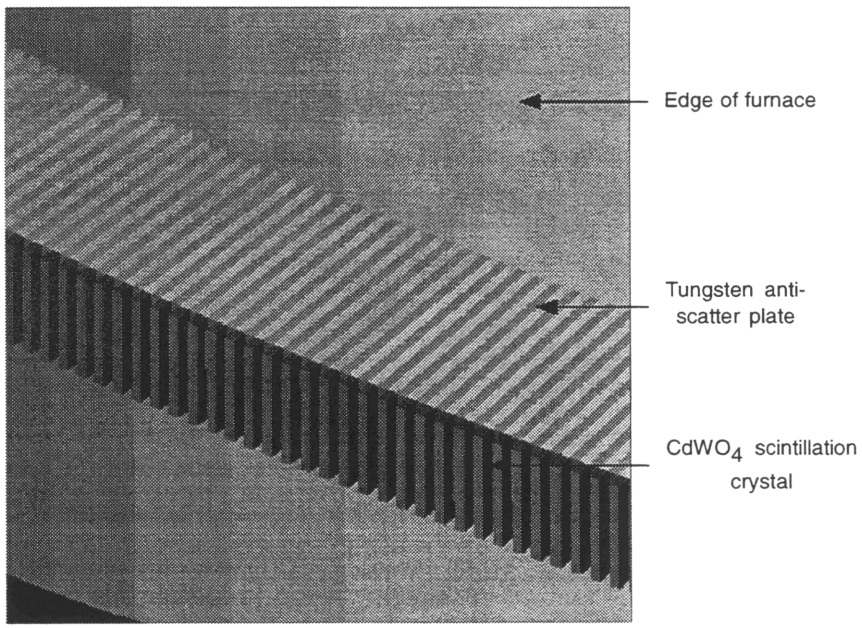

Figure 5.7. Detail of the MCNP model used to calculate the scatter functions.

The result of the Monte Carlo simulation is a function of the detector index. The detector index is chosen to range from -191 to 191, so that the center detector is at index 0. From this point on, this function will be referred to as a *scatter function*. It is shown in Figure 5.8 for the case when no anti-scatter plates are used.

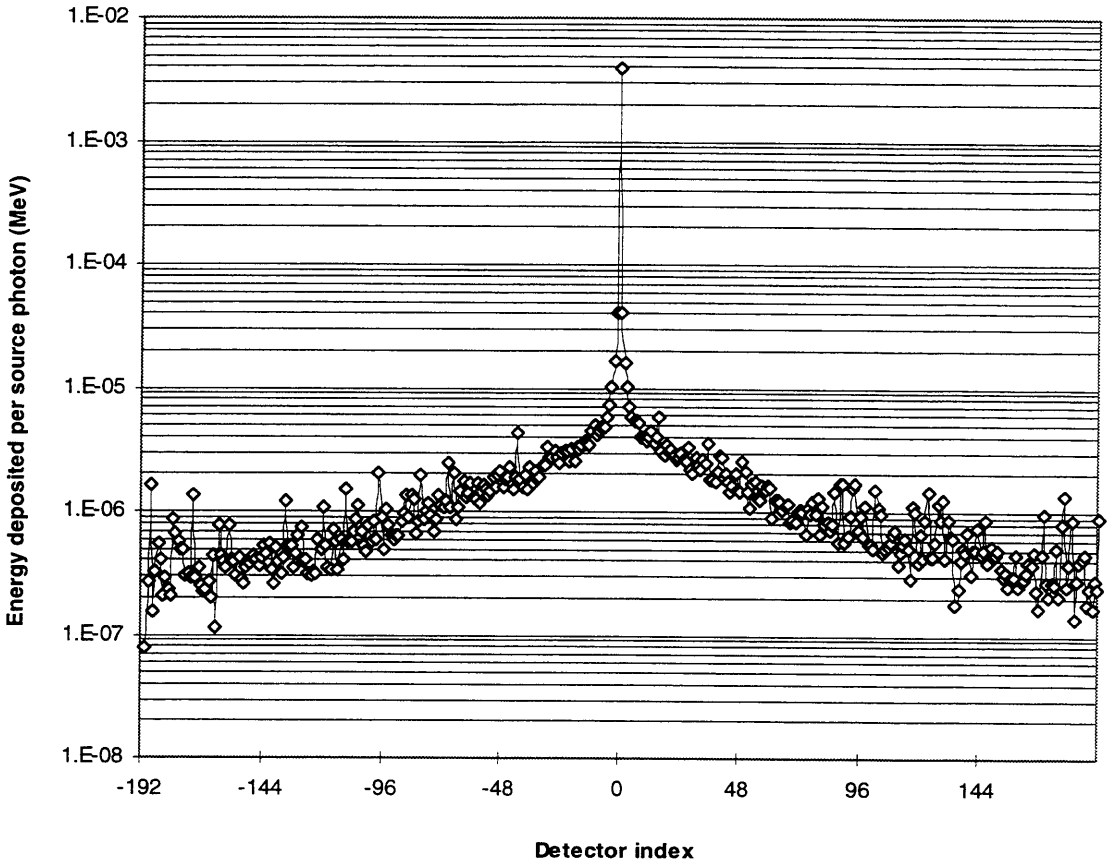

Figure 5.8. Scatter function of the detector system without collimation

As expected, a strong peak appears at the center, where the beam is directed. As one moves off center, the energy deposition profile drops sharply. The increasing jaggedness of the curve as the detector index increases is due to the smaller number of x-rays that are collected. This effect is one of *quantum noise*.

The scatter function was also calculated with the anti-scatter plate assembly taken into account. The results are shown in the next figure.

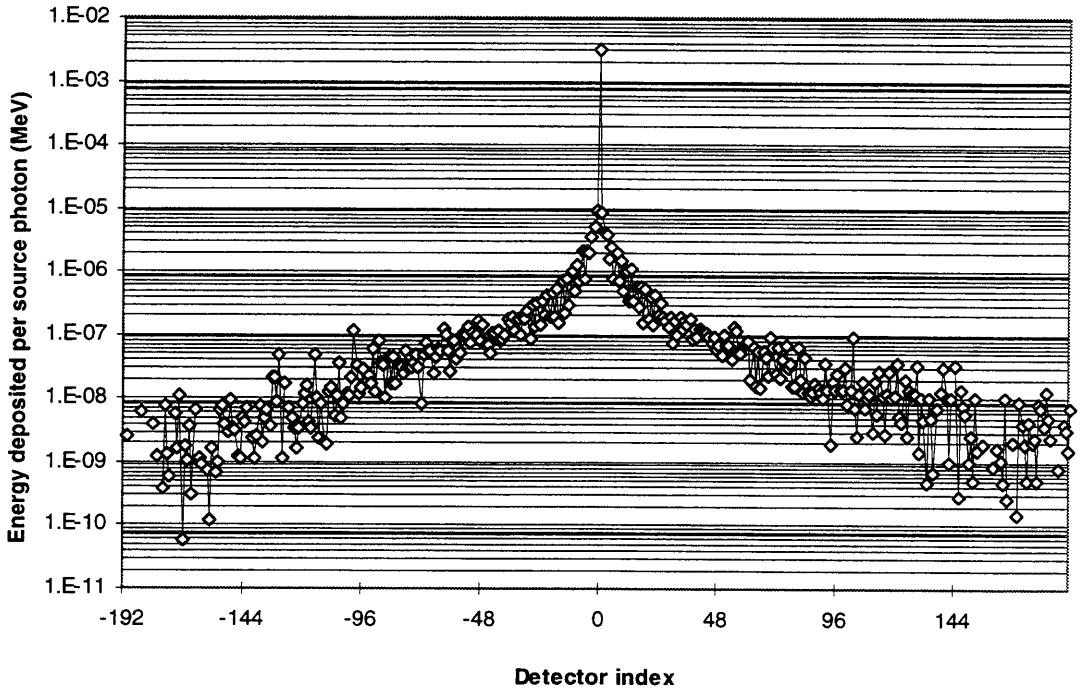

Figure 5.9. Scatter function of the detector system with collimation

This data is important in that it can be used to estimate how much of the signal measured by a crystal is attributable to unscattered photons, and how much is attributable to Compton scattered photons. A reasonable assumption is to equate the energy deposited into detector 1 from a beam aimed at detector 0 to the energy deposited in detector 0 from a beam aimed at detector 1. If we adopt the nomenclature that $E_{i,j}$ is equal to the energy deposited in detector j by a beam aimed at detector i, the previous statement is equivalent to the following expression:

$$E_{i,j} = E_{j,i} \qquad \text{Eq. 5.4}$$

The scatter functions calculated are equal to $E_{0,j}$. Because the worst case of scatter is going to occur when the beam traverses the center of the furnace, we can further qualify Eq. 5.4 by stating the following:

$$E_{i,0} \leq E_{0,i} \qquad \text{Eq. 5.5}$$

We can now place an upper limit on the energy $E_{scattered}$ deposited in detector 0 due to contributions from all other beam fragments not directly focused on it:

$$E_{scattered} \leq \sum_{i \neq 0} E_{i,0} \qquad \text{Eq. 5.6}$$

Because the MINAC 6 beam is limited to 30°, we only need to consider indices the absolute value of which is lower than 120.

Evaluating $E_{i,0}$ is a simple task in the case of the scatter function that does not involve collimators. When one considers the collimated scatter functions, Eq. 5.4 does not hold true because the scatter function $E'_{0,i}$ of a beam impinging directly onto a scatter plate is different than the function $E''_{0,I}$ of a beam that does not directly hit a plate, such as the one depicted in Figure 5.9. Equation Eq. 5.5 can be reformulated for such cases as:

$$E_{i,0} \leq \begin{cases} E'_{0,i} \text{ if } i \text{ is even} \\ E''_{0,i} \text{ if } i \text{ is odd} \end{cases} \qquad \text{Eq. 5.7}$$

Figure 5.10 shows the function $E_{0,j}$ for both non-collimated and collimated detector arrays.

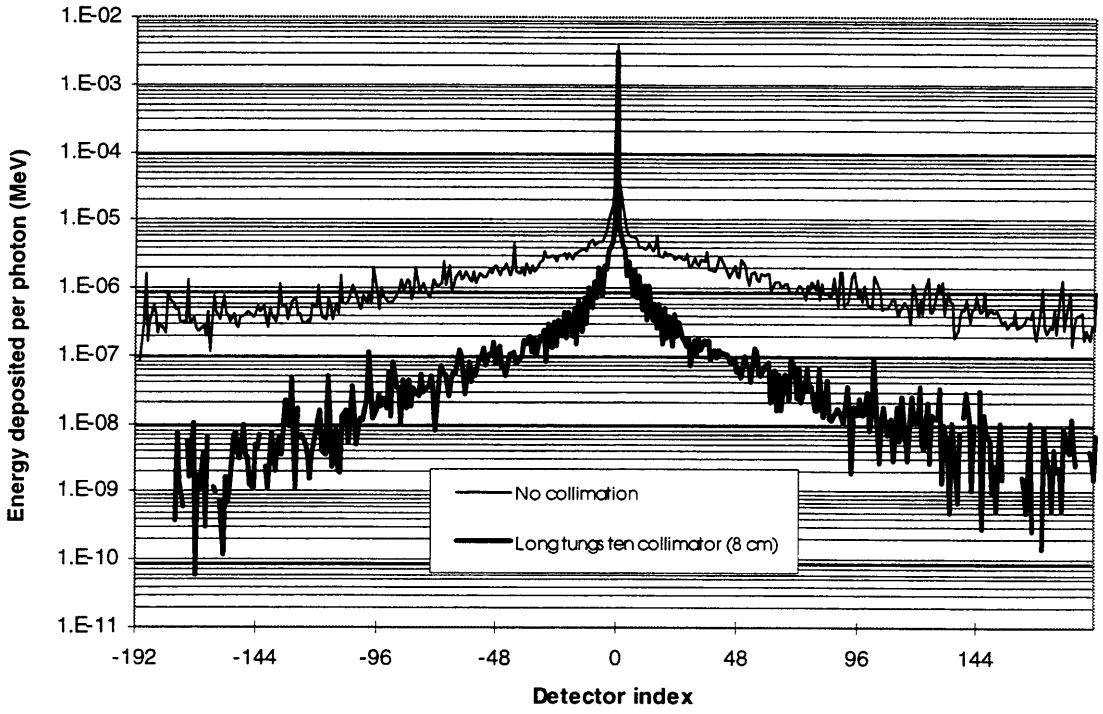

Figure 5.10. $E_{0,j}$ scatter function for non-collimated and collimated detectors

This figure is a striking example of the ability of the scatter plates to significantly reduce the scatter detected at the center detector while preserving the unscattered signal. To obtain a quantitative grip of this issue, we introduce the concept of *unscattered to scattered ratio (U/S)*, defined in Eq. 5.8.

$$U/S = \frac{E_{0,0}}{E_{scattered}} \qquad \text{Eq. 5.8}$$

This ratio was evaluated for both the uncollimated and the collimated scenarios. The result were found to be 6.2 and 40.7 respectively. This result shows that the collimation system specified in section 5.3.1 is effective at solving the problem of Compton scattered photons reducing the contrast of the signal.

6. FACILITY DESIGN

We now review the general design characteristics of the tomographic system, as well as the radiation shielding issues important for the safety of the operators.

6.1. Experiment Layout

Because the 30° fan beam does not cover the entire area of the furnace, the system cannot create an image by scanning only 180°. To overcome this limitation, one can limit the beam to half of the object, subsequently performing two 180° scans to obtain a complete sinogram that can be used for traditional tomographic reconstruction.

This method of collecting the data is an attractive one, and as we will see it imposes stringent restrictions on the positioning of the furnace within the beam. If the furnace is placed against the anti-scatter plates, its center is 51 cm away from the x-ray source. Assuming one edge of the beam traverses the center of the furnace, the other edge will fall exactly at the perimeter of the furnace. This implies that there is no freedom in the choice of the position of the object. Figure 6.1 is a schematic of the layout of the experiment, taking into account the requirement stated above. It shows the accelerator head, furnace and detector array placed on a 122cm x 244cm precision table.

After the beam travels through the furnace, it is stopped by a 30.5 cm deep beam stopper made of lead. The beam stopper is designed to be re-entrant, so that radiation scattered off its surface is intercepted. It is part of the shielding design of the facility, which we will investigate in the next section.

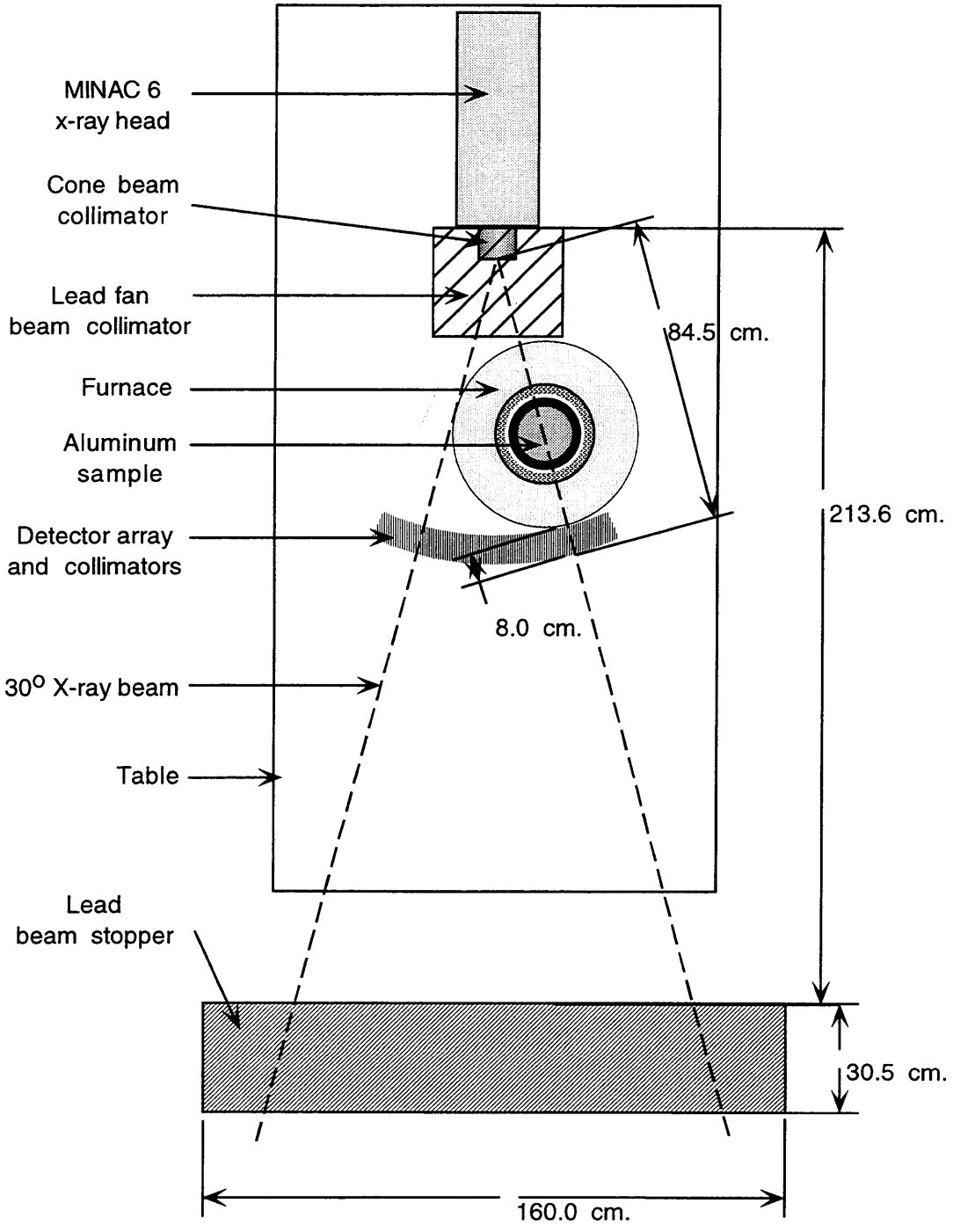

Figure 6.1. CastScan experiment layout

6.2. Shielding and Room Design

The layout of the shielded room is shown in Figure 6.2.

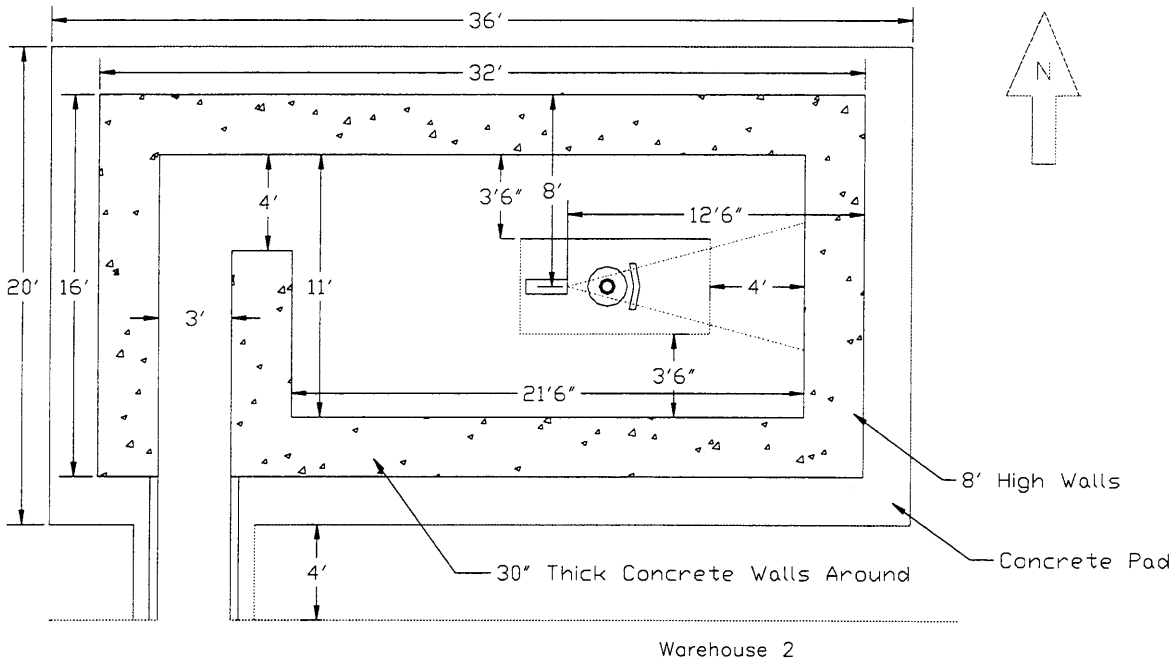

Figure 6.2. Shielded room layout

The shielded room is equipped with 30 inch concrete walls. Its entrance follows a *maze* pattern, allowing for an open design where it is impossible to be outside the room and in the line of sight of the beam or its scatter. A re-entrant beam stopper in the forward direction attenuates the primary beam from the accelerator. This beam stop is constructed of lead and has a thickness of 30.5 cm. In this setup, there are two areas of concern for radiation dose levels: the radiation on the beam axis and the radiation scattered off the object.

The MINAC 6 accelerator emits radiation at a rate of 300 R/min (18,000 R/hr) at 1 meter. In addition, it was measured experimentally that the dose rate at a distance of one meter from a 30 x 30 x 20 cm steel block, and at an angle of 90° from the beam axis, was 3 R/min. This dose is due to both the radiation scattered off the object and the radiation leaked from the accelerator. To eliminate the leakage radiation, the accelerator

x-ray head is surrounded by a 30 cm thick lead shield. The spectrum of the scattered radiation was calculated using MCNP. The primary and scattered beam spectra were fed into the computer code Photcoef to calculate attenuation curves for both lead and concrete. These curves include the buildup of photons due to the contribution of photons scattered back into the beam, and are shown in Figure 6.3.

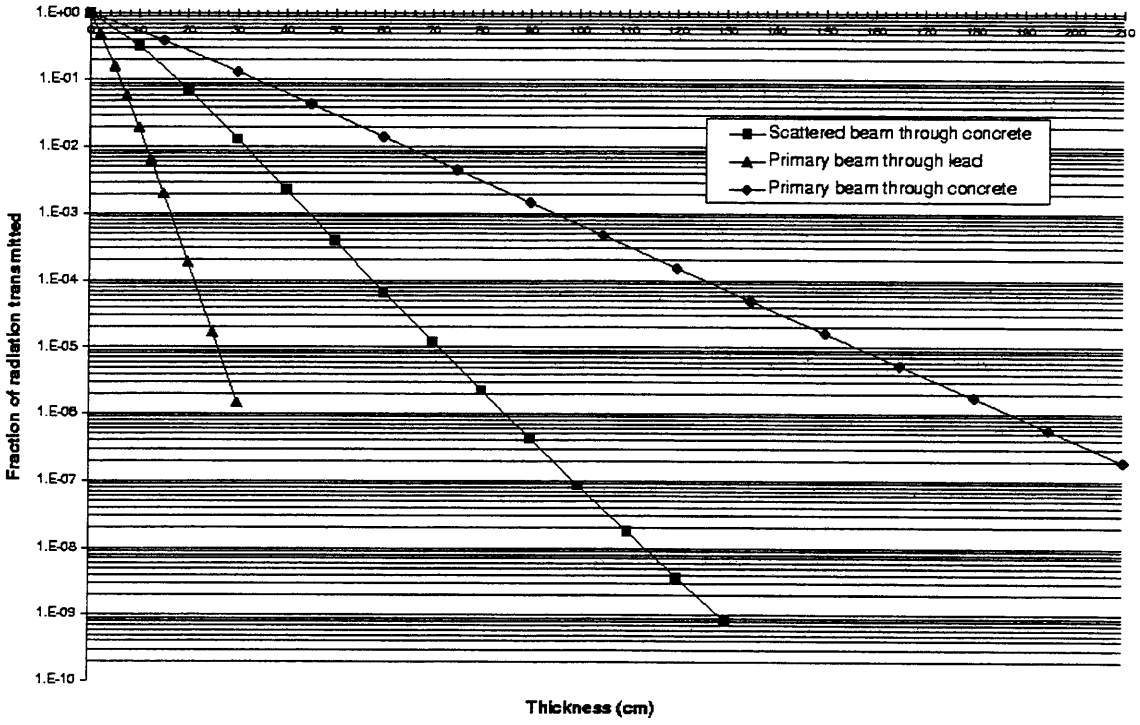

Figure 6.3. Attenuation curves through lead and concrete
for the MINAC 6 primary and scattered beams

According to these calculations, the primary beam stopper will cause the radiation to be reduced by a factor of at least $2x10^{-6}$. The concrete wall will attenuate the primary beam by an additional factor of $4x10^{-3}$. According to NCRP Report No. 51 [12], these attenuation factors are $3x10^{-6}$ and $4x10^{-3}$ respectively. Using the more conservative NCRP numbers, we estimate that the overall attenuation factor for the primary beam to be of at least $1.2x10^{-8}$. The distance from the source to the closest outside wall is approximately 3.5 meters. Taking into account attenuation and the inverse square decline in dose rate with distance, the expected dose rate outside the shielded facility due to the primary beam (300 R/min at 1 m) is at most .02 mR/hr.

In addition we need to consider the dose due to radiation scattered off the object under study. The expected attenuation from the 30 inch concrete wall for this spectrum is $5x10^{-6}$. The minimum distance from the object to the exterior of the shielded facility is 2.4 meters. The 3 R/min dose rate at one meter from the object should therefore be reduced to 0.16 mR/hr.

As a final check of these values, and to estimate the amount of radiation present at the entrance of the maze section of the facility, an MCNP simulation was carried out. This simulation accounted for the 30 degree cone beam emitting a photon spectrum such as the one expected from MINAC 6. Other inputs to the simulation included a lead collimator to limit the beam to a fan, the furnace that will be imaged, and the beam stopper. In addition, the room walls, ceiling and floor were accounted for. Dose rates were estimated in three different volumes. First, the energy deposited in a small volume placed inside the beam at one meter was used as a reference, corresponding to the specified dose rate of 300 R/min. Second, a volume was placed at 90 degrees on the exterior of the north wall. Finally, a volume was placed at the entrance of the maze. A total of thirty million photons were simulated. The MCNP input code is given in Appendix D.

The ratios of dose deposition were found to be the following: at 90°, the dose deposition rate was $7.6x10^{-9}$ that at our reference, corresponding to a dose rate of $2.28x10^{-6}$ R/min, or 0.14 mR/hour. This number is fairly close to the one estimated from the shielding curves. At the entrance of the maze, the dose deposition rate was found to be $7.9x10^{-10}$ that of the reference, corresponding to a dose rate of $1.4x10^{-2}$mR/hour.

Overall, the dose rate outside the shielded facility should never exceed 0.18 mR/hour when the accelerator is on. This dose rate is below the 2 mR/hour limit. Assuming a wildly overestimated 2000 hours of operation a year, the maximum yearly dose is 360 mR/year, again below the 500 mR/year limit.

7. DATA AND SOFTWARE

The CastScan experiment is comprised of many individual components that need to operate in conjunction with each other. We now review what they are and the computer tools used to coordinate them.

7.1. Controls and Sensors

The devices in this experiment fall into two categories. Some are operated and adjusted prior to the imaging sequence, and the others are an active part of the computed tomography process. Because the later need to be precisely coordinated, they are controlled by computers. The others are manually operated.

Among the manually operated devices are the furnace and the air compressor unit that supplies the cooling system with the coolant necessary to create a stable solidification front in the aluminum sample. A group of 16 thermocouples, shown in Figure 4.2, provide the operator with a rough temperature profile of the sample, allowing him or her to determine whether a solidification front is present or not.

The MINAC 6 linac is also manually operated. After a search procedure to ensure nobody is in the shielded room during linac operation, the room is secured. The linac control panel is located in a separate office, along with the computer systems. From this control panel, the linac can be turned on and off, and its performance can be tuned and monitored. Once the beam is judged satisfactory, the computers are used to coordinate an imaging sequence.

During an imaging sequence, the computers are used to translate and rotate the furnace within the beam. They also acquire the data measured by the detector array at each angular position. The radiation output of the linac is measured by an ionization chamber and is used to normalize the intensity measurements. The following section details some of the aspects of the computer control environment.

7.2. Control Environment

The stepping motors moving the furnace, the thermocouples and the thermocouples are controlled from within a single program written in the IDL language (Research Systems, Inc.). This program provides an easy to use graphical user interface within the Windows 95 operating system. All the parameters of an imaging sequence can be input within this environment. Once the operator is satisfied with them, the main program calls a series of MS-DOS executables which control the devices. This organization allows one to use a computer that is not equipped with Windows or IDL to acquire data. The parameters would then have to be entered manually or via the intermediary of batch files. Once the data is collected, it is passed along to the main IDL executable, which then allows the user to store it for further retrieval. The program converts the data to a sinogram format and performs conventional backprojection using a filtered backprojection algorithm. All images generated can then be saved in multiple formats such as bitmaps or the Postscript language. A flowchart of the organization of the CastScan software environment as well as a snapshot of the computer interface are included next.

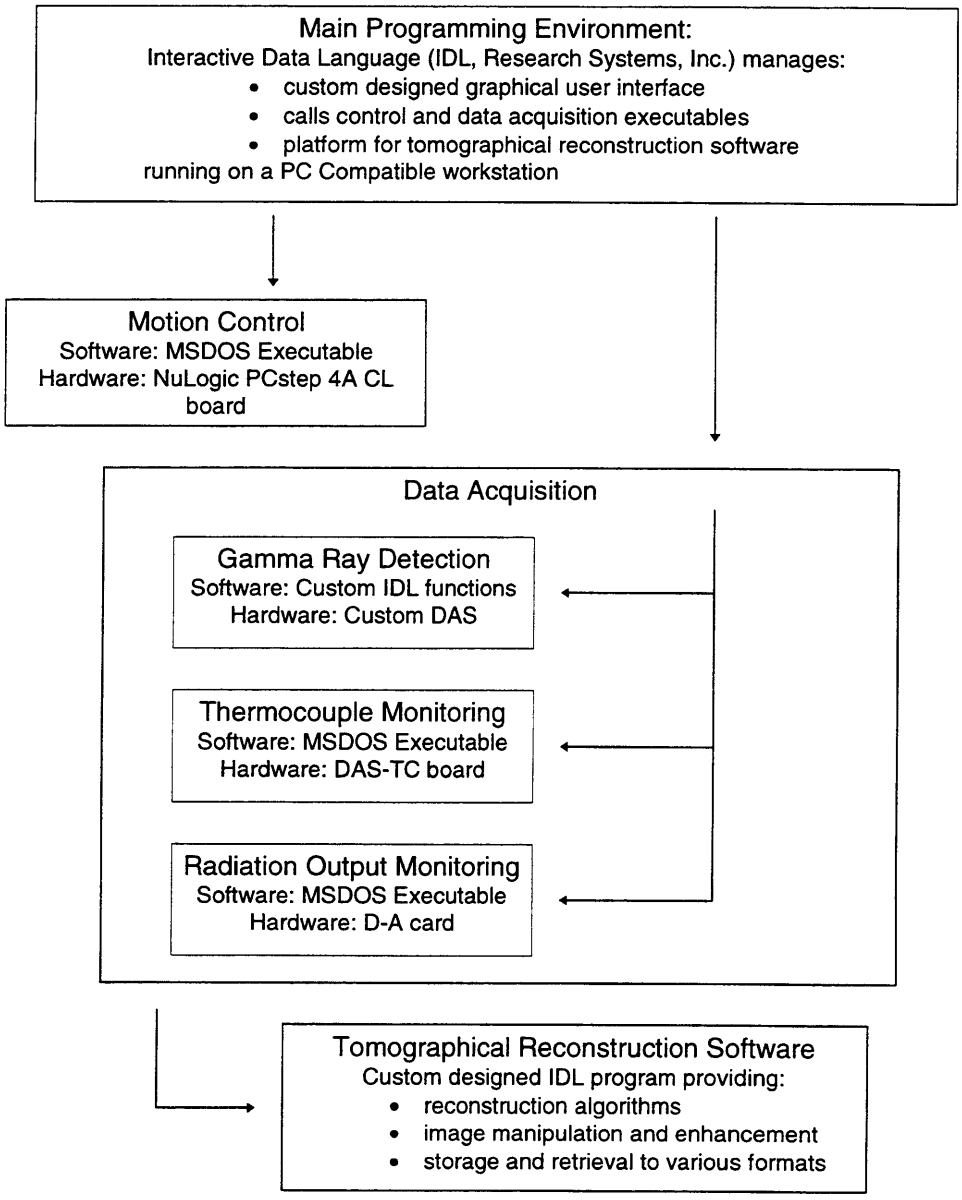

Figure 7.1. Chart of the CastScan software hierarchy

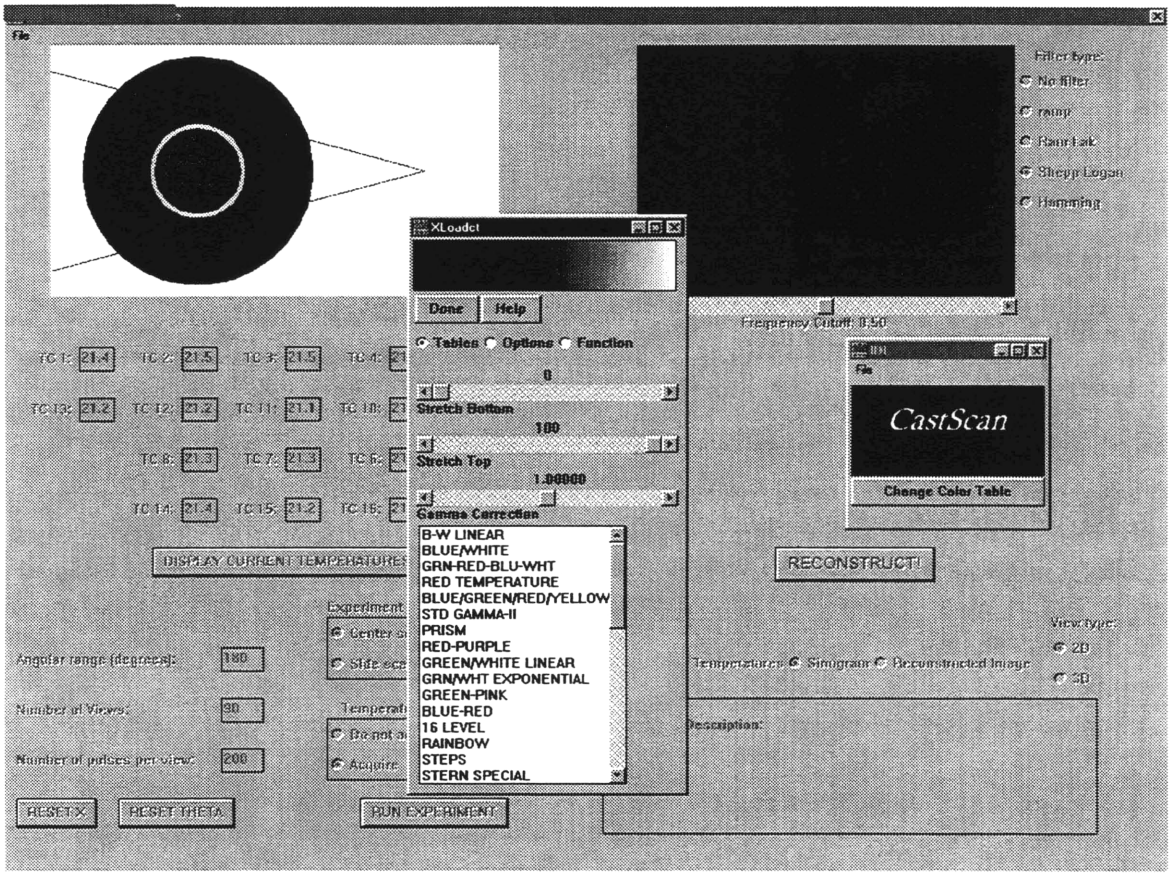

Figure 7.2. Snapshot of the CastScan control and reconstruction interface.

8. PERFORMANCE GOALS

To judge a tomographic system's performance, we need to know its maximum resolution as well as how this resolution changes as a function of imaging time.

8.1. Resolution

Because of the finite size of the source and the detector elements, the resolution in x-ray computed tomography has a lower limit. To determine this resolution, one needs to examine the situation from the point of view of the detector element. Each point along the width of the detector element receives photons from a finite angular range due to the width of the source. Each one of these positions is therefore sensitive to the attenuation coefficients of all the points situated inside this "fan". Of course this sensitivity depends on the distance between the source and the point the attenuation coefficient of which we are considering. Let us define $s(x,y,z)$ to be the sensitivity at a coordinate y along the detector width to the attenuation coefficient of a point situated at a position (x,z) from the source. The geometry is explained in the following figure.

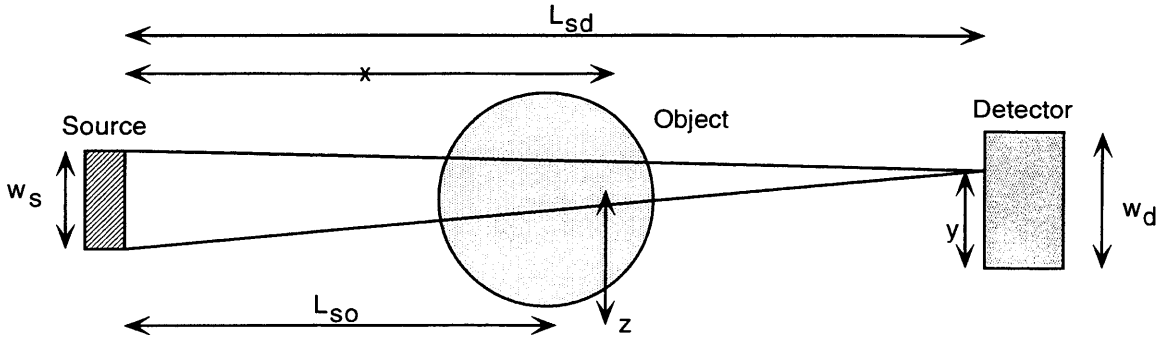

Figure 8.1. Source-detector geometry in resolution determination

The function $s(x,y,z)$ has the shape of a tophat function. The area under the plateau is constant, so it is equal to:

$$s(x,y,z) = tophat\left(y \cdot \frac{x}{L_{sd}}, w_s \cdot \frac{(L_{sd} - x)}{L_{sd}}, z \right) \qquad \text{Eq. 8.1}$$

where the first parameter in the *tophat* function is the starting point of the plateau, the second is its width, and the third is the variable it spans..

Because we are interested at the overall sensitivity of the detector to a point located at x, we need to integrate $s(x,y,z)$ over the width of the detector. The overall detector sensitivity is named $S(x,z)$.

$$S(x,z) = \int_0^{w_d} s(x,y,z)dy \qquad \text{Eq. 8.2}$$

This function was calculated numerically using a program written in the IDL language. The code is given in Appendix C. A surface plot of $S(x,z)$ is shown in Figure 8.2, using the experiment parameters w_s=2mm, w_d=1.8 mm, and L_{sd} = 84.5 cm.

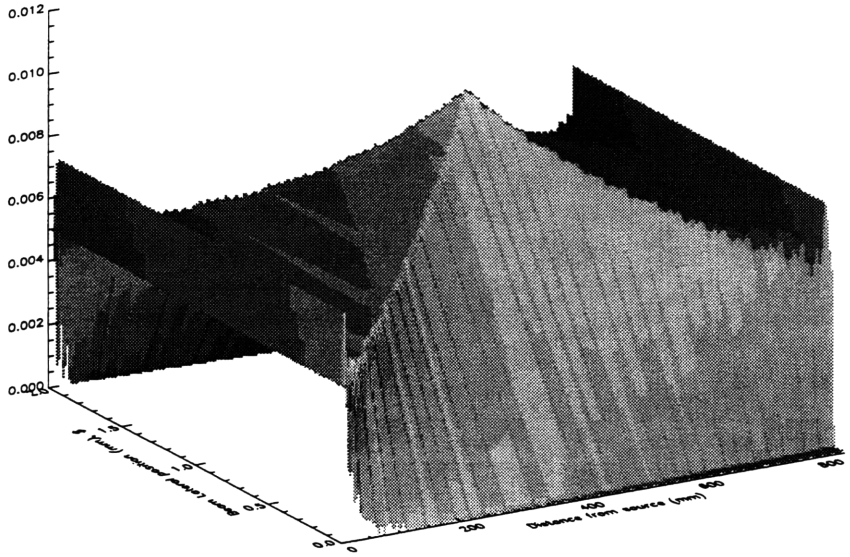

Figure 8.2. Surface plot of the *S(x,z)* sensitivity function for the CastScan experiment

The resolution of the system for an object centered at position x is defined as the full-width half-maximum (FWHM) of the *S(x,z)* curve. The FWHM was calculated for this experiment, and is plotted in Figure 8.3.

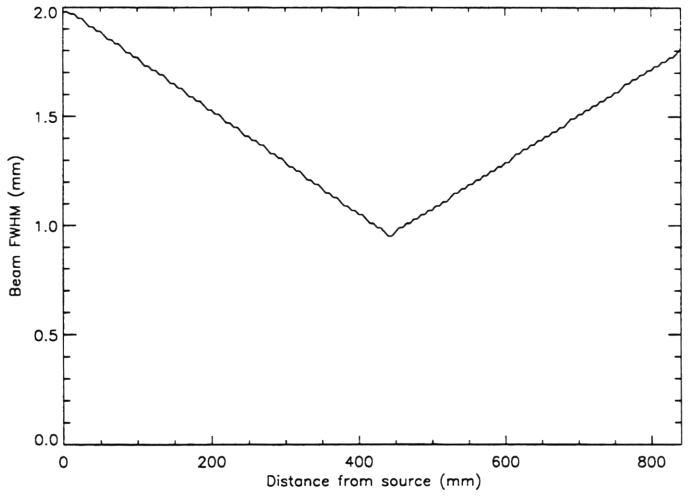

Figure 8.3. Predicted planar resolution of the CastScan system as a function of the object position

The minimum of this resolution is found at x = 44cm. If an object is placed at this position, it can be imaged with a resolution of 0.95 mm in the plane. Because we are restricted to placing the furnace at x = 51 cm, the resolution of our system is at best 1.1 mm.

The vertical resolution of the system can be determined in a similar fashion. A computation identical to that carried out above is done, but the detector width parameter is chosen to be equal to 20mm, the height of the scintillation crystals. The resulting resolution versus position plot is given next.

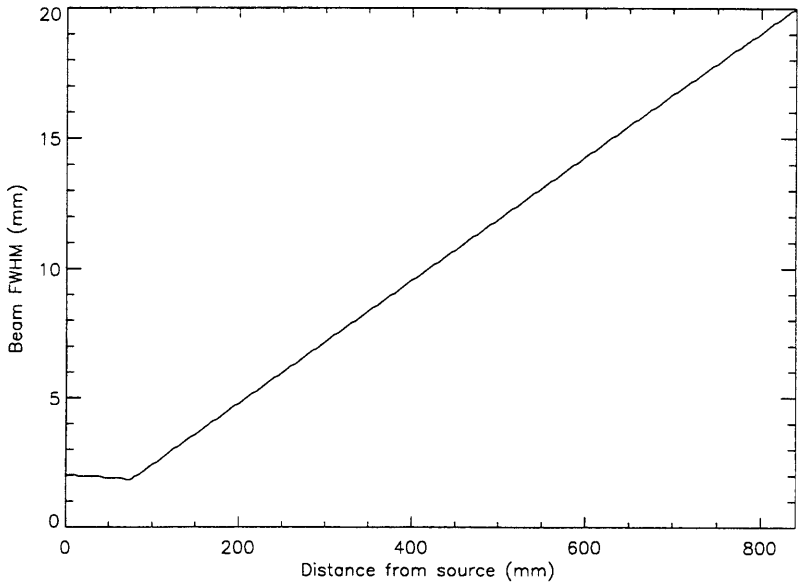

Figure 8.4. Predicted vertical resolution of the CastScan system as a function of the object position

Because we are more interested in the cross-sectional information in the sample, the minimum vertical resolution position is not a great concern. However this curve is useful to determine what the vertical resolution is for our particular design. At x = 51 cm, we find that it is equal to 12 mm.

To properly reconstruct an image of the object we examine, the number of angular increments N_θ the attenuation data is collected at must meet a minimum criterion.

Consider a system that meets the planar resolution requirements to measure an object of diameter D. If this system samples the attenuation along N_z translational steps, the object is scanned with a resolution equal to $r = D/N_z$. To achieve the same resolution in the θ dimension, we divide the perimeter $2\pi D$ of the circle containing the object by the resolution r. For a conventional tomography system which scans 180°, this number can be divided by two and becomes:

$$N_\theta = \frac{\pi}{2} N_z \qquad \text{Eq. 8.3}$$

In the case of this experiment, the requirement of two 180° scans means acquiring data at twice this number, i.e. πN_z.

8.2. Imaging Time

Because photons are individual bundles of energy, the intensity measured by the detector system is really the sum of many individual contributions. Because of this, any signal measured by our system is subject to an inherent source of noise. Poisson statistics dictate that the ratio of the true signal to the level of random fluctuations, also known as the *signal to noise ratio (SNR)*, is a function of the number N of detected photons:

$$SNR \equiv \frac{N}{\sigma_n} = \frac{N}{\sqrt{N}} = \sqrt{N} \qquad \text{Eq. 8.4}$$

where $\sigma_N = \sqrt{N}$ is the statistical variance is N. This equation means that the SNR in the number of detected photons increases as the square root of the number of photons. For this reason, it is important to use a source as strong as possible, in order to reduce the statistical noise.

Assuming that we wish to be capable of measuring a change of density $\Delta\rho$ over a distance Δx, the signal is equal to:

$$\begin{aligned} signal &= N\mu_m(\rho+\Delta\rho)\Delta x - N\mu_m\rho\Delta x \\ &= N\mu_m\Delta\rho\Delta x \end{aligned} \qquad \text{Eq. 8.5}$$

where μ_m is the mass attenuation coefficient. Because the noise is equal to the square root of N, we find:

$$SNR = \sqrt{N}\mu\left(\frac{\Delta\rho}{\rho}\right)\Delta x \qquad \text{Eq. 8.6}$$

where our sensitivity to density is now unitless.

We need to relate the number N of detected photons to the number N_0 of photons emitted by the source. These photons are attenuated by the object that is imaged, and then are subject to a detection efficiency as discussed previously. This conversion factor can be obtained from the MCNP calculation performed to calculate the scatter function shown in Figure 5.9. The center of the curve shows the energy deposited inside the crystal for each photon emitted. This number is equal to 3.55 keV/photon emitted. Because the average photon energy in the beam was found to be 1.29 MeV (section 3.2.3), we can determine that the overall probability of a photon traversing the center of the object and depositing its energy in the detector to be the ratio of these to numbers, i.e.:

$$p = \frac{N}{N_0} = 2.41\times10^{-3} \text{ per photon} \qquad \text{Eq. 8.7}$$

We can now reformulate Eq. 8.6 to obtain the number of photons N_0 that must be emitted to achieve a given *SNR*.

$$N_0 = \frac{1}{p}\left[\frac{SNR}{\mu\left(\frac{\Delta\rho}{\rho}\right)\Delta x}\right]^2 \qquad \text{Eq. 8.8}$$

The photon flux of MINAC 6 was found to be equal to be 8.4 x 10^9 photons/cm^2/s at 1 meter in section 3.2.3. Because the flux decreases as the square of the distance from the source, the detectors, placed 84.5 cm away, are subjected to a photon flux of ϕ = 1.18x10^{10} photons/cm^2/s. The detection area A is a function of the resolution desired. It is given by:

$$A = h_d \cdot \Delta x \cdot \frac{L_{sd}}{L_{so}} \qquad \text{Eq. 8.9}$$

where L_{sd} is the source to detector distance, L_{so} is the source to object distance and h_d is the detector height.

Using this information, the time T required to obtain a given SNR is given by:

$$t_{acquisition} = \frac{N_0}{\phi \cdot A} = \frac{4 L_{so} \cdot SNR^2}{p \cdot \phi \cdot h_d \cdot L_{sd} \cdot \Delta x^3 \cdot \mu^2 \cdot \left(\frac{\Delta\rho}{\rho}\right)^2} \qquad \text{Eq. 8.10}$$

A factor of four has been added to take into account the fact that only half of the detectors are used and the fact that the object needs to be rotated through twice 180° instead of only once.

It is now possible to calculate this acquisition time for our experiment configuration. The following parameters will be used:

- p = 2.41 x 10^{-3} /photon
- ϕ = 1.18 x 10^{10} photons/cm^2/s
- h_d = 2 cm
- L_{sd} = 84.5 cm, L_{so} = 51 cm
- SNR = 1
- $\mu_{aluminum,\ 1.29\ MeV}$ = 0.146 cm^{-1}
- $\Delta\rho/\rho$ = 1 %

The resolution Δx as a function of the acquisition time is shown in Figure 8.5.

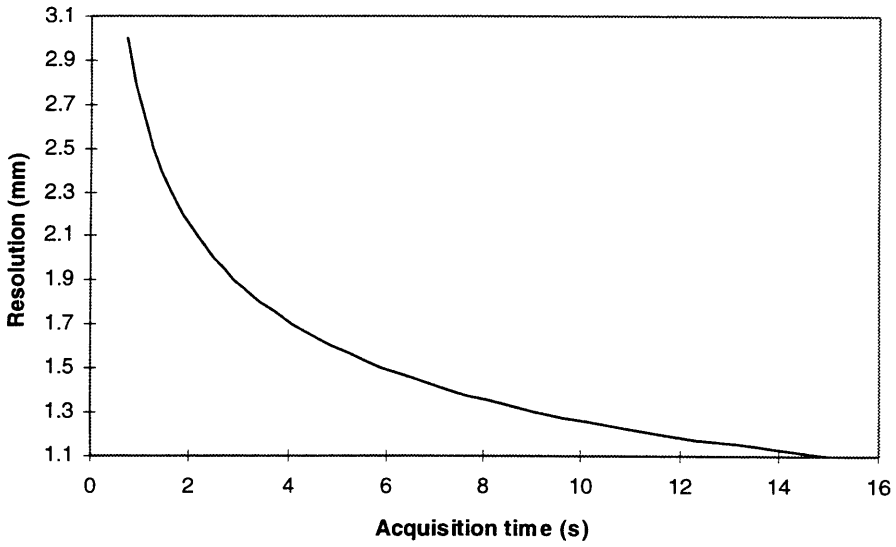

Figure 8.5. Chart of resolution versus data acquisition time for the CastScan system

For the system's optimal resolution, the acquisition time is approximately 15 seconds. Because the acquisition time is a inverse cube function of the resolution, it is apparent that sacrificing resolution can lead to vast reductions in acquisition time.

As a final note, it is important to realize that this estimate only takes into account the time during which data is collected. The actual imaging times depends on several other factors, including the speed at which the furnace can be rotated. This speed is essentially limited by the power of the stepping motors driving the rotary table. Another time consuming factor to account for is the tomographic reconstruction time, which increases with resolution. This time is a function of the speed of the computer running the algorithms, but is on the order of a minute on a contemporary personal computer. Overall, one can estimate that the complete imaging time of the CastScan system will be on the order of several minutes.

Overall, one can estimate that the complete imaging time of the CastScan system will be on the order of several minutes.

8.3. Dynamic Range

The Data Acquisition System (DAS) used to measure the charge created within the photodiodes must have a sufficient *dynamic range (DR)* to be useful. The dynamic range is the ratio of the highest signal expected to be measured by the system to the smallest signal variation it must be capable of measuring. The maximum expected signal is equal to the intensity of the unrestricted beam impinging upon the detectors. The minimum signal is equal to the change in intensity caused by a change in density $\Delta\rho$ over a distance Δx. The equation for this signal is given in Eq. 8.5, without taking attenuation through the object into account. The combined density thickness of the furnace and its contents is equal to 72 g/cm^2. Using a mass attenuation coefficient μ_m equal to 0.052 cm^2/g, the attenuation a of the photon beam through the center of the furnace is equal to 2.4%. An expression for the dynamic range is given in the following equation:

$$DR = \frac{N_0}{(N_0 a)\mu_m \cdot \Delta\rho \cdot \Delta x} = \frac{1}{a \cdot \mu \cdot \Delta x \cdot \left(\frac{\Delta\rho}{\rho}\right)} \qquad \text{Eq. 8.11}$$

Using the parameters Δx = 0.11cm, $\Delta\rho/\rho$ = 1 %, a = 2.4 %, and μ = 0.146 cm^{-1}, one finds the necessary dynamic range of the DAS to be 2.6×10^5. Because most data acquisition systems provide information in a digital format interpretable by a computer, the dynamic range is often specified in terms of n bit(s), where $DR \leq 2^n$. Using this nomenclature, the CastScan DAS must achieve a minimum dynamic range of 18 bits. In practice, it may be possible to reduce this dynamic range by adding absorber material to reduce the intensity of the open beam impinging on the detectors. This does present the drawback of increasing the amount of unwanted signal caused by scattered radiation.

9. CONCLUSIONS AND FUTURE WORK

The overall imaging time of a computed tomography scanner is a function of the data acquisition time, the motion time and the reconstruction time. Current technology allows one to easily improve the capabilities of the CastScan system in terms of the last two parameters. Faster motors and computers are available, for which the main issue to consider is cost. To reduce data acquisition time, an issue important to the continuous casting industry, a number of options are available. These fall into three principal categories:

- data collection efficiency improvements,
- usage of *a priori* information,
- reconstruction algorithms relying on incomplete data sets.

9.1. Efficiency Improvements

Examining Eq. 8.10, it appears that changing some parameters can yield shorter acquisition time without sacrificing planar or vertical resolution. The most obvious change is to use a greater photon flux ϕ. This translates into using a higher output source, such as a higher current linac.

If one is restricted to a given source, increasing the parameter p, the photon collection efficiency, is an available option. This can easily be done with the CastScan system by using deeper scintillation crystals. The photon collection efficiency can thus be improved from about 5% to about 45%. Reducing the thickness and density of the furnace will allow a greater number of photons to reach the detectors.

9.2. *A Priori* Information

The CastScan system provides images of the entire cross section of the experimental apparatus used to melt the aluminum, including the furnace and its thick insulation. The crucible itself is filled with solid and liquid aluminum, the densities of which are known. The only uncertainty in the scanned object lies in the position of the solidification front within the aluminum. This represents a small fraction of the entire scanned volume. A possibility of reducing data acquisition time relies on using the *a priori* knowledge about the density of the object in an iterated reconstruction algorithm. This algorithm relies on modifying a backprojected image until its computer simulated sinogram converges towards the sinogram obtained through measurements. The density of the furnace, the crucible, the outer and inner regions of aluminum can be given as a constraint. Consequently the data collection needs only focus on the areas of the sinogram representing paths going through the solidification front. This method allows one to reduce detection time by focusing the beam on the center of the furnace only; it can also allow an increase of the resolution in the solidification region.

9.3. Incomplete Data Sets and Limited Angle Tomography

In general, using traditional filtered backprojection on a data set that does not cover the full angular or translational range yield artifacts that make images difficult or impossible to interpret, both qualitatively and quantitatively. In an industrial environment, one may face physical restriction that prevent the collection of a complete sinogram. If the sinogram is incomplete in the angle of rotation dimension, the only solution to obtain an image lies in *limited angle tomography* algorithms. A possible track for future research is the application of these algorithms to our problem. A combination of the abundance of *a priori* knowledge about the scanned object and of its inherent physical symmetry improve the prospects of success in this particular line of research.

APPENDIX A. MINAC 6 Spectrum Computation - MCNP Code

```
mcnp simulation - MINAC 6 source spectrum
c
c Cell cards
1       2 -19.26 1 -2 -7 imp:p=1 imp:e=1
2       3 -8.92 2 -3 -7 imp:p=1 imp:e=1
3       4 -11.34 4 -5 -8 imp:p=1 imp:e=0
5       2 -19.26 6 -10 -8 7 imp:p=1 imp:e=0
6       2 -19.26 10 -4 -8 9 imp:p=1 imp:e=0
10      1 -.00127 -100 -6 imp:p=1 imp:e=0
11      1 -.00127 -100 5 #20 #21 imp:p=1 imp:e=0
12      1 -0.00127 6 -5 8 -100 imp:p=1 imp:e=0
13      1 -0.00127 6 -1 -7 imp:p=1 imp:e=1
14      1 -0.00127 3 -10 -7 imp:p=1 imp:e=0
15      1 -0.00127 10 -4 -9 imp:p=1 imp:e=0
20      1 -.00127 -30 12 -13 imp:p=1 imp:e=0
21      1 -.00127 14 -15 -31 imp:p=1 imp:e=0
100     0 100 imp:p=0 imp:e=0

c Surface cards
1       PX  0
2       PX .0889
3       PX .18542
4       PX 7.17042
5       PX 7.27042
6       PX -2.35458
7       CX 0.873125
8       CX 5.715
9       KX -1.1240629 0.07179677
10      PX 2.314483
12      px 100.0
13      px 100.0001
14      px 100.0002
15      px 100.0003
30      cx 26.7949
31      cx 8.7489
100     SX .14271 130

c Data cards
mode    p e
m1      7014 .78 8016 .22  $air
m2      74184 1            $tungsten
m3      29064 1            $copper
m4      82207 1            $lead
sdef    pos=-.000001 0 0 erg=6 vec=1 0 0 dir=1 par=3
f12:p   12 14              $Photon flux at 1cm at 5 and 30 degrees
E12     .1 117I 6
nps     500000
```

APPENDIX B. Scatter Function Computation - MCNP Code

This MCNP input file will calculate the spread function for this experiment's configuration, using 8cm long tungsten anti-scatter plates.

```
MINAC 6 Spectrum - 8cm tungsten coll. centered on air
c
c
c
1       2 -2.7 -1 -7 8 imp:p=1
2       3 -2.20 1 -2  -7 8 imp:p=1
3       1 -0.00127 2 -3 -7 8 imp:p=1
4       4 -1.5 3 -4 -7 8 imp:p=1
5       5 -0.5 4 -5 -7 8 imp:p=1
6       6 -7.9 5 -6 -7 8 imp:p=1
10      1 -0.00127 -11 101 -484 12 -13 imp:p=1
20      1 -0.00127 -30 #1 #2 #3 #4 #5 #6 #40 #41
#(60 -51 -52 53) imp:p=1
30      0 30 imp:p=0
40      40 -11.3 52 -41 60 -44 101 -484 imp:p=1
41      40 -11.3 -53 42 60 -44 101 -484 imp:p=1
50       1 -0.00127 60 -51 -52 53 (-101 : 484)
imp:p=1
101     10 -7.9 50 -51 -52 53 101 -102 imp:p=1
102     11 -7.9 50 -51 -52 53 102 -103 imp:p=1
103     10 -7.9 50 -51 -52 53 103 -104 imp:p=1
104     11 -7.9 50 -51 -52 53 104 -105 imp:p=1
105     10 -7.9 50 -51 -52 53 105 -106 imp:p=1
106     11 -7.9 50 -51 -52 53 106 -107 imp:p=1
107     10 -7.9 50 -51 -52 53 107 -108 imp:p=1
108     11 -7.9 50 -51 -52 53 108 -109 imp:p=1
109     10 -7.9 50 -51 -52 53 109 -110 imp:p=1
110     11 -7.9 50 -51 -52 53 110 -111 imp:p=1
111     10 -7.9 50 -51 -52 53 111 -112 imp:p=1
112     11 -7.9 50 -51 -52 53 112 -113 imp:p=1
113     10 -7.9 50 -51 -52 53 113 -114 imp:p=1
114     11 -7.9 50 -51 -52 53 114 -115 imp:p=1
115     10 -7.9 50 -51 -52 53 115 -116 imp:p=1
116     11 -7.9 50 -51 -52 53 116 -117 imp:p=1
117     10 -7.9 50 -51 -52 53 117 -118 imp:p=1
118     11 -7.9 50 -51 -52 53 118 -119 imp:p=1
119     10 -7.9 50 -51 -52 53 119 -120 imp:p=1
120     11 -7.9 50 -51 -52 53 120 -121 imp:p=1
121     10 -7.9 50 -51 -52 53 121 -122 imp:p=1
122     11 -7.9 50 -51 -52 53 122 -123 imp:p=1
123     10 -7.9 50 -51 -52 53 123 -124 imp:p=1
124     11 -7.9 50 -51 -52 53 124 -125 imp:p=1
125     10 -7.9 50 -51 -52 53 125 -126 imp:p=1
126     11 -7.9 50 -51 -52 53 126 -127 imp:p=1
127     10 -7.9 50 -51 -52 53 127 -128 imp:p=1
128     11 -7.9 50 -51 -52 53 128 -129 imp:p=1
129     10 -7.9 50 -51 -52 53 129 -130 imp:p=1
130     11 -7.9 50 -51 -52 53 130 -131 imp:p=1
131     10 -7.9 50 -51 -52 53 131 -132 imp:p=1
132     11 -7.9 50 -51 -52 53 132 -133 imp:p=1
133     10 -7.9 50 -51 -52 53 133 -134 imp:p=1
134     11 -7.9 50 -51 -52 53 134 -135 imp:p=1
135     10 -7.9 50 -51 -52 53 135 -136 imp:p=1
136     11 -7.9 50 -51 -52 53 136 -137 imp:p=1
137     10 -7.9 50 -51 -52 53 137 -138 imp:p=1
138     11 -7.9 50 -51 -52 53 138 -139 imp:p=1
139     10 -7.9 50 -51 -52 53 139 -140 imp:p=1
140     11 -7.9 50 -51 -52 53 140 -141 imp:p=1
141     10 -7.9 50 -51 -52 53 141 -142 imp:p=1
142     11 -7.9 50 -51 -52 53 142 -143 imp:p=1
143     10 -7.9 50 -51 -52 53 143 -144 imp:p=1
144     11 -7.9 50 -51 -52 53 144 -145 imp:p=1
145     10 -7.9 50 -51 -52 53 145 -146 imp:p=1
146     11 -7.9 50 -51 -52 53 146 -147 imp:p=1
147     10 -7.9 50 -51 -52 53 147 -148 imp:p=1
148     11 -7.9 50 -51 -52 53 148 -149 imp:p=1
149     10 -7.9 50 -51 -52 53 149 -150 imp:p=1
150     11 -7.9 50 -51 -52 53 150 -151 imp:p=1
151     10 -7.9 50 -51 -52 53 151 -152 imp:p=1
152     11 -7.9 50 -51 -52 53 152 -153 imp:p=1
153     10 -7.9 50 -51 -52 53 153 -154 imp:p=1
154     11 -7.9 50 -51 -52 53 154 -155 imp:p=1
155     10 -7.9 50 -51 -52 53 155 -156 imp:p=1
156     11 -7.9 50 -51 -52 53 156 -157 imp:p=1
157     10 -7.9 50 -51 -52 53 157 -158 imp:p=1
158     11 -7.9 50 -51 -52 53 158 -159 imp:p=1
159     10 -7.9 50 -51 -52 53 159 -160 imp:p=1
160     11 -7.9 50 -51 -52 53 160 -161 imp:p=1
161     10 -7.9 50 -51 -52 53 161 -162 imp:p=1
162     11 -7.9 50 -51 -52 53 162 -163 imp:p=1
163     10 -7.9 50 -51 -52 53 163 -164 imp:p=1
164     11 -7.9 50 -51 -52 53 164 -165 imp:p=1
165     10 -7.9 50 -51 -52 53 165 -166 imp:p=1
166     11 -7.9 50 -51 -52 53 166 -167 imp:p=1
167     10 -7.9 50 -51 -52 53 167 -168 imp:p=1
168     11 -7.9 50 -51 -52 53 168 -169 imp:p=1
169     10 -7.9 50 -51 -52 53 169 -170 imp:p=1
170     11 -7.9 50 -51 -52 53 170 -171 imp:p=1
171     10 -7.9 50 -51 -52 53 171 -172 imp:p=1
172     11 -7.9 50 -51 -52 53 172 -173 imp:p=1
173     10 -7.9 50 -51 -52 53 173 -174 imp:p=1
174     11 -7.9 50 -51 -52 53 174 -175 imp:p=1
175     10 -7.9 50 -51 -52 53 175 -176 imp:p=1
176     11 -7.9 50 -51 -52 53 176 -177 imp:p=1
177     10 -7.9 50 -51 -52 53 177 -178 imp:p=1
178     11 -7.9 50 -51 -52 53 178 -179 imp:p=1
179     10 -7.9 50 -51 -52 53 179 -180 imp:p=1
180     11 -7.9 50 -51 -52 53 180 -181 imp:p=1
181     10 -7.9 50 -51 -52 53 181 -182 imp:p=1
182     11 -7.9 50 -51 -52 53 182 -183 imp:p=1
183     10 -7.9 50 -51 -52 53 183 -184 imp:p=1
184     11 -7.9 50 -51 -52 53 184 -185 imp:p=1
185     10 -7.9 50 -51 -52 53 185 -186 imp:p=1
186     11 -7.9 50 -51 -52 53 186 -187 imp:p=1
187     10 -7.9 50 -51 -52 53 187 -188 imp:p=1
188     11 -7.9 50 -51 -52 53 188 -189 imp:p=1
189     10 -7.9 50 -51 -52 53 189 -190 imp:p=1
190     11 -7.9 50 -51 -52 53 190 -191 imp:p=1
191     10 -7.9 50 -51 -52 53 191 -192 imp:p=1
192     11 -7.9 50 -51 -52 53 192 -193 imp:p=1
193     10 -7.9 50 -51 -52 53 193 -194 imp:p=1
194     11 -7.9 50 -51 -52 53 194 -195 imp:p=1
195     10 -7.9 50 -51 -52 53 195 -196 imp:p=1
196     11 -7.9 50 -51 -52 53 196 -197 imp:p=1
197     10 -7.9 50 -51 -52 53 197 -198 imp:p=1
198     11 -7.9 50 -51 -52 53 198 -199 imp:p=1
199     10 -7.9 50 -51 -52 53 199 -200 imp:p=1
200     11 -7.9 50 -51 -52 53 200 -201 imp:p=1
201     10 -7.9 50 -51 -52 53 201 -202 imp:p=1
202     11 -7.9 50 -51 -52 53 202 -203 imp:p=1
203     10 -7.9 50 -51 -52 53 203 -204 imp:p=1
204     11 -7.9 50 -51 -52 53 204 -205 imp:p=1
205     10 -7.9 50 -51 -52 53 205 -206 imp:p=1
206     11 -7.9 50 -51 -52 53 206 -207 imp:p=1
207     10 -7.9 50 -51 -52 53 207 -208 imp:p=1
```

```
208     11 -7.9 50 -51 -52 53 208 -209 imp:p=1
209     10 -7.9 50 -51 -52 53 209 -210 imp:p=1
210     11 -7.9 50 -51 -52 53 210 -211 imp:p=1
211     10 -7.9 50 -51 -52 53 211 -212 imp:p=1
212     11 -7.9 50 -51 -52 53 212 -213 imp:p=1
213     10 -7.9 50 -51 -52 53 213 -214 imp:p=1
214     11 -7.9 50 -51 -52 53 214 -215 imp:p=1
215     10 -7.9 50 -51 -52 53 215 -216 imp:p=1
216     11 -7.9 50 -51 -52 53 216 -217 imp:p=1
217     10 -7.9 50 -51 -52 53 217 -218 imp:p=1
218     11 -7.9 50 -51 -52 53 218 -219 imp:p=1
219     10 -7.9 50 -51 -52 53 219 -220 imp:p=1
220     11 -7.9 50 -51 -52 53 220 -221 imp:p=1
221     10 -7.9 50 -51 -52 53 221 -222 imp:p=1
222     11 -7.9 50 -51 -52 53 222 -223 imp:p=1
223     10 -7.9 50 -51 -52 53 223 -224 imp:p=1
224     11 -7.9 50 -51 -52 53 224 -225 imp:p=1
225     10 -7.9 50 -51 -52 53 225 -226 imp:p=1
226     11 -7.9 50 -51 -52 53 226 -227 imp:p=1
227     10 -7.9 50 -51 -52 53 227 -228 imp:p=1
228     11 -7.9 50 -51 -52 53 228 -229 imp:p=1
229     10 -7.9 50 -51 -52 53 229 -230 imp:p=1
230     11 -7.9 50 -51 -52 53 230 -231 imp:p=1
231     10 -7.9 50 -51 -52 53 231 -232 imp:p=1
232     11 -7.9 50 -51 -52 53 232 -233 imp:p=1
233     10 -7.9 50 -51 -52 53 233 -234 imp:p=1
234     11 -7.9 50 -51 -52 53 234 -235 imp:p=1
235     10 -7.9 50 -51 -52 53 235 -236 imp:p=1
236     11 -7.9 50 -51 -52 53 236 -237 imp:p=1
237     10 -7.9 50 -51 -52 53 237 -238 imp:p=1
238     11 -7.9 50 -51 -52 53 238 -239 imp:p=1
239     10 -7.9 50 -51 -52 53 239 -240 imp:p=1
240     11 -7.9 50 -51 -52 53 240 -241 imp:p=1
241     10 -7.9 50 -51 -52 53 241 -242 imp:p=1
242     11 -7.9 50 -51 -52 53 242 -243 imp:p=1
243     10 -7.9 50 -51 -52 53 243 -244 imp:p=1
244     11 -7.9 50 -51 -52 53 244 -245 imp:p=1
245     10 -7.9 50 -51 -52 53 245 -246 imp:p=1
246     11 -7.9 50 -51 -52 53 246 -247 imp:p=1
247     10 -7.9 50 -51 -52 53 247 -248 imp:p=1
248     11 -7.9 50 -51 -52 53 248 -249 imp:p=1
249     10 -7.9 50 -51 -52 53 249 -250 imp:p=1
250     11 -7.9 50 -51 -52 53 250 -251 imp:p=1
251     10 -7.9 50 -51 -52 53 251 -252 imp:p=1
252     11 -7.9 50 -51 -52 53 252 -253 imp:p=1
253     10 -7.9 50 -51 -52 53 253 -254 imp:p=1
254     11 -7.9 50 -51 -52 53 254 -255 imp:p=1
255     10 -7.9 50 -51 -52 53 255 -256 imp:p=1
256     11 -7.9 50 -51 -52 53 256 -257 imp:p=1
257     10 -7.9 50 -51 -52 53 257 -258 imp:p=1
258     11 -7.9 50 -51 -52 53 258 -259 imp:p=1
259     10 -7.9 50 -51 -52 53 259 -260 imp:p=1
260     11 -7.9 50 -51 -52 53 260 -261 imp:p=1
261     10 -7.9 50 -51 -52 53 261 -262 imp:p=1
262     11 -7.9 50 -51 -52 53 262 -263 imp:p=1
263     10 -7.9 50 -51 -52 53 263 -264 imp:p=1
264     11 -7.9 50 -51 -52 53 264 -265 imp:p=1
265     10 -7.9 50 -51 -52 53 265 -266 imp:p=1
266     11 -7.9 50 -51 -52 53 266 -267 imp:p=1
267     10 -7.9 50 -51 -52 53 267 -268 imp:p=1
268     11 -7.9 50 -51 -52 53 268 -269 imp:p=1
269     10 -7.9 50 -51 -52 53 269 -270 imp:p=1
270     11 -7.9 50 -51 -52 53 270 -271 imp:p=1
271     10 -7.9 50 -51 -52 53 271 -272 imp:p=1
272     11 -7.9 50 -51 -52 53 272 -273 imp:p=1
273     10 -7.9 50 -51 -52 53 273 -274 imp:p=1
274     11 -7.9 50 -51 -52 53 274 -275 imp:p=1
275     10 -7.9 50 -51 -52 53 275 -276 imp:p=1
276     11 -7.9 50 -51 -52 53 276 -277 imp:p=1
277     10 -7.9 50 -51 -52 53 277 -278 imp:p=1
278     11 -7.9 50 -51 -52 53 278 -279 imp:p=1
279     10 -7.9 50 -51 -52 53 279 -280 imp:p=1
280     11 -7.9 50 -51 -52 53 280 -281 imp:p=1
281     10 -7.9 50 -51 -52 53 281 -282 imp:p=1
282     11 -7.9 50 -51 -52 53 282 -283 imp:p=1
283     10 -7.9 50 -51 -52 53 283 -284 imp:p=1
284     11 -7.9 50 -51 -52 53 284 -285 imp:p=1
285     10 -7.9 50 -51 -52 53 285 -286 imp:p=1
286     11 -7.9 50 -51 -52 53 286 -287 imp:p=1
287     10 -7.9 50 -51 -52 53 287 -288 imp:p=1
288     11 -7.9 50 -51 -52 53 288 -289 imp:p=1
289     10 -7.9 50 -51 -52 53 289 -290 imp:p=1
290     11 -7.9 50 -51 -52 53 290 -291 imp:p=1
291     10 -7.9 50 -51 -52 53 291 -292 imp:p=1
292     11 -7.9 50 -51 -52 53 292 -293 imp:p=1
293     10 -7.9 50 -51 -52 53 293 -294 imp:p=1
294     11 -7.9 50 -51 -52 53 294 -295 imp:p=1
295     10 -7.9 50 -51 -52 53 295 -296 imp:p=1
296     11 -7.9 50 -51 -52 53 296 -297 imp:p=1
297     10 -7.9 50 -51 -52 53 297 -298 imp:p=1
298     11 -7.9 50 -51 -52 53 298 -299 imp:p=1
299     10 -7.9 50 -51 -52 53 299 -300 imp:p=1
300     11 -7.9 50 -51 -52 53 300 -301 imp:p=1
301     10 -7.9 50 -51 -52 53 301 -302 imp:p=1
302     11 -7.9 50 -51 -52 53 302 -303 imp:p=1
303     10 -7.9 50 -51 -52 53 303 -304 imp:p=1
304     11 -7.9 50 -51 -52 53 304 -305 imp:p=1
305     10 -7.9 50 -51 -52 53 305 -306 imp:p=1
306     11 -7.9 50 -51 -52 53 306 -307 imp:p=1
307     10 -7.9 50 -51 -52 53 307 -308 imp:p=1
308     11 -7.9 50 -51 -52 53 308 -309 imp:p=1
309     10 -7.9 50 -51 -52 53 309 -310 imp:p=1
310     11 -7.9 50 -51 -52 53 310 -311 imp:p=1
311     10 -7.9 50 -51 -52 53 311 -312 imp:p=1
312     11 -7.9 50 -51 -52 53 312 -313 imp:p=1
313     10 -7.9 50 -51 -52 53 313 -314 imp:p=1
314     11 -7.9 50 -51 -52 53 314 -315 imp:p=1
315     10 -7.9 50 -51 -52 53 315 -316 imp:p=1
316     11 -7.9 50 -51 -52 53 316 -317 imp:p=1
317     10 -7.9 50 -51 -52 53 317 -318 imp:p=1
318     11 -7.9 50 -51 -52 53 318 -319 imp:p=1
319     10 -7.9 50 -51 -52 53 319 -320 imp:p=1
320     11 -7.9 50 -51 -52 53 320 -321 imp:p=1
321     10 -7.9 50 -51 -52 53 321 -322 imp:p=1
322     11 -7.9 50 -51 -52 53 322 -323 imp:p=1
323     10 -7.9 50 -51 -52 53 323 -324 imp:p=1
324     11 -7.9 50 -51 -52 53 324 -325 imp:p=1
325     10 -7.9 50 -51 -52 53 325 -326 imp:p=1
326     11 -7.9 50 -51 -52 53 326 -327 imp:p=1
327     10 -7.9 50 -51 -52 53 327 -328 imp:p=1
328     11 -7.9 50 -51 -52 53 328 -329 imp:p=1
329     10 -7.9 50 -51 -52 53 329 -330 imp:p=1
330     11 -7.9 50 -51 -52 53 330 -331 imp:p=1
331     10 -7.9 50 -51 -52 53 331 -332 imp:p=1
332     11 -7.9 50 -51 -52 53 332 -333 imp:p=1
333     10 -7.9 50 -51 -52 53 333 -334 imp:p=1
334     11 -7.9 50 -51 -52 53 334 -335 imp:p=1
335     10 -7.9 50 -51 -52 53 335 -336 imp:p=1
336     11 -7.9 50 -51 -52 53 336 -337 imp:p=1
337     10 -7.9 50 -51 -52 53 337 -338 imp:p=1
338     11 -7.9 50 -51 -52 53 338 -339 imp:p=1
339     10 -7.9 50 -51 -52 53 339 -340 imp:p=1
340     11 -7.9 50 -51 -52 53 340 -341 imp:p=1
341     10 -7.9 50 -51 -52 53 341 -342 imp:p=1
342     11 -7.9 50 -51 -52 53 342 -343 imp:p=1
343     10 -7.9 50 -51 -52 53 343 -344 imp:p=1
344     11 -7.9 50 -51 -52 53 344 -345 imp:p=1
345     10 -7.9 50 -51 -52 53 345 -346 imp:p=1
346     11 -7.9 50 -51 -52 53 346 -347 imp:p=1
347     10 -7.9 50 -51 -52 53 347 -348 imp:p=1
348     11 -7.9 50 -51 -52 53 348 -349 imp:p=1
349     10 -7.9 50 -51 -52 53 349 -350 imp:p=1
350     11 -7.9 50 -51 -52 53 350 -351 imp:p=1
351     10 -7.9 50 -51 -52 53 351 -352 imp:p=1
352     11 -7.9 50 -51 -52 53 352 -353 imp:p=1
353     10 -7.9 50 -51 -52 53 353 -354 imp:p=1
354     11 -7.9 50 -51 -52 53 354 -355 imp:p=1
355     10 -7.9 50 -51 -52 53 355 -356 imp:p=1
356     11 -7.9 50 -51 -52 53 356 -357 imp:p=1
357     10 -7.9 50 -51 -52 53 357 -358 imp:p=1
358     11 -7.9 50 -51 -52 53 358 -359 imp:p=1
359     10 -7.9 50 -51 -52 53 359 -360 imp:p=1
```

```
360     11 -7.9 50 -51 -52 53 360 -361 imp:p=1
361     10 -7.9 50 -51 -52 53 361 -362 imp:p=1
362     11 -7.9 50 -51 -52 53 362 -363 imp:p=1
363     10 -7.9 50 -51 -52 53 363 -364 imp:p=1
364     11 -7.9 50 -51 -52 53 364 -365 imp:p=1
365     10 -7.9 50 -51 -52 53 365 -366 imp:p=1
366     11 -7.9 50 -51 -52 53 366 -367 imp:p=1
367     10 -7.9 50 -51 -52 53 367 -368 imp:p=1
368     11 -7.9 50 -51 -52 53 368 -369 imp:p=1
369     10 -7.9 50 -51 -52 53 369 -370 imp:p=1
370     11 -7.9 50 -51 -52 53 370 -371 imp:p=1
371     10 -7.9 50 -51 -52 53 371 -372 imp:p=1
372     11 -7.9 50 -51 -52 53 372 -373 imp:p=1
373     10 -7.9 50 -51 -52 53 373 -374 imp:p=1
374     11 -7.9 50 -51 -52 53 374 -375 imp:p=1
375     10 -7.9 50 -51 -52 53 375 -376 imp:p=1
376     11 -7.9 50 -51 -52 53 376 -377 imp:p=1
377     10 -7.9 50 -51 -52 53 377 -378 imp:p=1
378     11 -7.9 50 -51 -52 53 378 -379 imp:p=1
379     10 -7.9 50 -51 -52 53 379 -380 imp:p=1
380     11 -7.9 50 -51 -52 53 380 -381 imp:p=1
381     10 -7.9 50 -51 -52 53 381 -382 imp:p=1
382     11 -7.9 50 -51 -52 53 382 -383 imp:p=1
383     10 -7.9 50 -51 -52 53 383 -384 imp:p=1
384     11 -7.9 50 -51 -52 53 384 -385 imp:p=1
385     10 -7.9 50 -51 -52 53 385 -386 imp:p=1
386     11 -7.9 50 -51 -52 53 386 -387 imp:p=1
387     10 -7.9 50 -51 -52 53 387 -388 imp:p=1
388     11 -7.9 50 -51 -52 53 388 -389 imp:p=1
389     10 -7.9 50 -51 -52 53 389 -390 imp:p=1
390     11 -7.9 50 -51 -52 53 390 -391 imp:p=1
391     10 -7.9 50 -51 -52 53 391 -392 imp:p=1
392     11 -7.9 50 -51 -52 53 392 -393 imp:p=1
393     10 -7.9 50 -51 -52 53 393 -394 imp:p=1
394     11 -7.9 50 -51 -52 53 394 -395 imp:p=1
395     10 -7.9 50 -51 -52 53 395 -396 imp:p=1
396     11 -7.9 50 -51 -52 53 396 -397 imp:p=1
397     10 -7.9 50 -51 -52 53 397 -398 imp:p=1
398     11 -7.9 50 -51 -52 53 398 -399 imp:p=1
399     10 -7.9 50 -51 -52 53 399 -400 imp:p=1
400     11 -7.9 50 -51 -52 53 400 -401 imp:p=1
401     10 -7.9 50 -51 -52 53 401 -402 imp:p=1
402     11 -7.9 50 -51 -52 53 402 -403 imp:p=1
403     10 -7.9 50 -51 -52 53 403 -404 imp:p=1
404     11 -7.9 50 -51 -52 53 404 -405 imp:p=1
405     10 -7.9 50 -51 -52 53 405 -406 imp:p=1
406     11 -7.9 50 -51 -52 53 406 -407 imp:p=1
407     10 -7.9 50 -51 -52 53 407 -408 imp:p=1
408     11 -7.9 50 -51 -52 53 408 -409 imp:p=1
409     10 -7.9 50 -51 -52 53 409 -410 imp:p=1
410     11 -7.9 50 -51 -52 53 410 -411 imp:p=1
411     10 -7.9 50 -51 -52 53 411 -412 imp:p=1
412     11 -7.9 50 -51 -52 53 412 -413 imp:p=1
413     10 -7.9 50 -51 -52 53 413 -414 imp:p=1
414     11 -7.9 50 -51 -52 53 414 -415 imp:p=1
415     10 -7.9 50 -51 -52 53 415 -416 imp:p=1
416     11 -7.9 50 -51 -52 53 416 -417 imp:p=1
417     10 -7.9 50 -51 -52 53 417 -418 imp:p=1
418     11 -7.9 50 -51 -52 53 418 -419 imp:p=1
419     10 -7.9 50 -51 -52 53 419 -420 imp:p=1
420     11 -7.9 50 -51 -52 53 420 -421 imp:p=1
421     10 -7.9 50 -51 -52 53 421 -422 imp:p=1
422     11 -7.9 50 -51 -52 53 422 -423 imp:p=1
423     10 -7.9 50 -51 -52 53 423 -424 imp:p=1
424     11 -7.9 50 -51 -52 53 424 -425 imp:p=1
425     10 -7.9 50 -51 -52 53 425 -426 imp:p=1
426     11 -7.9 50 -51 -52 53 426 -427 imp:p=1
427     10 -7.9 50 -51 -52 53 427 -428 imp:p=1
428     11 -7.9 50 -51 -52 53 428 -429 imp:p=1
429     10 -7.9 50 -51 -52 53 429 -430 imp:p=1
430     11 -7.9 50 -51 -52 53 430 -431 imp:p=1
431     10 -7.9 50 -51 -52 53 431 -432 imp:p=1
432     11 -7.9 50 -51 -52 53 432 -433 imp:p=1
433     10 -7.9 50 -51 -52 53 433 -434 imp:p=1
434     11 -7.9 50 -51 -52 53 434 -435 imp:p=1
435     10 -7.9 50 -51 -52 53 435 -436 imp:p=1
436     11 -7.9 50 -51 -52 53 436 -437 imp:p=1
437     10 -7.9 50 -51 -52 53 437 -438 imp:p=1
438     11 -7.9 50 -51 -52 53 438 -439 imp:p=1
439     10 -7.9 50 -51 -52 53 439 -440 imp:p=1
440     11 -7.9 50 -51 -52 53 440 -441 imp:p=1
441     10 -7.9 50 -51 -52 53 441 -442 imp:p=1
442     11 -7.9 50 -51 -52 53 442 -443 imp:p=1
443     10 -7.9 50 -51 -52 53 443 -444 imp:p=1
444     11 -7.9 50 -51 -52 53 444 -445 imp:p=1
445     10 -7.9 50 -51 -52 53 445 -446 imp:p=1
446     11 -7.9 50 -51 -52 53 446 -447 imp:p=1
447     10 -7.9 50 -51 -52 53 447 -448 imp:p=1
448     11 -7.9 50 -51 -52 53 448 -449 imp:p=1
449     10 -7.9 50 -51 -52 53 449 -450 imp:p=1
450     11 -7.9 50 -51 -52 53 450 -451 imp:p=1
451     10 -7.9 50 -51 -52 53 451 -452 imp:p=1
452     11 -7.9 50 -51 -52 53 452 -453 imp:p=1
453     10 -7.9 50 -51 -52 53 453 -454 imp:p=1
454     11 -7.9 50 -51 -52 53 454 -455 imp:p=1
455     10 -7.9 50 -51 -52 53 455 -456 imp:p=1
456     11 -7.9 50 -51 -52 53 456 -457 imp:p=1
457     10 -7.9 50 -51 -52 53 457 -458 imp:p=1
458     11 -7.9 50 -51 -52 53 458 -459 imp:p=1
459     10 -7.9 50 -51 -52 53 459 -460 imp:p=1
460     11 -7.9 50 -51 -52 53 460 -461 imp:p=1
461     10 -7.9 50 -51 -52 53 461 -462 imp:p=1
462     11 -7.9 50 -51 -52 53 462 -463 imp:p=1
463     10 -7.9 50 -51 -52 53 463 -464 imp:p=1
464     11 -7.9 50 -51 -52 53 464 -465 imp:p=1
465     10 -7.9 50 -51 -52 53 465 -466 imp:p=1
466     11 -7.9 50 -51 -52 53 466 -467 imp:p=1
467     10 -7.9 50 -51 -52 53 467 -468 imp:p=1
468     11 -7.9 50 -51 -52 53 468 -469 imp:p=1
469     10 -7.9 50 -51 -52 53 469 -470 imp:p=1
470     11 -7.9 50 -51 -52 53 470 -471 imp:p=1
471     10 -7.9 50 -51 -52 53 471 -472 imp:p=1
472     11 -7.9 50 -51 -52 53 472 -473 imp:p=1
473     10 -7.9 50 -51 -52 53 473 -474 imp:p=1
474     11 -7.9 50 -51 -52 53 474 -475 imp:p=1
475     10 -7.9 50 -51 -52 53 475 -476 imp:p=1
476     11 -7.9 50 -51 -52 53 476 -477 imp:p=1
477     10 -7.9 50 -51 -52 53 477 -478 imp:p=1
478     11 -7.9 50 -51 -52 53 478 -479 imp:p=1
479     10 -7.9 50 -51 -52 53 479 -480 imp:p=1
480     11 -7.9 50 -51 -52 53 480 -481 imp:p=1
481     10 -7.9 50 -51 -52 53 481 -482 imp:p=1
482     11 -7.9 50 -51 -52 53 482 -483 imp:p=1
483     10 -7.9 50 -51 -52 53 483 -484 imp:p=1
501     21 -0.00127 -50 60 -52 53 101 -102 imp:p=1
502     20 -19.3 -50 60 -52 53 102 -103 imp:p=1
503     21 -0.00127 -50 60 -52 53 103 -104 imp:p=1
504     20 -19.3 -50 60 -52 53 104 -105 imp:p=1
505     21 -0.00127 -50 60 -52 53 105 -106 imp:p=1
506     20 -19.3 -50 60 -52 53 106 -107 imp:p=1
507     21 -0.00127 -50 60 -52 53 107 -108 imp:p=1
508     20 -19.3 -50 60 -52 53 108 -109 imp:p=1
509     21 -0.00127 -50 60 -52 53 109 -110 imp:p=1
510     20 -19.3 -50 60 -52 53 110 -111 imp:p=1
511     21 -0.00127 -50 60 -52 53 111 -112 imp:p=1
512     20 -19.3 -50 60 -52 53 112 -113 imp:p=1
513     21 -0.00127 -50 60 -52 53 113 -114 imp:p=1
514     20 -19.3 -50 60 -52 53 114 -115 imp:p=1
515     21 -0.00127 -50 60 -52 53 115 -116 imp:p=1
516     20 -19.3 -50 60 -52 53 116 -117 imp:p=1
517     21 -0.00127 -50 60 -52 53 117 -118 imp:p=1
518     20 -19.3 -50 60 -52 53 118 -119 imp:p=1
519     21 -0.00127 -50 60 -52 53 119 -120 imp:p=1
520     20 -19.3 -50 60 -52 53 120 -121 imp:p=1
521     21 -0.00127 -50 60 -52 53 121 -122 imp:p=1
522     20 -19.3 -50 60 -52 53 122 -123 imp:p=1
523     21 -0.00127 -50 60 -52 53 123 -124 imp:p=1
524     20 -19.3 -50 60 -52 53 124 -125 imp:p=1
525     21 -0.00127 -50 60 -52 53 125 -126 imp:p=1
526     20 -19.3 -50 60 -52 53 126 -127 imp:p=1
527     21 -0.00127 -50 60 -52 53 127 -128 imp:p=1
528     20 -19.3 -50 60 -52 53 128 -129 imp:p=1
```

```
529       21 -0.00127 -50 60 -52 53 129 -130
imp:p=1
530     20 -19.3 -50 60 -52 53 130 -131 imp:p=1
531       21 -0.00127 -50 60 -52 53 131 -132
imp:p=1
532     20 -19.3 -50 60 -52 53 132 -133 imp:p=1
533       21 -0.00127 -50 60 -52 53 133 -134
imp:p=1
534     20 -19.3 -50 60 -52 53 134 -135 imp:p=1
535       21 -0.00127 -50 60 -52 53 135 -136
imp:p=1
536     20 -19.3 -50 60 -52 53 136 -137 imp:p=1
537       21 -0.00127 -50 60 -52 53 137 -138
imp:p=1
538     20 -19.3 -50 60 -52 53 138 -139 imp:p=1
539       21 -0.00127 -50 60 -52 53 139 -140
imp:p=1
540     20 -19.3 -50 60 -52 53 140 -141 imp:p=1
541       21 -0.00127 -50 60 -52 53 141 -142
imp:p=1
542     20 -19.3 -50 60 -52 53 142 -143 imp:p=1
543       21 -0.00127 -50 60 -52 53 143 -144
imp:p=1
544     20 -19.3 -50 60 -52 53 144 -145 imp:p=1
545       21 -0.00127 -50 60 -52 53 145 -146
imp:p=1
546     20 -19.3 -50 60 -52 53 146 -147 imp:p=1
547       21 -0.00127 -50 60 -52 53 147 -148
imp:p=1
548     20 -19.3 -50 60 -52 53 148 -149 imp:p=1
549       21 -0.00127 -50 60 -52 53 149 -150
imp:p=1
550     20 -19.3 -50 60 -52 53 150 -151 imp:p=1
551       21 -0.00127 -50 60 -52 53 151 -152
imp:p=1
552     20 -19.3 -50 60 -52 53 152 -153 imp:p=1
553       21 -0.00127 -50 60 -52 53 153 -154
imp:p=1
554     20 -19.3 -50 60 -52 53 154 -155 imp:p=1
555       21 -0.00127 -50 60 -52 53 155 -156
imp:p=1
556     20 -19.3 -50 60 -52 53 156 -157 imp:p=1
557       21 -0.00127 -50 60 -52 53 157 -158
imp:p=1
558     20 -19.3 -50 60 -52 53 158 -159 imp:p=1
559       21 -0.00127 -50 60 -52 53 159 -160
imp:p=1
560     20 -19.3 -50 60 -52 53 160 -161 imp:p=1
561       21 -0.00127 -50 60 -52 53 161 -162
imp:p=1
562     20 -19.3 -50 60 -52 53 162 -163 imp:p=1
563       21 -0.00127 -50 60 -52 53 163 -164
imp:p=1
564     20 -19.3 -50 60 -52 53 164 -165 imp:p=1
565       21 -0.00127 -50 60 -52 53 165 -166
imp:p=1
566     20 -19.3 -50 60 -52 53 166 -167 imp:p=1
567       21 -0.00127 -50 60 -52 53 167 -168
imp:p=1
568     20 -19.3 -50 60 -52 53 168 -169 imp:p=1
569       21 -0.00127 -50 60 -52 53 169 -170
imp:p=1
570     20 -19.3 -50 60 -52 53 170 -171 imp:p=1
571       21 -0.00127 -50 60 -52 53 171 -172
imp:p=1
572     20 -19.3 -50 60 -52 53 172 -173 imp:p=1
573       21 -0.00127 -50 60 -52 53 173 -174
imp:p=1
574     20 -19.3 -50 60 -52 53 174 -175 imp:p=1
575       21 -0.00127 -50 60 -52 53 175 -176
imp:p=1
576     20 -19.3 -50 60 -52 53 176 -177 imp:p=1
577       21 -0.00127 -50 60 -52 53 177 -178
imp:p=1
578     20 -19.3 -50 60 -52 53 178 -179 imp:p=1
579     21 -0.00127 -50 60 -52 53 179 -180 imp:p=1
580     20 -19.3 -50 60 -52 53 180 -181 imp:p=1
581     21 -0.00127 -50 60 -52 53 181 -182 imp:p=1
582     20 -19.3 -50 60 -52 53 182 -183 imp:p=1
583     21 -0.00127 -50 60 -52 53 183 -184 imp:p=1
584     20 -19.3 -50 60 -52 53 184 -185 imp:p=1
585     21 -0.00127 -50 60 -52 53 185 -186 imp:p=1
586     20 -19.3 -50 60 -52 53 186 -187 imp:p=1
587     21 -0.00127 -50 60 -52 53 187 -188 imp:p=1
588     20 -19.3 -50 60 -52 53 188 -189 imp:p=1
589     21 -0.00127 -50 60 -52 53 189 -190 imp:p=1
590     20 -19.3 -50 60 -52 53 190 -191 imp:p=1
591     21 -0.00127 -50 60 -52 53 191 -192 imp:p=1
592     20 -19.3 -50 60 -52 53 192 -193 imp:p=1
593     21 -0.00127 -50 60 -52 53 193 -194 imp:p=1
594     20 -19.3 -50 60 -52 53 194 -195 imp:p=1
595     21 -0.00127 -50 60 -52 53 195 -196 imp:p=1
596     20 -19.3 -50 60 -52 53 196 -197 imp:p=1
597     21 -0.00127 -50 60 -52 53 197 -198 imp:p=1
598     20 -19.3 -50 60 -52 53 198 -199 imp:p=1
599     21 -0.00127 -50 60 -52 53 199 -200 imp:p=1
600     20 -19.3 -50 60 -52 53 200 -201 imp:p=1
601     21 -0.00127 -50 60 -52 53 201 -202 imp:p=1
602     20 -19.3 -50 60 -52 53 202 -203 imp:p=1
603     21 -0.00127 -50 60 -52 53 203 -204 imp:p=1
604     20 -19.3 -50 60 -52 53 204 -205 imp:p=1
605     21 -0.00127 -50 60 -52 53 205 -206 imp:p=1
606     20 -19.3 -50 60 -52 53 206 -207 imp:p=1
607     21 -0.00127 -50 60 -52 53 207 -208 imp:p=1
608     20 -19.3 -50 60 -52 53 208 -209 imp:p=1
609     21 -0.00127 -50 60 -52 53 209 -210 imp:p=1
610     20 -19.3 -50 60 -52 53 210 -211 imp:p=1
611     21 -0.00127 -50 60 -52 53 211 -212 imp:p=1
612     20 -19.3 -50 60 -52 53 212 -213 imp:p=1
613     21 -0.00127 -50 60 -52 53 213 -214 imp:p=1
614     20 -19.3 -50 60 -52 53 214 -215 imp:p=1
615     21 -0.00127 -50 60 -52 53 215 -216 imp:p=1
616     20 -19.3 -50 60 -52 53 216 -217 imp:p=1
617     21 -0.00127 -50 60 -52 53 217 -218 imp:p=1
618     20 -19.3 -50 60 -52 53 218 -219 imp:p=1
619     21 -0.00127 -50 60 -52 53 219 -220 imp:p=1
620     20 -19.3 -50 60 -52 53 220 -221 imp:p=1
621     21 -0.00127 -50 60 -52 53 221 -222 imp:p=1
622     20 -19.3 -50 60 -52 53 222 -223 imp:p=1
623     21 -0.00127 -50 60 -52 53 223 -224 imp:p=1
624     20 -19.3 -50 60 -52 53 224 -225 imp:p=1
625     21 -0.00127 -50 60 -52 53 225 -226 imp:p=1
626     20 -19.3 -50 60 -52 53 226 -227 imp:p=1
627     21 -0.00127 -50 60 -52 53 227 -228 imp:p=1
628     20 -19.3 -50 60 -52 53 228 -229 imp:p=1
629     21 -0.00127 -50 60 -52 53 229 -230 imp:p=1
630     20 -19.3 -50 60 -52 53 230 -231 imp:p=1
631     21 -0.00127 -50 60 -52 53 231 -232 imp:p=1
632     20 -19.3 -50 60 -52 53 232 -233 imp:p=1
633     21 -0.00127 -50 60 -52 53 233 -234 imp:p=1
634     20 -19.3 -50 60 -52 53 234 -235 imp:p=1
635     21 -0.00127 -50 60 -52 53 235 -236 imp:p=1
636     20 -19.3 -50 60 -52 53 236 -237 imp:p=1
637     21 -0.00127 -50 60 -52 53 237 -238 imp:p=1
638     20 -19.3 -50 60 -52 53 238 -239 imp:p=1
639     21 -0.00127 -50 60 -52 53 239 -240 imp:p=1
640     20 -19.3 -50 60 -52 53 240 -241 imp:p=1
641     21 -0.00127 -50 60 -52 53 241 -242 imp:p=1
642     20 -19.3 -50 60 -52 53 242 -243 imp:p=1
643     21 -0.00127 -50 60 -52 53 243 -244 imp:p=1
644     20 -19.3 -50 60 -52 53 244 -245 imp:p=1
645     21 -0.00127 -50 60 -52 53 245 -246 imp:p=1
646     20 -19.3 -50 60 -52 53 246 -247 imp:p=1
647     21 -0.00127 -50 60 -52 53 247 -248 imp:p=1
648     20 -19.3 -50 60 -52 53 248 -249 imp:p=1
649     21 -0.00127 -50 60 -52 53 249 -250 imp:p=1
650     20 -19.3 -50 60 -52 53 250 -251 imp:p=1
651     21 -0.00127 -50 60 -52 53 251 -252 imp:p=1
652     20 -19.3 -50 60 -52 53 252 -253 imp:p=1
653     21 -0.00127 -50 60 -52 53 253 -254 imp:p=1
654     20 -19.3 -50 60 -52 53 254 -255 imp:p=1
```

```
655       21  -0.00127  -50  60  -52  53  255  -256
imp:p=1
656     20 -19.3 -50 60 -52 53 256 -257 imp:p=1
657       21  -0.00127  -50  60  -52  53  257  -258
imp:p=1
658     20 -19.3 -50 60 -52 53 258 -259 imp:p=1
659       21  -0.00127  -50  60  -52  53  259  -260
imp:p=1
660     20 -19.3 -50 60 -52 53 260 -261 imp:p=1
661       21  -0.00127  -50  60  -52  53  261  -262
imp:p=1
662     20 -19.3 -50 60 -52 53 262 -263 imp:p=1
663       21  -0.00127  -50  60  -52  53  263  -264
imp:p=1
664     20 -19.3 -50 60 -52 53 264 -265 imp:p=1
665       21  -0.00127  -50  60  -52  53  265  -266
imp:p=1
666     20 -19.3 -50 60 -52 53 266 -267 imp:p=1
667       21  -0.00127  -50  60  -52  53  267  -268
imp:p=1
668     20 -19.3 -50 60 -52 53 268 -269 imp:p=1
669       21  -0.00127  -50  60  -52  53  269  -270
imp:p=1
670     20 -19.3 -50 60 -52 53 270 -271 imp:p=1
671       21  -0.00127  -50  60  -52  53  271  -272
imp:p=1
672     20 -19.3 -50 60 -52 53 272 -273 imp:p=1
673       21  -0.00127  -50  60  -52  53  273  -274
imp:p=1
674     20 -19.3 -50 60 -52 53 274 -275 imp:p=1
675       21  -0.00127  -50  60  -52  53  275  -276
imp:p=1
676     20 -19.3 -50 60 -52 53 276 -277 imp:p=1
677       21  -0.00127  -50  60  -52  53  277  -278
imp:p=1
678     20 -19.3 -50 60 -52 53 278 -279 imp:p=1
679       21  -0.00127  -50  60  -52  53  279  -280
imp:p=1
680     20 -19.3 -50 60 -52 53 280 -281 imp:p=1
681       21  -0.00127  -50  60  -52  53  281  -282
imp:p=1
682     20 -19.3 -50 60 -52 53 282 -283 imp:p=1
683       21  -0.00127  -50  60  -52  53  283  -284
imp:p=1
684     20 -19.3 -50 60 -52 53 284 -285 imp:p=1
685       21  -0.00127  -50  60  -52  53  285  -286
imp:p=1
686     20 -19.3 -50 60 -52 53 286 -287 imp:p=1
687       21  -0.00127  -50  60  -52  53  287  -288
imp:p=1
688     20 -19.3 -50 60 -52 53 288 -289 imp:p=1
689       21  -0.00127  -50  60  -52  53  289  -290
imp:p=1
690     20 -19.3 -50 60 -52 53 290 -291 imp:p=1
691       21  -0.00127  -50  60  -52  53  291  -292
imp:p=1
692     20 -19.3 -50 60 -52 53 292 -293 imp:p=1
693       21  -0.00127  -50  60  -52  53  293  -294
imp:p=1
694     20 -19.3 -50 60 -52 53 294 -295 imp:p=1
695       21  -0.00127  -50  60  -52  53  295  -296
imp:p=1
696     20 -19.3 -50 60 -52 53 296 -297 imp:p=1
697       21  -0.00127  -50  60  -52  53  297  -298
imp:p=1
698     20 -19.3 -50 60 -52 53 298 -299 imp:p=1
699       21  -0.00127  -50  60  -52  53  299  -300
imp:p=1
700     20 -19.3 -50 60 -52 53 300 -301 imp:p=1
701       21  -0.00127  -50  60  -52  53  301  -302
imp:p=1
702     20 -19.3 -50 60 -52 53 302 -303 imp:p=1
703       21  -0.00127  -50  60  -52  53  303  -304
imp:p=1
704     20 -19.3 -50 60 -52 53 304 -305 imp:p=1
705     21 -0.00127 -50 60 -52 53 305 -306 imp:p=1
706     20 -19.3 -50 60 -52 53 306 -307 imp:p=1
707     21 -0.00127 -50 60 -52 53 307 -308 imp:p=1
708     20 -19.3 -50 60 -52 53 308 -309 imp:p=1
709     21 -0.00127 -50 60 -52 53 309 -310 imp:p=1
710     20 -19.3 -50 60 -52 53 310 -311 imp:p=1
711     21 -0.00127 -50 60 -52 53 311 -312 imp:p=1
712     20 -19.3 -50 60 -52 53 312 -313 imp:p=1
713     21 -0.00127 -50 60 -52 53 313 -314 imp:p=1
714     20 -19.3 -50 60 -52 53 314 -315 imp:p=1
715     21 -0.00127 -50 60 -52 53 315 -316 imp:p=1
716     20 -19.3 -50 60 -52 53 316 -317 imp:p=1
717     21 -0.00127 -50 60 -52 53 317 -318 imp:p=1
718     20 -19.3 -50 60 -52 53 318 -319 imp:p=1
719     21 -0.00127 -50 60 -52 53 319 -320 imp:p=1
720     20 -19.3 -50 60 -52 53 320 -321 imp:p=1
721     21 -0.00127 -50 60 -52 53 321 -322 imp:p=1
722     20 -19.3 -50 60 -52 53 322 -323 imp:p=1
723     21 -0.00127 -50 60 -52 53 323 -324 imp:p=1
724     20 -19.3 -50 60 -52 53 324 -325 imp:p=1
725     21 -0.00127 -50 60 -52 53 325 -326 imp:p=1
726     20 -19.3 -50 60 -52 53 326 -327 imp:p=1
727     21 -0.00127 -50 60 -52 53 327 -328 imp:p=1
728     20 -19.3 -50 60 -52 53 328 -329 imp:p=1
729     21 -0.00127 -50 60 -52 53 329 -330 imp:p=1
730     20 -19.3 -50 60 -52 53 330 -331 imp:p=1
731     21 -0.00127 -50 60 -52 53 331 -332 imp:p=1
732     20 -19.3 -50 60 -52 53 332 -333 imp:p=1
733     21 -0.00127 -50 60 -52 53 333 -334 imp:p=1
734     20 -19.3 -50 60 -52 53 334 -335 imp:p=1
735     21 -0.00127 -50 60 -52 53 335 -336 imp:p=1
736     20 -19.3 -50 60 -52 53 336 -337 imp:p=1
737     21 -0.00127 -50 60 -52 53 337 -338 imp:p=1
738     20 -19.3 -50 60 -52 53 338 -339 imp:p=1
739     21 -0.00127 -50 60 -52 53 339 -340 imp:p=1
740     20 -19.3 -50 60 -52 53 340 -341 imp:p=1
741     21 -0.00127 -50 60 -52 53 341 -342 imp:p=1
742     20 -19.3 -50 60 -52 53 342 -343 imp:p=1
743     21 -0.00127 -50 60 -52 53 343 -344 imp:p=1
744     20 -19.3 -50 60 -52 53 344 -345 imp:p=1
745     21 -0.00127 -50 60 -52 53 345 -346 imp:p=1
746     20 -19.3 -50 60 -52 53 346 -347 imp:p=1
747     21 -0.00127 -50 60 -52 53 347 -348 imp:p=1
748     20 -19.3 -50 60 -52 53 348 -349 imp:p=1
749     21 -0.00127 -50 60 -52 53 349 -350 imp:p=1
750     20 -19.3 -50 60 -52 53 350 -351 imp:p=1
751     21 -0.00127 -50 60 -52 53 351 -352 imp:p=1
752     20 -19.3 -50 60 -52 53 352 -353 imp:p=1
753     21 -0.00127 -50 60 -52 53 353 -354 imp:p=1
754     20 -19.3 -50 60 -52 53 354 -355 imp:p=1
755     21 -0.00127 -50 60 -52 53 355 -356 imp:p=1
756     20 -19.3 -50 60 -52 53 356 -357 imp:p=1
757     21 -0.00127 -50 60 -52 53 357 -358 imp:p=1
758     20 -19.3 -50 60 -52 53 358 -359 imp:p=1
759     21 -0.00127 -50 60 -52 53 359 -360 imp:p=1
760     20 -19.3 -50 60 -52 53 360 -361 imp:p=1
761     21 -0.00127 -50 60 -52 53 361 -362 imp:p=1
762     20 -19.3 -50 60 -52 53 362 -363 imp:p=1
763     21 -0.00127 -50 60 -52 53 363 -364 imp:p=1
764     20 -19.3 -50 60 -52 53 364 -365 imp:p=1
765     21 -0.00127 -50 60 -52 53 365 -366 imp:p=1
766     20 -19.3 -50 60 -52 53 366 -367 imp:p=1
767     21 -0.00127 -50 60 -52 53 367 -368 imp:p=1
768     20 -19.3 -50 60 -52 53 368 -369 imp:p=1
769     21 -0.00127 -50 60 -52 53 369 -370 imp:p=1
770     20 -19.3 -50 60 -52 53 370 -371 imp:p=1
771     21 -0.00127 -50 60 -52 53 371 -372 imp:p=1
772     20 -19.3 -50 60 -52 53 372 -373 imp:p=1
773     21 -0.00127 -50 60 -52 53 373 -374 imp:p=1
774     20 -19.3 -50 60 -52 53 374 -375 imp:p=1
775     21 -0.00127 -50 60 -52 53 375 -376 imp:p=1
776     20 -19.3 -50 60 -52 53 376 -377 imp:p=1
777     21 -0.00127 -50 60 -52 53 377 -378 imp:p=1
778     20 -19.3 -50 60 -52 53 378 -379 imp:p=1
779     21 -0.00127 -50 60 -52 53 379 -380 imp:p=1
780     20 -19.3 -50 60 -52 53 380 -381 imp:p=1
```

```
781        21  -0.00127  -50  60  -52  53  381  -382
imp:p=1
782     20 -19.3 -50 60 -52 53 382 -383 imp:p=1
783        21  -0.00127  -50  60  -52  53  383  -384
imp:p=1
784     20 -19.3 -50 60 -52 53 384 -385 imp:p=1
785        21  -0.00127  -50  60  -52  53  385  -386
imp:p=1
786     20 -19.3 -50 60 -52 53 386 -387 imp:p=1
787        21  -0.00127  -50  60  -52  53  387  -388
imp:p=1
788     20 -19.3 -50 60 -52 53 388 -389 imp:p=1
789        21  -0.00127  -50  60  -52  53  389  -390
imp:p=1
790     20 -19.3 -50 60 -52 53 390 -391 imp:p=1
791        21  -0.00127  -50  60  -52  53  391  -392
imp:p=1
792     20 -19.3 -50 60 -52 53 392 -393 imp:p=1
793        21  -0.00127  -50  60  -52  53  393  -394
imp:p=1
794     20 -19.3 -50 60 -52 53 394 -395 imp:p=1
795        21  -0.00127  -50  60  -52  53  395  -396
imp:p=1
796     20 -19.3 -50 60 -52 53 396 -397 imp:p=1
797        21  -0.00127  -50  60  -52  53  397  -398
imp:p=1
798     20 -19.3 -50 60 -52 53 398 -399 imp:p=1
799        21  -0.00127  -50  60  -52  53  399  -400
imp:p=1
800     20 -19.3 -50 60 -52 53 400 -401 imp:p=1
801        21  -0.00127  -50  60  -52  53  401  -402
imp:p=1
802     20 -19.3 -50 60 -52 53 402 -403 imp:p=1
803        21  -0.00127  -50  60  -52  53  403  -404
imp:p=1
804     20 -19.3 -50 60 -52 53 404 -405 imp:p=1
805        21  -0.00127  -50  60  -52  53  405  -406
imp:p=1
806     20 -19.3 -50 60 -52 53 406 -407 imp:p=1
807        21  -0.00127  -50  60  -52  53  407  -408
imp:p=1
808     20 -19.3 -50 60 -52 53 408 -409 imp:p=1
809        21  -0.00127  -50  60  -52  53  409  -410
imp:p=1
810     20 -19.3 -50 60 -52 53 410 -411 imp:p=1
811        21  -0.00127  -50  60  -52  53  411  -412
imp:p=1
812     20 -19.3 -50 60 -52 53 412 -413 imp:p=1
813        21  -0.00127  -50  60  -52  53  413  -414
imp:p=1
814     20 -19.3 -50 60 -52 53 414 -415 imp:p=1
815        21  -0.00127  -50  60  -52  53  415  -416
imp:p=1
816     20 -19.3 -50 60 -52 53 416 -417 imp:p=1
817        21  -0.00127  -50  60  -52  53  417  -418
imp:p=1
818     20 -19.3 -50 60 -52 53 418 -419 imp:p=1
819        21  -0.00127  -50  60  -52  53  419  -420
imp:p=1
820     20 -19.3 -50 60 -52 53 420 -421 imp:p=1
821        21  -0.00127  -50  60  -52  53  421  -422
imp:p=1
822     20 -19.3 -50 60 -52 53 422 -423 imp:p=1
823        21  -0.00127  -50  60  -52  53  423  -424
imp:p=1
824     20 -19.3 -50 60 -52 53 424 -425 imp:p=1
825        21  -0.00127  -50  60  -52  53  425  -426
imp:p=1
826     20 -19.3 -50 60 -52 53 426 -427 imp:p=1
827        21  -0.00127  -50  60  -52  53  427  -428
imp:p=1
828     20 -19.3 -50 60 -52 53 428 -429 imp:p=1
829        21  -0.00127  -50  60  -52  53  429  -430
imp:p=1
830     20 -19.3 -50 60 -52 53 430 -431 imp:p=1
831     21 -0.00127 -50 60 -52 53 431 -432 imp:p=1
832     20 -19.3 -50 60 -52 53 432 -433 imp:p=1
833     21 -0.00127 -50 60 -52 53 433 -434 imp:p=1
834     20 -19.3 -50 60 -52 53 434 -435 imp:p=1
835     21 -0.00127 -50 60 -52 53 435 -436 imp:p=1
836     20 -19.3 -50 60 -52 53 436 -437 imp:p=1
837     21 -0.00127 -50 60 -52 53 437 -438 imp:p=1
838     20 -19.3 -50 60 -52 53 438 -439 imp:p=1
839     21 -0.00127 -50 60 -52 53 439 -440 imp:p=1
840     20 -19.3 -50 60 -52 53 440 -441 imp:p=1
841     21 -0.00127 -50 60 -52 53 441 -442 imp:p=1
842     20 -19.3 -50 60 -52 53 442 -443 imp:p=1
843     21 -0.00127 -50 60 -52 53 443 -444 imp:p=1
844     20 -19.3 -50 60 -52 53 444 -445 imp:p=1
845     21 -0.00127 -50 60 -52 53 445 -446 imp:p=1
846     20 -19.3 -50 60 -52 53 446 -447 imp:p=1
847     21 -0.00127 -50 60 -52 53 447 -448 imp:p=1
848     20 -19.3 -50 60 -52 53 448 -449 imp:p=1
849     21 -0.00127 -50 60 -52 53 449 -450 imp:p=1
850     20 -19.3 -50 60 -52 53 450 -451 imp:p=1
851     21 -0.00127 -50 60 -52 53 451 -452 imp:p=1
852     20 -19.3 -50 60 -52 53 452 -453 imp:p=1
853     21 -0.00127 -50 60 -52 53 453 -454 imp:p=1
854     20 -19.3 -50 60 -52 53 454 -455 imp:p=1
855     21 -0.00127 -50 60 -52 53 455 -456 imp:p=1
856     20 -19.3 -50 60 -52 53 456 -457 imp:p=1
857     21 -0.00127 -50 60 -52 53 457 -458 imp:p=1
858     20 -19.3 -50 60 -52 53 458 -459 imp:p=1
859     21 -0.00127 -50 60 -52 53 459 -460 imp:p=1
860     20 -19.3 -50 60 -52 53 460 -461 imp:p=1
861     21 -0.00127 -50 60 -52 53 461 -462 imp:p=1
862     20 -19.3 -50 60 -52 53 462 -463 imp:p=1
863     21 -0.00127 -50 60 -52 53 463 -464 imp:p=1
864     20 -19.3 -50 60 -52 53 464 -465 imp:p=1
865     21 -0.00127 -50 60 -52 53 465 -466 imp:p=1
866     20 -19.3 -50 60 -52 53 466 -467 imp:p=1
867     21 -0.00127 -50 60 -52 53 467 -468 imp:p=1
868     20 -19.3 -50 60 -52 53 468 -469 imp:p=1
869     21 -0.00127 -50 60 -52 53 469 -470 imp:p=1
870     20 -19.3 -50 60 -52 53 470 -471 imp:p=1
871     21 -0.00127 -50 60 -52 53 471 -472 imp:p=1
872     20 -19.3 -50 60 -52 53 472 -473 imp:p=1
873     21 -0.00127 -50 60 -52 53 473 -474 imp:p=1
874     20 -19.3 -50 60 -52 53 474 -475 imp:p=1
875     21 -0.00127 -50 60 -52 53 475 -476 imp:p=1
876     20 -19.3 -50 60 -52 53 476 -477 imp:p=1
877     21 -0.00127 -50 60 -52 53 477 -478 imp:p=1
878     20 -19.3 -50 60 -52 53 478 -479 imp:p=1
879     21 -0.00127 -50 60 -52 53 479 -480 imp:p=1
880     20 -19.3 -50 60 -52 53 480 -481 imp:p=1
881     21 -0.00127 -50 60 -52 53 481 -482 imp:p=1
882     20 -19.3 -50 60 -52 53 482 -483 imp:p=1
883     21 -0.00127 -50 60 -52 53 483 -484 imp:p=1
900      0 14 -15 16 -17 -12 13 imp:p=1

1       cz 7.6
2       cz 9.5
3       cz 10.5
4       cz 13.4
5       cz 25.4
6       cz 25.52
7       pz 15
8       pz -15
11       sx -50 .1
12       p -1 0 -84.5 50
13       p 1 0 -84.5 -50
14      sx -50 .09
15      sx -50 .11
16      p 0.00109083 1 0 -0.05454159
17      p -0.00109083 1 0 0.05454159
30      so 1000.0
41      pz 5.08
42      pz -5.08
44      c/z -50 0 86.66
50      c/z -50 0 84.5
51      c/z -50 0 84.8
```

```
52      pz 1
53      pz -1
60      c/z -50 0 76.5
101     p 0.441313 1 0 -22.0657
102     p 0.438709 1 0 -21.9355
103     p 0.436110 1 0 -21.8055
104     p 0.433516 1 0 -21.6758
105     p 0.430927 1 0 -21.5463
106     p 0.428342 1 0 -21.4171
107     p 0.425763 1 0 -21.2881
108     p 0.423188 1 0 -21.1594
109     p 0.420618 1 0 -21.0309
110     p 0.418053 1 0 -20.9026
111     p 0.415492 1 0 -20.7746
112     p 0.412936 1 0 -20.6468
113     p 0.410385 1 0 -20.5192
114     p 0.407838 1 0 -20.3919
115     p 0.405296 1 0 -20.2648
116     p 0.402758 1 0 -20.1379
117     p 0.400225 1 0 -20.0112
118     p 0.397696 1 0 -19.8848
119     p 0.395171 1 0 -19.7586
120     p 0.392651 1 0 -19.6325
121     p 0.390135 1 0 -19.5068
122     p 0.387623 1 0 -19.3812
123     p 0.385116 1 0 -19.2558
124     p 0.382613 1 0 -19.1306
125     p 0.380114 1 0 -19.0057
126     p 0.377619 1 0 -18.8810
127     p 0.375129 1 0 -18.7564
128     p 0.372642 1 0 -18.6321
129     p 0.370159 1 0 -18.5080
130     p 0.367681 1 0 -18.3840
131     p 0.365206 1 0 -18.2603
132     p 0.362735 1 0 -18.1368
133     p 0.360269 1 0 -18.0134
134     p 0.357806 1 0 -17.8903
135     p 0.355347 1 0 -17.7673
136     p 0.352891 1 0 -17.6446
137     p 0.350440 1 0 -17.5220
138     p 0.347992 1 0 -17.3996
139     p 0.345548 1 0 -17.2774
140     p 0.343108 1 0 -17.1554
141     p 0.340671 1 0 -17.0336
142     p 0.338238 1 0 -16.9119
143     p 0.335809 1 0 -16.7904
144     p 0.333383 1 0 -16.6691
145     p 0.330960 1 0 -16.5480
146     p 0.328542 1 0 -16.4271
147     p 0.326126 1 0 -16.3063
148     p 0.323714 1 0 -16.1857
149     p 0.321306 1 0 -16.0653
150     p 0.318900 1 0 -15.9450
151     p 0.316498 1 0 -15.8249
152     p 0.314100 1 0 -15.7050
153     p 0.311705 1 0 -15.5852
154     p 0.309313 1 0 -15.4656
155     p 0.306924 1 0 -15.3462
156     p 0.304538 1 0 -15.2269
157     p 0.302156 1 0 -15.1078
158     p 0.299777 1 0 -14.9888
159     p 0.297400 1 0 -14.8700
160     p 0.295027 1 0 -14.7514
161     p 0.292657 1 0 -14.6329
162     p 0.290290 1 0 -14.5145
163     p 0.287926 1 0 -14.3963
164     p 0.285565 1 0 -14.2783
165     p 0.283207 1 0 -14.1604
166     p 0.280852 1 0 -14.0426
167     p 0.278500 1 0 -13.9250
168     p 0.276150 1 0 -13.8075
169     p 0.273804 1 0 -13.6902
170     p 0.271460 1 0 -13.5730
171     p 0.269119 1 0 -13.4559
172     p 0.266780 1 0 -13.3390
173     p 0.264445 1 0 -13.2222
174     p 0.262112 1 0 -13.1056
175     p 0.259782 1 0 -12.9891
176     p 0.257454 1 0 -12.8727
177     p 0.255129 1 0 -12.7565
178     p 0.252807 1 0 -12.6403
179     p 0.250487 1 0 -12.5243
180     p 0.248170 1 0 -12.4085
181     p 0.245855 1 0 -12.2927
182     p 0.243543 1 0 -12.1771
183     p 0.241233 1 0 -12.0616
184     p 0.238925 1 0 -11.9463
185     p 0.236620 1 0 -11.8310
186     p 0.234318 1 0 -11.7159
187     p 0.232017 1 0 -11.6009
188     p 0.229720 1 0 -11.4860
189     p 0.227424 1 0 -11.3712
190     p 0.225131 1 0 -11.2565
191     p 0.222839 1 0 -11.1420
192     p 0.220551 1 0 -11.0275
193     p 0.218264 1 0 -10.9132
194     p 0.215979 1 0 -10.7990
195     p 0.213697 1 0 -10.6848
196     p 0.211417 1 0 -10.5708
197     p 0.209139 1 0 -10.4569
198     p 0.206863 1 0 -10.3431
199     p 0.204589 1 0 -10.2294
200     p 0.202317 1 0 -10.1158
201     p 0.200047 1 0 -10.0023
202     p 0.197779 1 0 -9.88893
203     p 0.195513 1 0 -9.77563
204     p 0.193249 1 0 -9.66243
205     p 0.190986 1 0 -9.54932
206     p 0.188726 1 0 -9.43630
207     p 0.186468 1 0 -9.32338
208     p 0.184211 1 0 -9.21055
209     p 0.181956 1 0 -9.09781
210     p 0.179703 1 0 -8.98516
211     p 0.177452 1 0 -8.87260
212     p 0.175202 1 0 -8.76012
213     p 0.172955 1 0 -8.64773
214     p 0.170709 1 0 -8.53543
215     p 0.168464 1 0 -8.42321
216     p 0.166221 1 0 -8.31107
217     p 0.163980 1 0 -8.19902
218     p 0.161741 1 0 -8.08704
219     p 0.159503 1 0 -7.97514
220     p 0.157266 1 0 -7.86332
221     p 0.155032 1 0 -7.75158
222     p 0.152798 1 0 -7.63991
223     p 0.150566 1 0 -7.52832
224     p 0.148336 1 0 -7.41680
225     p 0.146107 1 0 -7.30535
226     p 0.143880 1 0 -7.19397
227     p 0.141653 1 0 -7.08267
228     p 0.139429 1 0 -6.97143
229     p 0.137205 1 0 -6.86026
230     p 0.134983 1 0 -6.74916
231     p 0.132762 1 0 -6.63812
232     p 0.130543 1 0 -6.52715
233     p 0.128325 1 0 -6.41624
234     p 0.126108 1 0 -6.30539
235     p 0.123892 1 0 -6.19460
236     p 0.121677 1 0 -6.08387
237     p 0.119464 1 0 -5.97320
238     p 0.117252 1 0 -5.86259
239     p 0.115041 1 0 -5.75204
240     p 0.112831 1 0 -5.64154
241     p 0.110622 1 0 -5.53109
242     p 0.108414 1 0 -5.42070
243     p 0.106207 1 0 -5.31036
244     p 0.104001 1 0 -5.20007
245     p 0.101797 1 0 -5.08984
246     p 0.0995929 1 0 -4.97965
247     p 0.0973901 1 0 -4.86951
248     p 0.0951882 1 0 -4.75941
249     p 0.0929872 1 0 -4.64936
```

```
250     p 0.0907872 1 0 -4.53936
251     p 0.0885879 1 0 -4.42940
252     p 0.0863896 1 0 -4.31948
253     p 0.0841921 1 0 -4.20960
254     p 0.0819953 1 0 -4.09977
255     p 0.0797994 1 0 -3.98997
256     p 0.0776042 1 0 -3.88021
257     p 0.0754098 1 0 -3.77049
258     p 0.0732161 1 0 -3.66080
259     p 0.0710231 1 0 -3.55115
260     p 0.0688307 1 0 -3.44154
261     p 0.0666391 1 0 -3.33195
262     p 0.0644480 1 0 -3.22240
263     p 0.0622576 1 0 -3.11288
264     p 0.0600678 1 0 -3.00339
265     p 0.0578785 1 0 -2.89393
266     p 0.0556898 1 0 -2.78449
267     p 0.0535017 1 0 -2.67508
268     p 0.0513140 1 0 -2.56570
269     p 0.0491269 1 0 -2.45634
270     p 0.0469402 1 0 -2.34701
271     p 0.0447539 1 0 -2.23770
272     p 0.0425681 1 0 -2.12840
273     p 0.0403827 1 0 -2.01913
274     p 0.0381976 1 0 -1.90988
275     p 0.0360130 1 0 -1.80065
276     p 0.0338287 1 0 -1.69143
277     p 0.0316446 1 0 -1.58223
278     p 0.0294610 1 0 -1.47305
279     p 0.0272775 1 0 -1.36388
280     p 0.0250944 1 0 -1.25472
281     p 0.0229115 1 0 -1.14557
282     p 0.0207288 1 0 -1.03644
283     p 0.0185462 1 0 -0.927312
284     p 0.0163639 1 0 -0.818196
285     p 0.0141818 1 0 -0.709088
286     p 0.0119997 1 0 -0.599986
287     p 0.00981779 1 0 -0.490890
288     p 0.00763596 1 0 -0.381798
289     p 0.00545421 1 0 -0.272710
290     p 0.00327250 1 0 -0.163625
291     p 0.00109083 1 0 -0.0545416
292     p -0.00109083 1 0 0.0545416
293     p -0.00327250 1 0 0.163625
294     p -0.00545421 1 0 0.272710
295     p -0.00763596 1 0 0.381798
296     p -0.00981779 1 0 0.490890
297     p -0.0119997 1 0 0.599986
298     p -0.0141818 1 0 0.709088
299     p -0.0163639 1 0 0.818196
300     p -0.0185462 1 0 0.927312
301     p -0.0207288 1 0 1.03644
302     p -0.0229115 1 0 1.14557
303     p -0.0250944 1 0 1.25472
304     p -0.0272775 1 0 1.36388
305     p -0.0294610 1 0 1.47305
306     p -0.0316446 1 0 1.58223
307     p -0.0338287 1 0 1.69143
308     p -0.0360130 1 0 1.80065
309     p -0.0381976 1 0 1.90988
310     p -0.0403827 1 0 2.01913
311     p -0.0425681 1 0 2.12840
312     p -0.0447539 1 0 2.23770
313     p -0.0469402 1 0 2.34701
314     p -0.0491269 1 0 2.45634
315     p -0.0513140 1 0 2.56570
316     p -0.0535017 1 0 2.67508
317     p -0.0556898 1 0 2.78449
318     p -0.0578785 1 0 2.89393
319     p -0.0600678 1 0 3.00339
320     p -0.0622576 1 0 3.11288
321     p -0.0644480 1 0 3.22240
322     p -0.0666391 1 0 3.33195
323     p -0.0688307 1 0 3.44154
324     p -0.0710231 1 0 3.55115
325     p -0.0732161 1 0 3.66080
326     p -0.0754098 1 0 3.77049
327     p -0.0776042 1 0 3.88021
328     p -0.0797994 1 0 3.98997
329     p -0.0819953 1 0 4.09977
330     p -0.0841921 1 0 4.20960
331     p -0.0863896 1 0 4.31948
332     p -0.0885879 1 0 4.42940
333     p -0.0907872 1 0 4.53936
334     p -0.0929872 1 0 4.64936
335     p -0.0951882 1 0 4.75941
336     p -0.0973901 1 0 4.86951
337     p -0.0995929 1 0 4.97965
338     p -0.101797 1 0 5.08984
339     p -0.104001 1 0 5.20007
340     p -0.106207 1 0 5.31036
341     p -0.108414 1 0 5.42070
342     p -0.110622 1 0 5.53109
343     p -0.112831 1 0 5.64154
344     p -0.115041 1 0 5.75204
345     p -0.117252 1 0 5.86259
346     p -0.119464 1 0 5.97320
347     p -0.121677 1 0 6.08387
348     p -0.123892 1 0 6.19460
349     p -0.126108 1 0 6.30539
350     p -0.128325 1 0 6.41624
351     p -0.130543 1 0 6.52715
352     p -0.132762 1 0 6.63812
353     p -0.134983 1 0 6.74916
354     p -0.137205 1 0 6.86026
355     p -0.139429 1 0 6.97143
356     p -0.141653 1 0 7.08267
357     p -0.143880 1 0 7.19397
358     p -0.146107 1 0 7.30535
359     p -0.148336 1 0 7.41680
360     p -0.150566 1 0 7.52832
361     p -0.152798 1 0 7.63991
362     p -0.155032 1 0 7.75158
363     p -0.157266 1 0 7.86332
364     p -0.159503 1 0 7.97514
365     p -0.161741 1 0 8.08704
366     p -0.163980 1 0 8.19902
367     p -0.166221 1 0 8.31107
368     p -0.168464 1 0 8.42321
369     p -0.170709 1 0 8.53543
370     p -0.172955 1 0 8.64773
371     p -0.175202 1 0 8.76012
372     p -0.177452 1 0 8.87260
373     p -0.179703 1 0 8.98516
374     p -0.181956 1 0 9.09781
375     p -0.184211 1 0 9.21055
376     p -0.186468 1 0 9.32338
377     p -0.188726 1 0 9.43630
378     p -0.190986 1 0 9.54932
379     p -0.193249 1 0 9.66243
380     p -0.195513 1 0 9.77563
381     p -0.197779 1 0 9.88893
382     p -0.200047 1 0 10.0023
383     p -0.202317 1 0 10.1158
384     p -0.204589 1 0 10.2294
385     p -0.206863 1 0 10.3431
386     p -0.209139 1 0 10.4569
387     p -0.211417 1 0 10.5708
388     p -0.213697 1 0 10.6848
389     p -0.215979 1 0 10.7990
390     p -0.218264 1 0 10.9132
391     p -0.220551 1 0 11.0275
392     p -0.222839 1 0 11.1420
393     p -0.225131 1 0 11.2565
394     p -0.227424 1 0 11.3712
395     p -0.229720 1 0 11.4860
396     p -0.232017 1 0 11.6009
397     p -0.234318 1 0 11.7159
398     p -0.236620 1 0 11.8310
399     p -0.238925 1 0 11.9463
400     p -0.241233 1 0 12.0616
401     p -0.243543 1 0 12.1771
```

```
402     p -0.245855 1 0 12.2927
403     p -0.248170 1 0 12.4085
404     p -0.250487 1 0 12.5243
405     p -0.252807 1 0 12.6403
406     p -0.255129 1 0 12.7565
407     p -0.257454 1 0 12.8727
408     p -0.259782 1 0 12.9891
409     p -0.262112 1 0 13.1056
410     p -0.264445 1 0 13.2222
411     p -0.266780 1 0 13.3390
412     p -0.269119 1 0 13.4559
413     p -0.271460 1 0 13.5730
414     p -0.273804 1 0 13.6902
415     p -0.276150 1 0 13.8075
416     p -0.278500 1 0 13.9250
417     p -0.280852 1 0 14.0426
418     p -0.283207 1 0 14.1604
419     p -0.285565 1 0 14.2783
420     p -0.287926 1 0 14.3963
421     p -0.290290 1 0 14.5145
422     p -0.292657 1 0 14.6329
423     p -0.295027 1 0 14.7514
424     p -0.297400 1 0 14.8700
425     p -0.299777 1 0 14.9888
426     p -0.302156 1 0 15.1078
427     p -0.304538 1 0 15.2269
428     p -0.306924 1 0 15.3462
429     p -0.309313 1 0 15.4656
430     p -0.311705 1 0 15.5852
431     p -0.314100 1 0 15.7050
432     p -0.316498 1 0 15.8249
433     p -0.318900 1 0 15.9450
434     p -0.321306 1 0 16.0653
435     p -0.323714 1 0 16.1857
436     p -0.326126 1 0 16.3063
437     p -0.328542 1 0 16.4271
438     p -0.330960 1 0 16.5480
439     p -0.333383 1 0 16.6691
440     p -0.335809 1 0 16.7904
441     p -0.338238 1 0 16.9119
442     p -0.340671 1 0 17.0336
443     p -0.343108 1 0 17.1554
444     p -0.345548 1 0 17.2774
445     p -0.347992 1 0 17.3996
446     p -0.350440 1 0 17.5220
447     p -0.352891 1 0 17.6446
448     p -0.355347 1 0 17.7673
449     p -0.357806 1 0 17.8903
450     p -0.360269 1 0 18.0134
451     p -0.362735 1 0 18.1368
452     p -0.365206 1 0 18.2603
453     p -0.367681 1 0 18.3840
454     p -0.370159 1 0 18.5080
455     p -0.372642 1 0 18.6321
456     p -0.375129 1 0 18.7564
457     p -0.377619 1 0 18.8810
458     p -0.380114 1 0 19.0057
459     p -0.382613 1 0 19.1306
460     p -0.385116 1 0 19.2558
461     p -0.387623 1 0 19.3812
462     p -0.390135 1 0 19.5068
463     p -0.392651 1 0 19.6325
464     p -0.395171 1 0 19.7586
465     p -0.397696 1 0 19.8848
466     p -0.400225 1 0 20.0112
467     p -0.402758 1 0 20.1379
468     p -0.405296 1 0 20.2648
469     p -0.407838 1 0 20.3919
470     p -0.410385 1 0 20.5192
471     p -0.412936 1 0 20.6468
472     p -0.415492 1 0 20.7746
473     p -0.418053 1 0 20.9026
474     p -0.420618 1 0 21.0309
475     p -0.423188 1 0 21.1594
476     p -0.425763 1 0 21.2881
477     p -0.428342 1 0 21.4171
478     p -0.430927 1 0 21.5463
479     p -0.433516 1 0 21.6758
480     p -0.436110 1 0 21.8055
481     p -0.438709 1 0 21.9355
482     p -0.441313 1 0 22.0657
483     p -0.443922 1 0 22.1961
484     p -0.446536 1 0 22.3268

mode    p
m1      7014 0.78 8016 0.22
m2      13027 1
m3      6012 1
m4      8016 0.67 14028 0.33
m5      8016 0.67 14028 0.33
m6      24052 0.2 26056 0.7 28059 0.1
m10     7014 0.78 8016 0.22
m11     74184 0.5 48112 0.5
m20     74184 1
m21     7014 0.78 8016 0.22
m40     82207 1
sdef      sur=11  dir=1  erg=D1  axs=1  0  0  ext=D3
ccc=900
SI3     H .999929386964 1
SP3     D 0 1
f6:p    101 381I 483
vol     12J 0.11061 381I 0.11061 384J
SI1     A 0.1 117I 6.00
SB1     0.1 117I 6.00
SP1     D &
  0.0026 &
  0.006135 &
  0.077262 &
  0.200829 &
  0.245488 &
  0.270285 &
  0.276133 &
  0.275658 &
  0.240378 &
  0.244559 &
  0.208765 &
  0.208993 &
  0.189345 &
  0.185969 &
  0.163017 &
  0.148788 &
  0.133495 &
  0.145094 &
  0.124181 &
  0.113446 &
  0.116133 &
  0.106771 &
  0.100577 &
  0.091048 &
  0.088891 &
  0.090863 &
  0.084028 &
  0.076445 &
  0.069985 &
  0.06613 &
  0.067011 &
  0.061604 &
  0.059176 &
  0.054042 &
  0.050185 &
  0.049736 &
  0.052049 &
  0.045888 &
  0.05146 &
  0.045329 &
  0.044589 &
  0.03617 &
  0.035994 &
  0.034671 &
  0.030122 &
  0.038276 &
  0.034885 &
```

```
   0.03122 &
   0.030346 &
   0.037031 &
   0.02626 &
   0.02173 &
   0.021335 &
   0.024956 &
   0.021486 &
   0.028397 &
   0.022173 &
   0.020651 &
   0.021311 &
   0.022417 &
   0.025586 &
   0.02281 &
   0.01784 &
   0.016964 &
   0.021158 &
   0.014624 &
   0.017429 &
   0.015485 &
   0.019368 &
   0.014834 &
   0.017644 &
   0.013134 &
   0.015706 &
   0.012041 &
   0.013347 &
   0.010086 &
   0.015925 &
   0.011645 &
   0.013566 &
   0.007134 &
   0.012696 &
   0.009044 &
   0.010547 &
   0.008149 &
   0.00925 &
   0.008176 &
   0.011395 &
   0.007521 &
   0.008608 &
   0.006232 &
   0.006037 &
   0.006879 &
   0.006905 &
   0.009473 &
   0.006035 &
   0.006849 &
   0.005598 &
   0.005611 &
   0.004967 &
   0.004514 &
   0.00493 &
   0.006864 &
   0.002154 &
   0.002808 &
   0.005356 &
   0.004095 &
   0.003015 &
   0.004726 &
   0.003237 &
   0.00323 &
   0.003016 &
   0.001933 &
   0.003452 &
   0.002374 &
   0.001723 &
   0.002557 &
   0.001291 &
   0.000212 &
   0.000428
nps     5000000
```

APPENDIX C. Resolution Calculation - IDL Code

```
FUNCTION FWHM, array
sz = size(array)
size = sz(1)
maximum = MAX(array, max_pos)
low = 0.
high= size -1.
FOR i = 0., max_pos do begin
       j = size - 1. - i
       if array(i) LT (maximum/2.) then low = i
       if array(j) LT (maximum/2.) then high = j
ENDFOR
fwhm_value = high - low - 1
RETURN, fwhm_value
END


PRO shape, s_width, d_width, dist
x_size = dist /5
x_pix2mm = dist / x_size
y_size = MAX([s_width * 100., d_width * 100.])
s_size = s_width * 100.
d_size = d_width * 100.
y_pix2mm = MAX([s_width, d_width]) / y_size
x_dim = FINDGEN(x_size) * x_pix2mm
y_dim = FINDGEN(y_size) * y_pix2mm

image = FLTARR(x_size , y_size)
source = FLTARR(x_size , y_size)
detector = FLTARR(x_size , y_size)

FOR x_index = 0., x_size-1 DO BEGIN
       y_start = ((y_size -1.) / 2.) * (x_index / (x_size - 1.))
       y_start = ((y_size -1.) / 2.) - ((((y_size -1.) / 2.) - y_start) / y_size *
s_size)
       y_end = y_size - 1. - y_start
       height = 1. / (y_end - y_start + 1.)
       source(x_index  , y_start:y_end) = height

       y_start = ((y_size - 1.) / 2.) * ((x_size -1 - x_index) / (x_size - 1.))
       y_start = ((y_size -1.) / 2.) - ((((y_size -1.) / 2.) - y_start) / y_size *
d_size)
       y_end = y_size -1. - y_start
       height = 1. / (y_end - y_start + 1.)
       detector(x_index  , y_start:y_end) = height

       temp1 = FLTARR(y_size)
       temp2 = FLTARR(y_size-1)
       for i=0, y_size-1 do temp1(i) = source(x_index, i)
       for i=0, y_size-2 do temp2(i) = detector(x_index, i)
       temp = CONVOL(temp1 , temp2, EDGE_WRAP = 1)
;      temp = FFT(FFT(temp1, -1) * FFT(temp2, -1), 1)
       image(x_index, *) = temp
ENDFOR

;WINDOW, 0, XSIZE = 300, YSIZE = 300
;WINDOW, 1, XSIZE = 300, YSIZE = 300
WINDOW, 2, XSIZE = 300, YSIZE = 300
WINDOW, 3, XSIZE = x_size, YSIZE = y_size
;WSET, 0
;shade_surf, source
;WSET, 1
;shade_surf, detector
WSET, 2
shade_surf, image, x_dim, y_dim, $
       XSTYLE = 1, $
```

```
        XTITLE = "Distance from source (mm)", $
        YTITLE = "Beam Lateral position (mm), $
        ZTITLE = "Beam Intensity"

WSET, 3
tvscl, image
fwhm_array = FLTARR(x_size)
FOR i = 0, x_size -1 DO BEGIN
        temp = fltarr(y_size)
        FOR j = 0, y_size - 1 DO BEGIN
                temp(j) = image(i,j)
        ENDFOR
        fwhm_array(i) = fwhm(temp)
ENDFOR

plot, x_dim, fwhm_array * y_pix2mm, $
        XSTYLE = 1, $
        XTITLE = "Distance from source (mm)", $
        YTITLE = "Beam FWHM (mm)

resolution = MIN(fwhm_array, best_position)
PRINT, "The best resolution is: "
PRINT, resolution * y_pix2mm
PRINT, "The ideal object position is:"
PRINT, best_position * x_pix2mm

set_plot, 'PS'
DEVICE, /ENCAP, FILENAME = "e:\incoming\3dprof.eps"
shade_surf, image, x_dim, y_dim, $
        XSTYLE = 1, $
        XTITLE = "Distance from source (mm)", $
        YTITLE = "Beam Lateral position (mm), $
        ZTITLE = "Beam Intensity"
DEVICE, /CLOSE

set_plot, 'PS'
DEVICE, /ENCAP, FILENAME = "e:\incoming\fwhmplot.eps"
plot, x_dim, fwhm_array * y_pix2mm, $
        XSTYLE = 1, $
        XTITLE = "Distance from source (mm)", $
        YTITLE = "Beam FWHM (mm)
DEVICE, /CLOSE
SET_PLOT, 'WIN'

END
```

APPENDIX D. Shielding Computation - MCNP Input Code

```
 Shielding calculation 10/27/96
c
c Furnace
1       2 -2.7 -1 -7 8 imp:p=1
2       3 -2.20 1 -2  -7 8 imp:p=1
3       1 -0.00127 2 -3 -7 8 imp:p=1
4       4 -1.5 3 -4 -7 8 imp:p=1
5       5 -0.5 4 -5 -7 8 imp:p=1
6       6 -7.9 5 -6 -7 8 imp:p=1
7       0 -7 8 -6 imp:p=0
c Walls
10      41 -2.3 10 -11 -16  17  22 -18 imp:p=1
11      41 -2.3 10 -11  16 -12 -18  19 imp:p=1
12      41 -2.3 10 -11 -19  22 -12  13 imp:p=1
13      41 -2.3 10 -11 -13  15  22 -21 imp:p=1
14      41 -2.3 10 -11  21 -20  15 -14 imp:p=1
c ceiling
15      41 -2.3 11 -40  17 -12 -18 22 imp:p=1
c floor
20      41 -2.3 -999 -10 imp:p=1
c lead shielding
c 30      40 -11.3 25 -13 28 -29 26 -27 imp:p=1
30      1 -0.00127 25 -13 28 -29 26 -27 imp:p=1
31      40 -11.3 -31 30 -32 33 36 -37 imp:p=1
32      40 -11.3 -31 30 -34 35 38 -39 imp:p=1
c dosimeters
50      1 -0.00127 50 -51 -52 imp:p=1
51      1 -0.00127 12 -60 -61 imp:p=1
52      1 -0.00127 10 -11 22 -70 -15 16 imp:p=1
53      1 -0.00127 10 -11 80 -81 18 -82 imp:p=1
c air around...
100     1 -0.00127 -999 40 imp:p=1
101     1 -0.00127 -999 10 -40 12 #51 imp:p=1
102     1 -0.00127 -999 10 -40 -17 imp:p=1
103       1 -0.00127 -999 10 -40 18 -12 17 #53
imp:p=1
104     1 -0.00127 -999 10 -40 -22 -12 17 imp:p=1
105       1 -0.00127 10 -11 22 -19 16 -15 #52
imp:p=1
106     1 -0.00127 10 -11 15 -14 20 -19 imp:p=1
107     1 -0.00127 10 -11 14 -13 21 -19 &
 #7 #30 #31 #32 #50 imp:p=1
666     0 999 imp:p=0
900     0 101 -102 -103 104 imp:p=1

1       cz 7.6
2       cz 9.5
3       cz 10.5
4       cz 13.4
5       cz 25.4
6       cz 25.52
7       pz 179
8       pz 137
c floor
10      pz 0
c ceiling
11      pz 243
40      pz 304
c perpendicular walls
12      px 331
13      px 254.8
14      px -400.52
15      px -476.72
16      px -568.16
17      px -644.36
c parallel walls
18      py 243.84
19      py 167.64
20      py 45.72
21      py -167.64
22      py -243.84
c beam stopper
25      px 214.32
26      pz 150.5
27      pz 165.5
28      py -80
29      py 80
c collimator
30      py -10.16
31      py 10.16
32      p 1 0 -84.5 -13401
33      p 1 0 -84.5 -14259.52
34      p 1 0 84.5 13216.5
35      p 1 0 84.5 12358.033
36      p 84.5 0 1 -4058.55
37      p 84.5 0 1 -2341.3898
38      p 84.5 0 -1 -4374.55
39      p 84.5 0 -1 -2657.3898
c dosimeter in front of beam at 1 meter
50      px 98
51      px 102
52      k/x -50 0 158 0.0001400511186
c dosimeter in front of beam behind wall
60      px 381
61      k/x -50 0 158 0.07179677
c dosimeter at the entrance of the room
70      py -193.84
c dosimeter at 90 degrees outside
80      px -30
81      px  30
82      py 293.84
c source surfaces
100     s -50 0 158 .01
101     s -50 0 158 .009
102     s -50 0 158 .011
103     k/x -50 0 158 0.07179677
104     px -50
c outside
999     so 1300.0

mode    p
m1      7014 0.78 8016 0.22
m2      13027 1
m3      6012 1
m4      8016 0.67 14028 0.33
m5      8016 0.67 14028 0.33
m6      24052 0.2 26056 0.7 28059 0.1
m40     82207 1
m41       8016  .545  20040  .32  14028  .075  16032
.005 &
 13027 .025 24052 .015 12024 .015
c Number of particles simulated
nps     38000000
f6:p    50 51 52 53
sdef    sur=100 erg=D1 axs=1 0 0 ext=D3 ccc=900
SI3     H .9659258262 1
SP3     D 0 1
SI1     A 0.1 117I 6.00
SB1     0.1 117I 6.00
SP1     D &
  0.0026 &
  0.006135 &
  0.077262 &
  0.200829 &
  0.245488 &
  0.270285 &
  0.276133 &
  0.275658 &
  0.240378 &
  0.244559 &
```

0.208765 &
0.208993 &
0.189345 &
0.185969 &
0.163017 &
0.148788 &
0.133495 &
0.145094 &
0.124181 &
0.113446 &
0.116133 &
0.106771 &
0.100577 &
0.091048 &
0.088891 &
0.090863 &
0.084028 &
0.076445 &
0.069985 &
0.06613 &
0.067011 &
0.061604 &
0.059176 &
0.054042 &
0.050185 &
0.049736 &
0.052049 &
0.045888 &
0.05146 &
0.045329 &
0.044589 &
0.03617 &
0.035994 &
0.034671 &
0.030122 &
0.038276 &
0.034885 &
0.03122 &
0.030346 &
0.037031 &
0.02626 &
0.02173 &
0.021335 &
0.024956 &
0.021486 &
0.028397 &
0.022173 &
0.020651 &
0.021311 &
0.022417 &
0.025586 &
0.02281 &
0.01784 &
0.016964 &
0.021158 &
0.014624 &
0.017429 &
0.015485 &
0.019368 &
0.014834 &
0.017644 &
0.013134 &
0.015706 &
0.012041 &
0.013347 &
0.010086 &
0.015925 &
0.011645 &
0.013566 &
0.007134 &
0.012696 &
0.009044 &
0.010547 &
0.008149 &
0.00925 &
0.008176 &
0.011395 &
0.007521 &
0.008608 &
0.006232 &
0.006037 &
0.006879 &
0.006905 &
0.009473 &
0.006035 &
0.006849 &
0.005598 &
0.005611 &
0.004967 &
0.004514 &
0.00493 &
0.006864 &
0.002154 &
0.002808 &
0.005356 &
0.004095 &
0.003015 &
0.004726 &
0.003237 &
0.00323 &
0.003016 &
0.001933 &
0.003452 &
0.002374 &
0.001723 &
0.002557 &
0.001291 &
0.000212 &
0.000428

REFERENCES

1 Irving, W.R.. *Continuous Casting of Steel.* Institute of Materials, London, 1993

2 Chun, J.-H., Lanza, R. C., Saka, N., Hytros, M. M.. *On-Line Monitoring of the Solidification Front in Metal Casting.* Annals of the CIRP, Vol. 44, pp. 181-184., 1995.

3 Hytros, M.. *A Feasibility Study of Solidification Front Monitoring via Tomographic Imaging.* SM Thesis, Department of Mechanical Engineering, Massachusetts Institute of Technology, Cambridge, MA.

4 Kim, D.. *The Design of a Gamma-Ray Tomographic Sensor for Detecting Mushy Zone in Continuous Casting.* SM Thesis, Department of Mechanical Engineering, Massachusetts Institute of Technology, Cambridge, MA.

5 Turner, J.E.. *Atoms, Radiation, and Radiation Protection.* McGraw-Hill, Inc., New York, 1992.

6 Knoll, G.F.. *Radiation Detection and Measurement.* John Wiley & Sons, New York, 2nd edition, 1989.

7 Cho, Z.-H., Jones, J.P., Singh, M.. *Foundations of Medical Imaging.* John Wiley & Sons, New York, 1993.

8 Oppenheim, A.V., Willsky, A.S.. *Signals and Systems.* Prentice Hall, Upper Saddle River, New Jersey, 2nd edition, 1997.

9 Johns, H.E., Cunningham, J.R.. *The Physics of Radiology.* Charles C. Thomas Publisher, Springfield, Illinois, 4th edition, 1983.

10 Kollath, R.. *Particle Accelerators.* Sir Isaac Pitman and Sons Ltd., London, 2nd edition, 1967

11 Livingston, M.S., Blewett, J.P.. *Particle Accelerators.* McGraw-Hill Book Company Inc., New York, 1962.

12 National Council on Radiation Protection, Report NCRP 51.